# Airborne turbulence and temperature measurements

Szymon P. Malinowski

University of Warsaw,
Institute of Geophysics


Acknowledgments: Krzysztof Haman, Wojciech Kumala, Bogdan Rosa, Andrzej Makulski, Rheinhold Busen, Hermann Gerber and many others


EUFAR-TETRAD International School
Hyeres, Sep. 10, 2010

## What is turbulence?

**turbulence** —
1. Irregular fluctuations occurring in fluid motions. It is characteristic of turbulence that the fluctuations occur in all three velocity components and are unpredictable in detail; however, statistically distinct properties of the turbulence can be identified and profitably analyzed. Turbulence exhibits a broad range of spatial and temporal scales resulting in efficient mixing of fluid properties.
2. Random and continuously changing air motions that are superposed on the mean motion of the air.

*Glossary of Meteorology, American Meteorological Society*

**turbulence** — In fluid mechanics, a flow condition (see turbulent flow) in which local speed and pressure change unpredictably as an average flow is maintained.

**atmospheric turbulence** — small-scale, irregular air motions characterized by winds that vary in speed and direction. Turbulence is important because it mixes and churns the atmosphere and causes water vapour, smoke, and other substances, as well as energy, to become distributed both vertically and horizontally.

*Britannica Online*

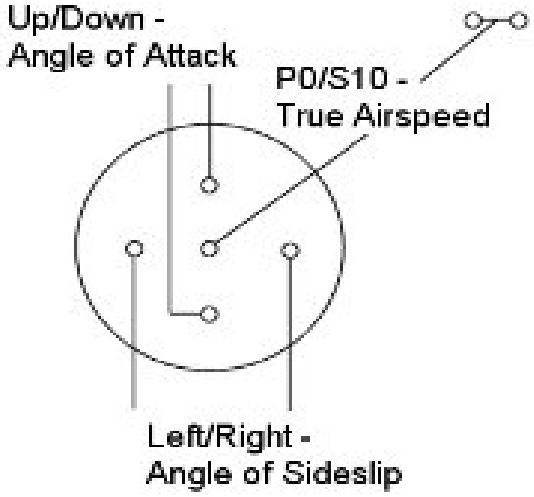


Probe Schematic


5-hole Arrangement in Radome

Internal Ports

The turbulence probe on the FAAM aircraft consists of a five-port pressure measurement system in the aircraft radome, combined with two scientific static ports - S10 - symetrically placed on either side of the aircraft. The system also utilises measurements from the RVSM-compliant air data computer and science measurements of the ambient air temperature, corrected for kinetic effects.

Outputs from the Turbulence system are the angles of attack and sideslip and a measurement of true airspeed. These data are used in conjunction with other core measurements of aircraft attitude and aircraft velocity components to derive northwards, eastwards and downwards components of wind velocity.

http://www.faam.ac.uk/index.php/science-instruments/turbulence/117-turbulence-probe


Rosemount temperature and General Eastern dew point sensors on right fuselage aft of radome


Flux instrumentation next to radome (Rosemount temperature, Lyman-alpha hygrometers)

Turbulence probe holes around radome

http://www.eol.ucar.edu/instrumentation/aircraft

The picture shows NOAA Long-EZ airplane on which the physical probe was primarily developed. Tim Crawford, whose vision brought the BAT probe into being, died of a massive stroke in September 2002. Since he was flying the Long-EZ at the time, we lost both him and the airplane. Nevertheless, a hallmark of his leadership was to develop the talents of those he was leading. He has left behind a group of capable people and a mature system.

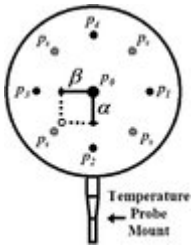


http://www.atdd.noaa.gov/?q=node/29

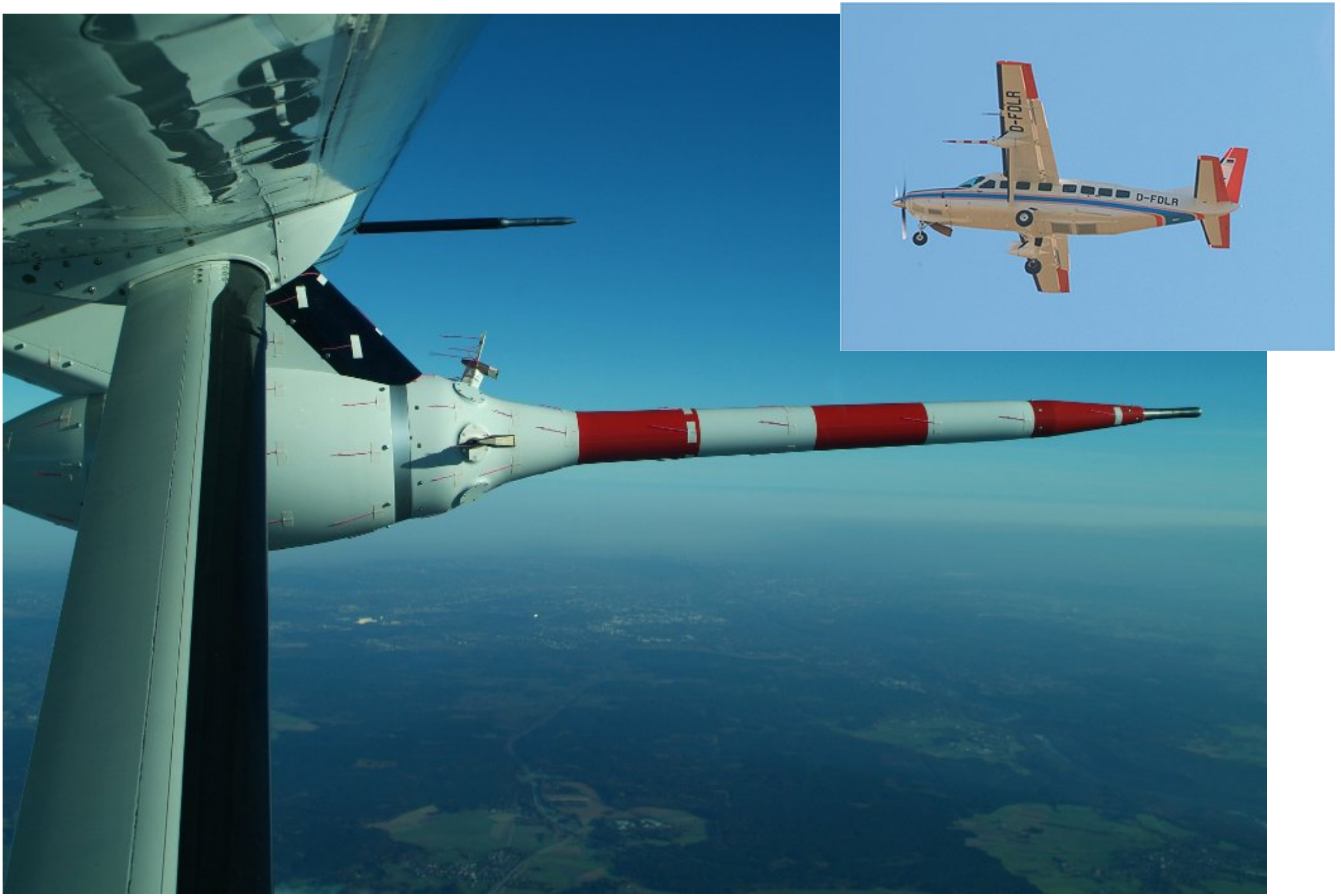


DLR Cessna 208B with turbulence probe
http://www.dlr.de/en/desktopdefault.aspx/tabid-4689/7762_read-11996/

# Turbulent Characteristics of Some Canadian Cumulus Clouds

J. I. MacPHERSON

*National Aeronautical Establishment, Ottawa, Ontario, Canada K1A 0R6*

G. A. ISAAC

*Atmospheric Environment Service, Downsview, Ontario, Canada M3H 5T4*

(Manuscript received 29 June 1976)

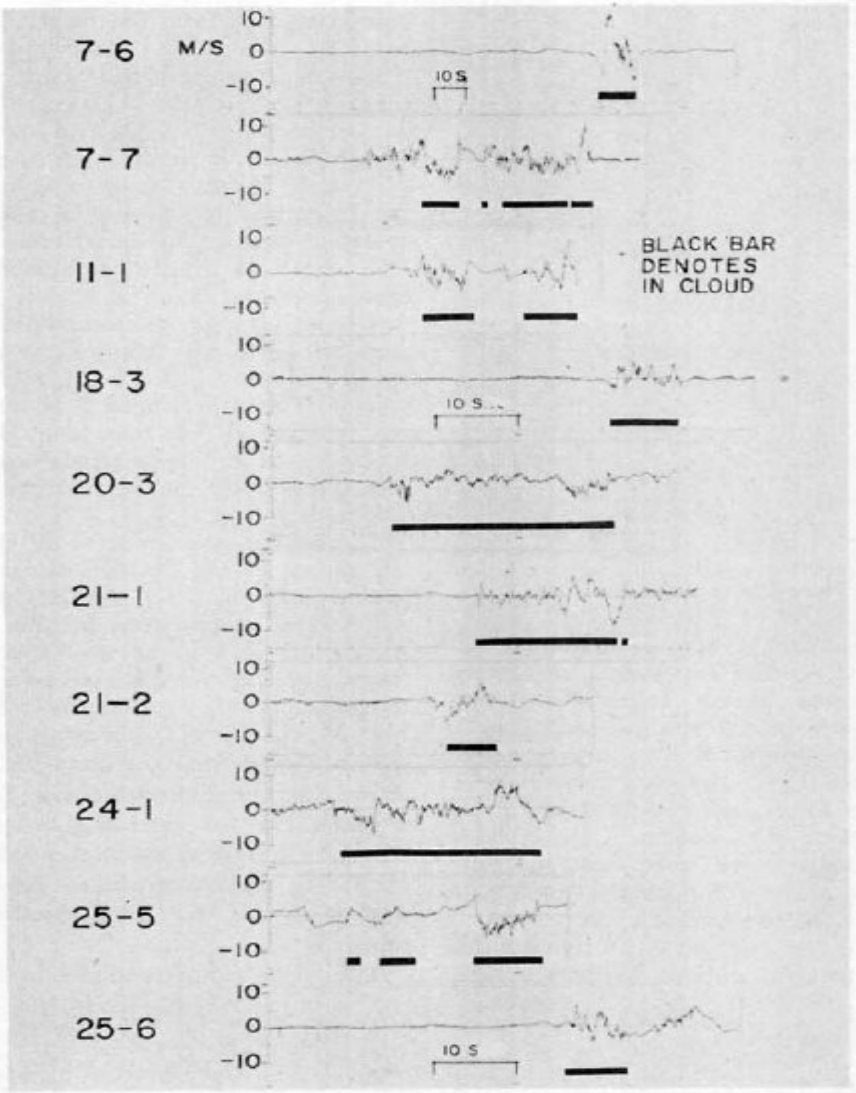


FIG. 6. Time histories of the vertical gust velocity for 10 of the cloud-top penetrations. Time scales vary as shown.


FIG. 1. National Aeronautical Establishment T-33 atmospheric research aircraft showing nose-mounted turbulence boom, fuselage pod housing Doppler radar, and AgI flare burning on wing-mounted pod.

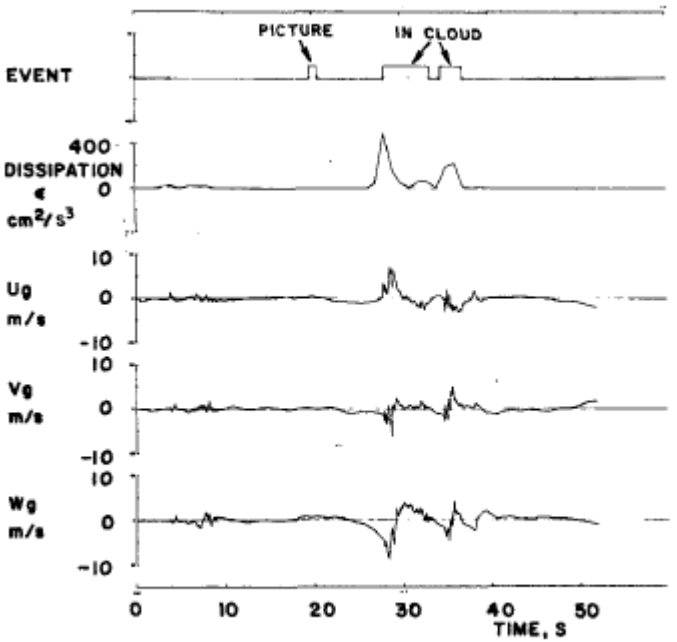


FIG. 4. Time histories for event marker, dissipation rate and three components of true gust velocity for run 20–5.

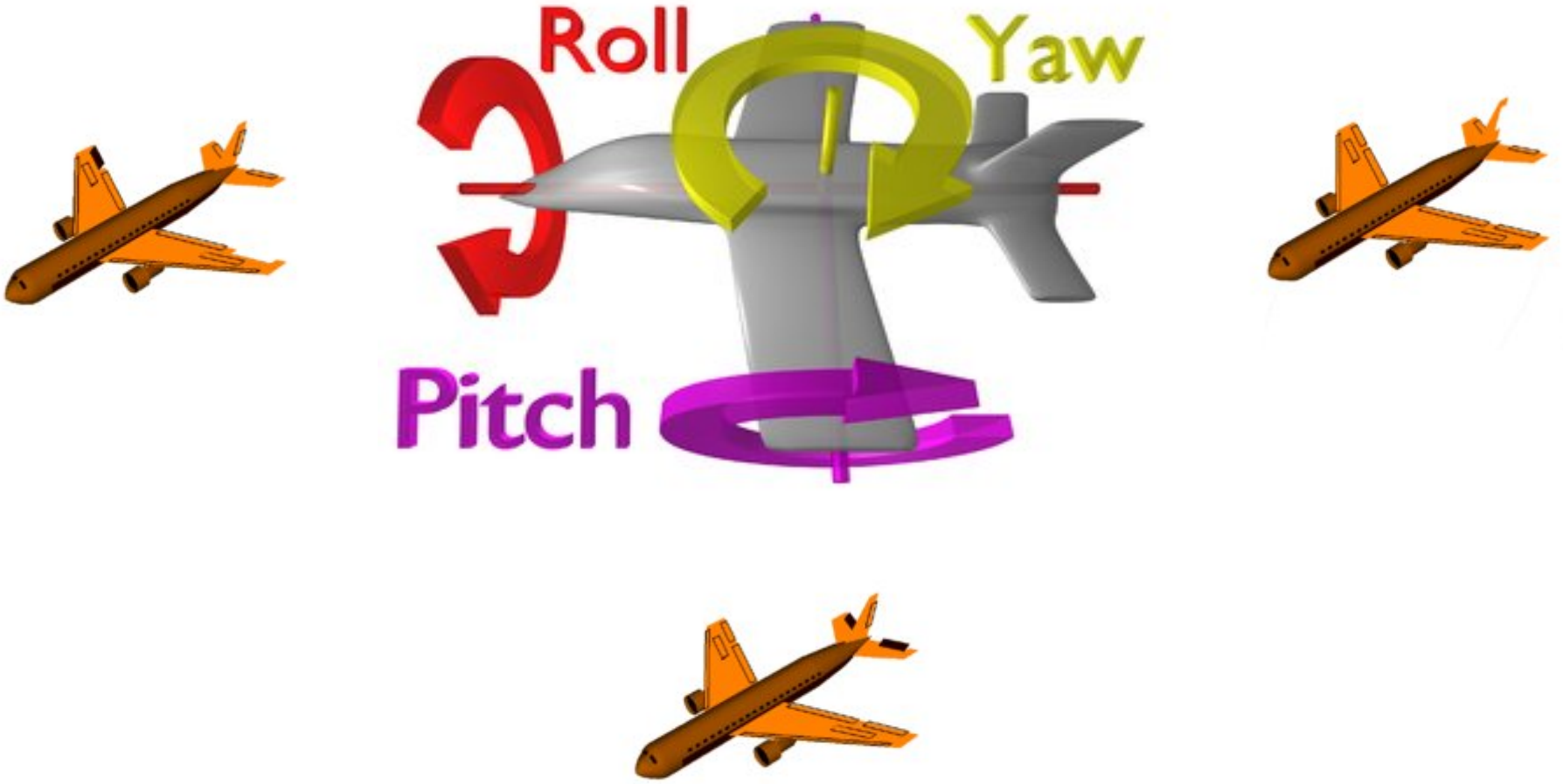


From Wikipedia

Atmos. Chem. Phys., 8, 5449–5463, 2008
www.atmos-chem-phys.net/8/5449/2008/


Atmospheric Chemistry and Physics

# Application of the Aventech AIMMS20AQ airborne probe for turbulence measurements during the Convective Storm Initiation Project

**K. M. Beswick[1], M. W. Gallagher[1], A. R. Webb[1], E. G. Norton[1], and F. Perry[2]**

[1]School of Earth, Atmosphere and Environmental Sciences, University of Manchester, UK
[2]School of Earth and Environment, University of Leeds, UK

Received: 13 November 2006 – Published in Atmos. Chem. Phys. Discuss.: 7 March 2007
Revised: 3 August 2008 – Accepted: 12 August 2008 – Published: 11 September 2008

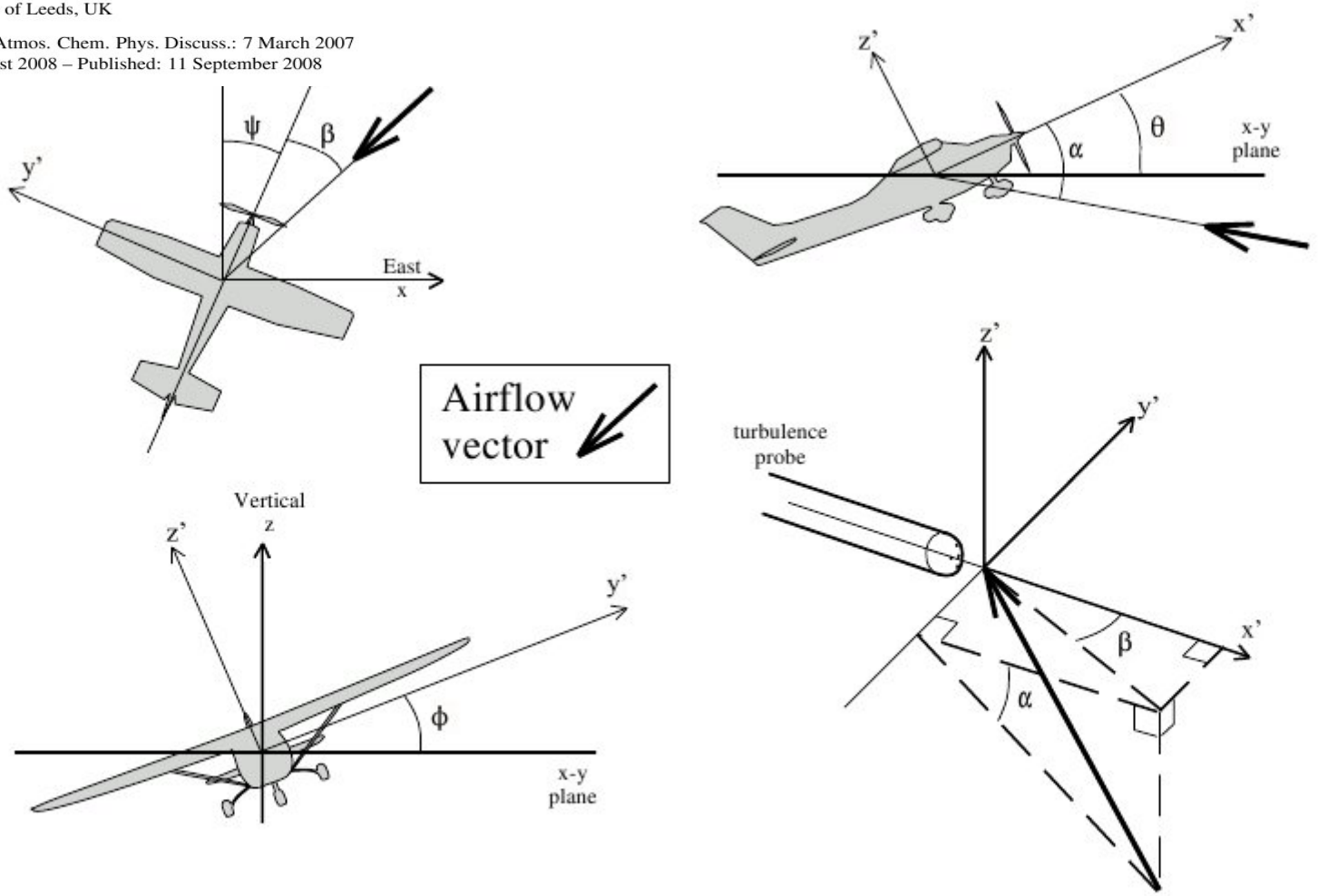


**Fig. 2.** The relationship between the Earth and aircraft coordinates. Earth coordinates are North, East and vertical, or $xyz$. Aircraft coordinates are longitudinal axis, lateral axis and vertical axis, or $x'y'z'$. $\psi$ = heading in $xyz$; $\theta$ = pitch in $xyz$; $\phi$ = roll in $xyz$; $\alpha$ = angle of attack in $x'y'z'$; $\beta$ = sideslip angle in $x'y'z'$.

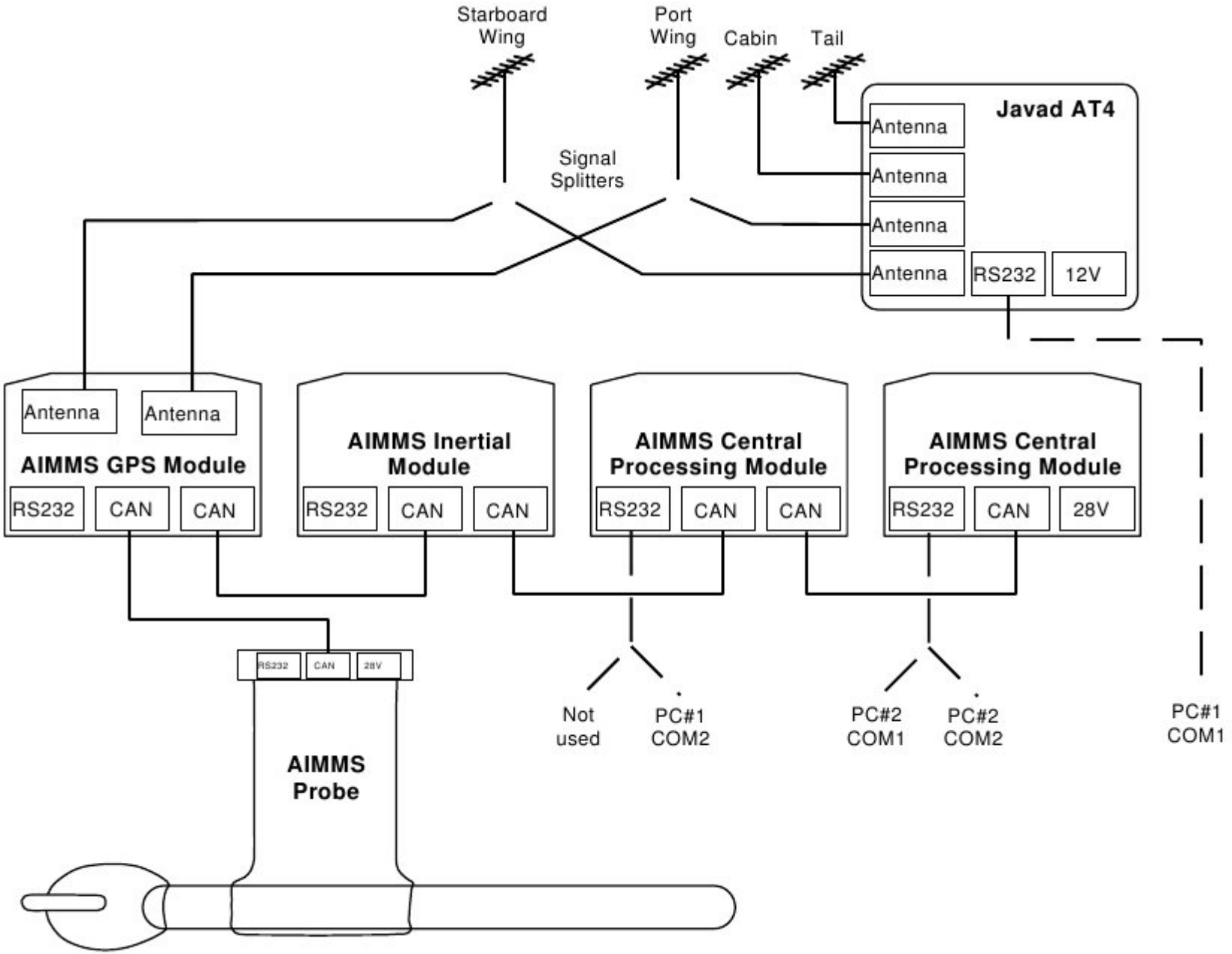


**Fig. 3.** Schematic of the Javad AT4 differential GPS and AIMMS modules. The figure shows the optional second CPM unit which allows on-line data to be displayed whilst the first CPM records high frequency data.

**Table 2.** AIMMS specifications.

| Module | Specification | |
|---|---|---|
| All modules | power: 12.5–37 VDC, 800–900 mA at 12.5 V | |
| | digital serial communication via 115 kbaud controller area network | |
| | Measurement frequency up to 20 Hz | |
| ADP | Overall weight | 3.36 kg |
| | Operating range | −20°C to +50°C |
| | Static pressure | range 0–110 kPa, accuracy 0.1 kPa±0.05% |
| | Pitot pressure | range 0–14 kPa, accuracy 0.02 kPa±0.05% |
| | Wind speed | horizontal: accuracy 0.5 $ms^{-1}$ |
| | | vertical: accuracy 0.75 $ms^{-1}$ |
| | Temperature | glass encapsulated bead thermistor |
| | | calibrated accuracy 0.05°C (0.3°C with dynamic heating correction) |
| | | resolution 0.01°C, time constant <5 s |
| | | mounted in ventilated reverse-flow chamber |
| | Relative Humidity | thermoset polymer capacitative |
| | | accuracy ±2% RH (0–100%) |
| | | resolution 0.1%, time constant <5 s at 20°C |
| | | mounted in ventilated reverse-flow chamber |
| | Compass heading | 3-axis magnetic field sensors |
| | Communication | external RS232 at 115 kbaud |
| IMU | Overall weight | 0.74 kg |
| | Accelerometer | 3-axis, range ±5 g, accuracy 0.005 g, operated at 40 Hz |
| | Rate gyro | 3-axis, operated at 40 Hz |
| GPS | Overall weight | 0.80 kg |
| | Heading | accuracy 0.1° |
| | Position | accuracy 0.01 m |
| | Antennae | shares two dual frequency antennae with AT4 DGPS |
| CPM | Overall weight | 0.60 kg |
| | Processor | Motorola DSP56F807 processor |
| | | 16 Mbit flash memory |
| | | external RS232 at 115k baud |

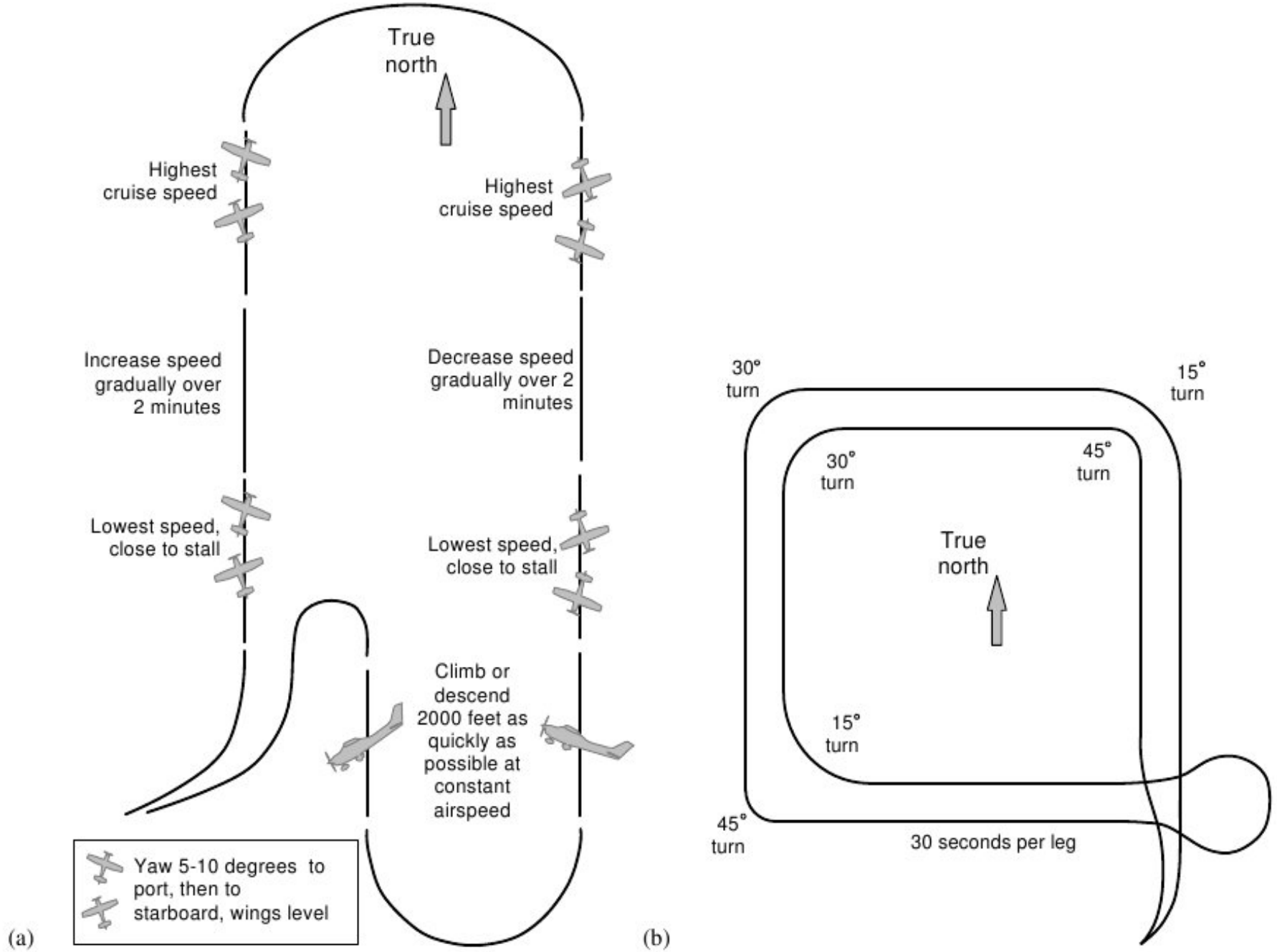


**Fig. 4.** Schematic diagram of the two airborne calibration procedures for the AIMMS sensor: **(a)** shows the flight plan for the aerodynamic calibration, whilst **(b)** shows the flight plan for the cross-axis calibration.

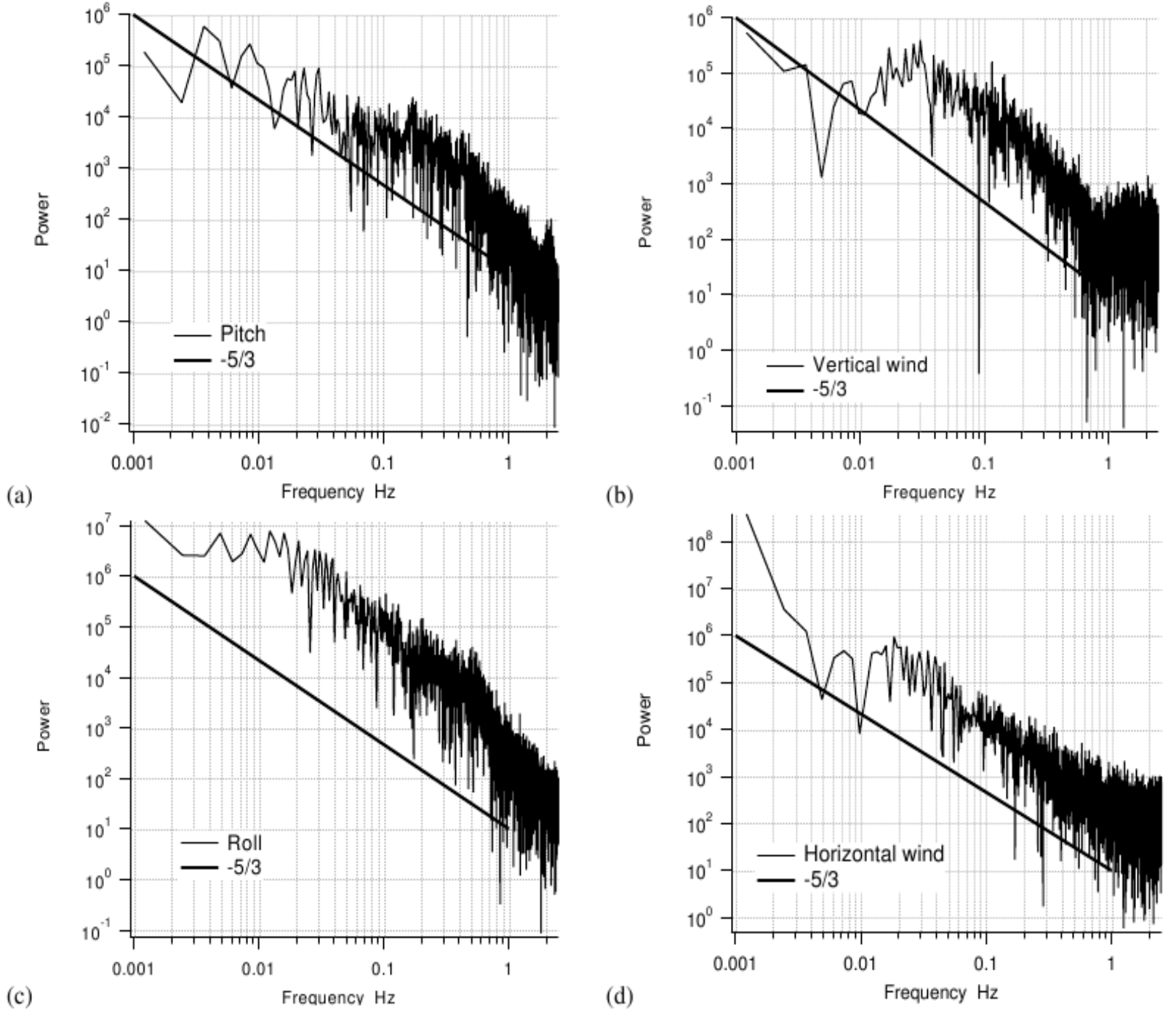


**Fig. 6.** Power spectral densities for AIMMS data from Flight 8 for **(a)** pitch, **(b)** roll, **(c)** vertical wind and **(d)** horizontal wind.

After WIKIPEDIA:

Temperature is a physical property that underlies the common notions of hot and cold. Something that feels hotter generally has a higher temperature, though temperature is not a direct measurement of heat.

Historically, two equivalent scientific concepts of temperature have developed: the macroscopic thermodynamic description, and a microscopic explanation based on statistical physics.

The thermodynamic definition of temperature, first stated by Lord Kelvin, is based entirely on empirical variables, as could be measured with a thermometer. Statistical physics provides a deeper understanding by describing the atomic behavior of matter, and derives macroscopic properties from statistical averages of microscopic properties.

Think to remember:

thermometer always measures its own temperature. To measure temperature of air one has to put the thermometer on the aircraft and this creates a lot of problems.

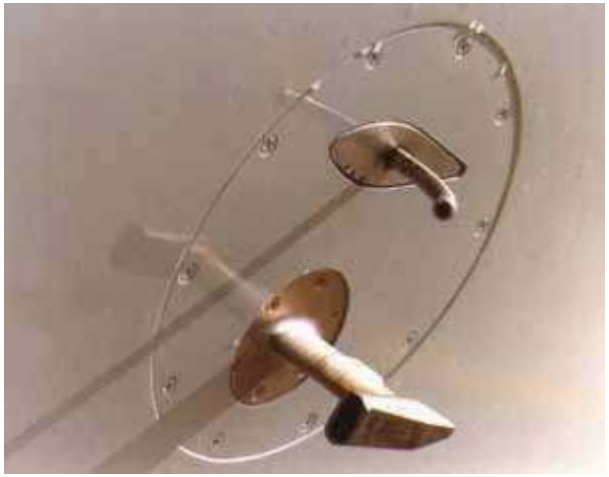

Rosemount housing

Thermometers and other sensors are often mounted in such housings

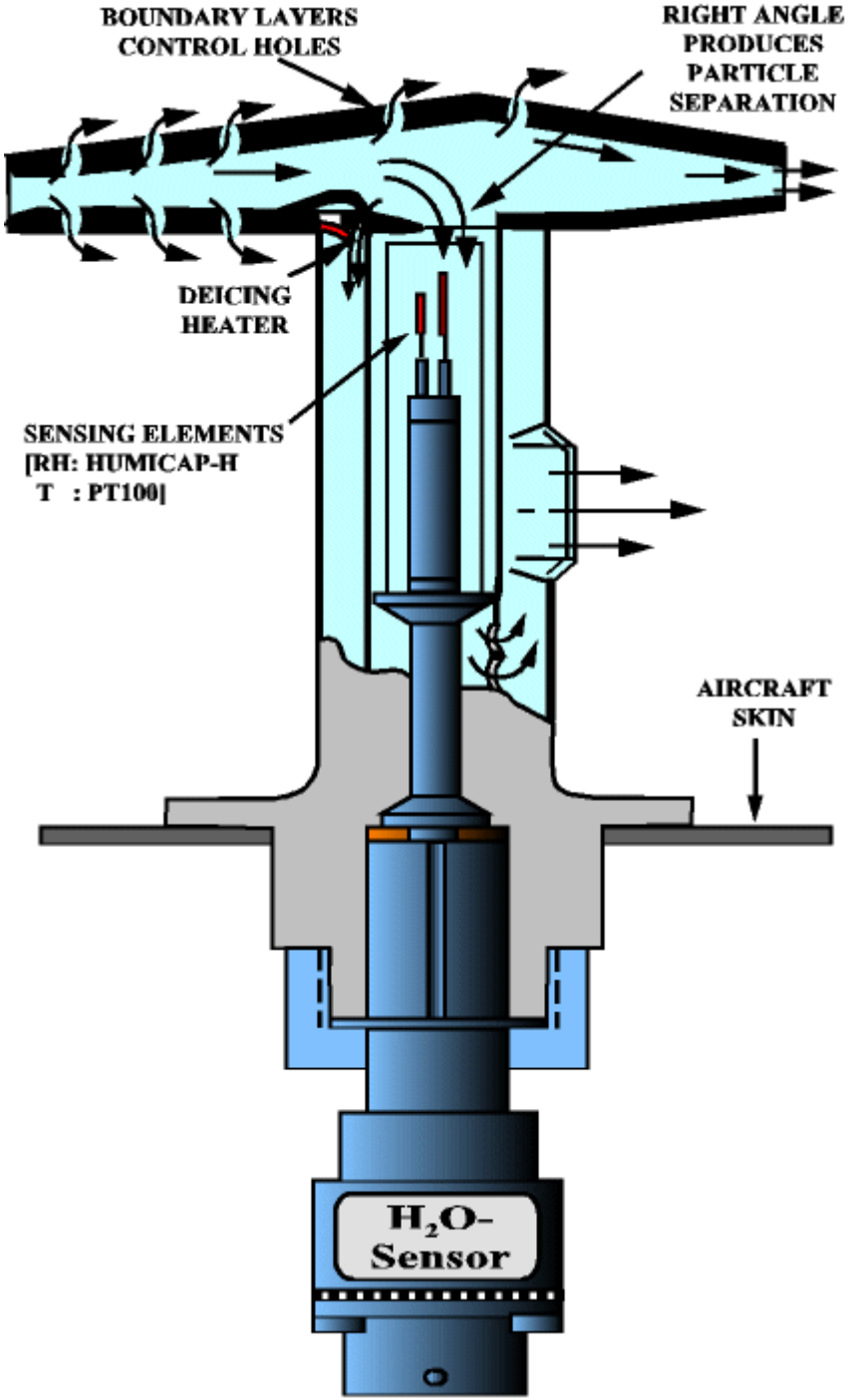


Juelich-MOSAIC

# Performance of Some Airborne Thermometers in Clouds

R. PAUL LAWSON*
*Department of Atmospheric Science, University of Wyoming, Laramie, Wyomimg*

WILLIAM A. COOPER
*National Center for Atmospheric Research,** Boulder, Colorado*

(Manuscript received 28 July 1989, in final form 27 November 1989)

The recovery temperature of an immersion thermometer, $T_r$, is the effective (i.e., average) temperature at the surface of the sensor when there is no net heat transfer to the airstream. The recovery temperature is affected by the thermometer housing (which slows and hence heats the air) and by the sensing element (which is heated by friction and by additional deceleration of the airflow in its vicinity). If the air in the housing is slowed adiabatically to a fraction $f$ of the free-stream airspeed $U_\infty$, conservation of energy requires that the air temperature will change from the free-stream temperature $T_\infty$ according to

$$T_h = T_\infty + r_h \frac{U_\infty^2}{2C_p} \qquad (1)$$

where $T_h$ is the temperature of the decelerated air in the housing, $U_\infty$ is now the true airspeed of the aircraft, $C_p$ is the specific heat of air at constant pressure and $r_h = 1 - f^2$ is the "recovery factor" of the housing. Then $r_h = (T_h - T_\infty)/(T_t - T_\infty)$, where $T_t$ is the stagnation temperature at $U_\infty$ (sometimes called the "total temperature"). If the sensing element is characterized by a recovery factor $r_s$ applicable at the slowed airspeed $fU_\infty$, the temperature of the sensing element will be

$$T_r = T_h + r_s \frac{f^2 U_\infty^2}{2C_p} = T_\infty + r \frac{U_\infty^2}{2C_p} \qquad (2)$$

where $r = 1 - f^2(1 - r_s)$ is the effective recovery factor of the thermometer. This dependence of the recovery factor on $f$ and $r_s$ assumes that frictional heating of the air by the housing is negligible.

While (2) defines the recovery temperature under adiabatic conditions at the surface of the sensor, in practice these conditions are rarely met in airborne thermometry. For a platinum resistance thermometer, additional errors result from conduction of heat from the housing to the sensor, self-heating (caused by the current used to measure the resistance), heating of the air by the housing, and radiative heat transfer. Resulting

At an aircraft speed of 100 m $s^{-1}$, compressional and viscous heating will warm the air approaching an immersion thermometer by about 5°C (if $r_h \approx 1$). Because this compressional heating occurs in a few milliseconds, while the time constant for response of the cloud vapor field to changes in ambient conditions is typically a few seconds (e.g., Politovich and Cooper

## Performance of Some Airborne Thermometers in Clouds

R. PAUL LAWSON*
*Department of Atmospheric Science, University of Wyoming, Laramie, Wyomimg*
WILLIAM A. COOPER
*National Center for Atmospheric Research,** Boulder, Colorado*
(Manuscript received 28 July 1989, in final form 27 November 1989)

Error due to wetting:

One can insert (5) into (3) and use the Bedingfield and Drew (1950) relationship for the ratio of heat-to-mass transfer coefficients (as did Lenschow and Pennell 1974) to obtain

$$T_{wb} - T_r = \frac{-1}{AP_o}\left(e_s(T_{wb}) - \frac{P_o}{P_\infty}e_\infty\right) \qquad (6)$$

where

$$A = \frac{C_p}{\epsilon L_v}(\mathrm{Sc}/\mathrm{Pr})^{0.56}\left(1 - \frac{\epsilon e_s(T_{wb})}{P_o}\right) \qquad (7)$$

is the psychrometric parameter, Sc is the Schmidt number and Pr is the Prandtl number. The quantity $(T_{wb} - T_r)$ is the error caused by sensor wetting, and its absolute value is equal to the wet-bulb depression.

Equation (6) is similar to the classical wet-bulb equation,

$$T'_{wb} - T_\infty = \frac{-1}{A'P_o}(e_s(T'_{wb}) - e_\infty) \qquad (8)$$

where the prime denotes quantities at low-velocity. In (6), $T_r$ replaces $T_\infty$ of (8) and the free-stream vapor pressure has been multiplied by the factor $P_o/P_\infty$, as is appropriate in a compressed airstream near the sensing element.

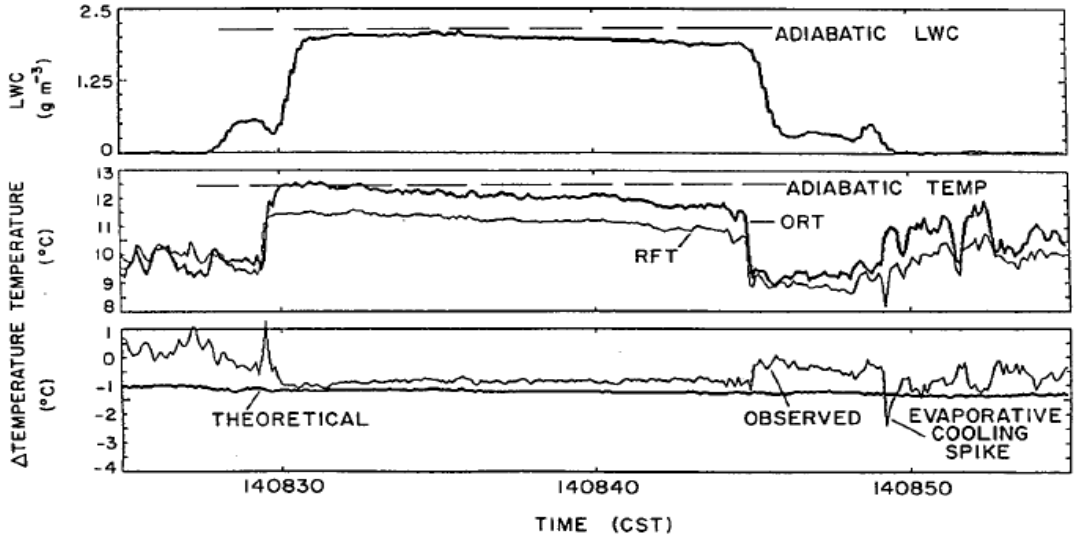


FIG. 9. Time series of measurements recorded during penetration by the NCAR King Air of an undiluted core in a warm cumulus cloud near New Iberia on 7 November 1985. The plotted adiabatic temperature and liquid water content were computed using measurements taken at cloud base by the NCAR Electra. The theoretical value of temperature for a wetted sensor was computed using (6) for the reverse-flow thermometer (RFT), and is compared with the observed temperature difference between the RFT and the Ophir radiometric thermometer. ($\Delta T$ = RFT − ORT.)

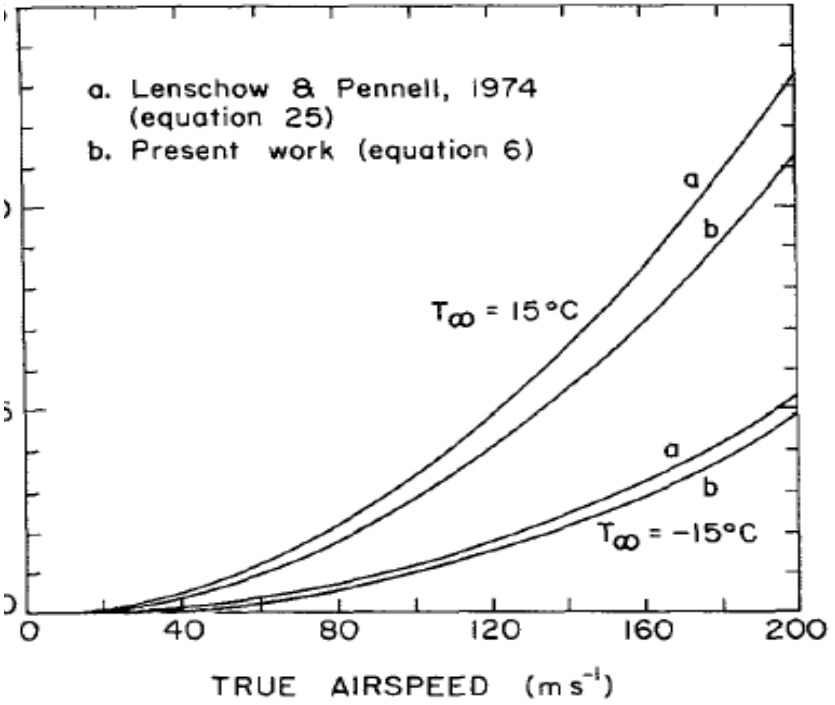


FIG. 1. Temperature error ($T_{wb} - T_r$) for a wetted sensor with $r = 1$ as a function of true airspeed at −15 and +15°C, using (25) from Lenschow and Pennell (1974) and (6) from the present work.

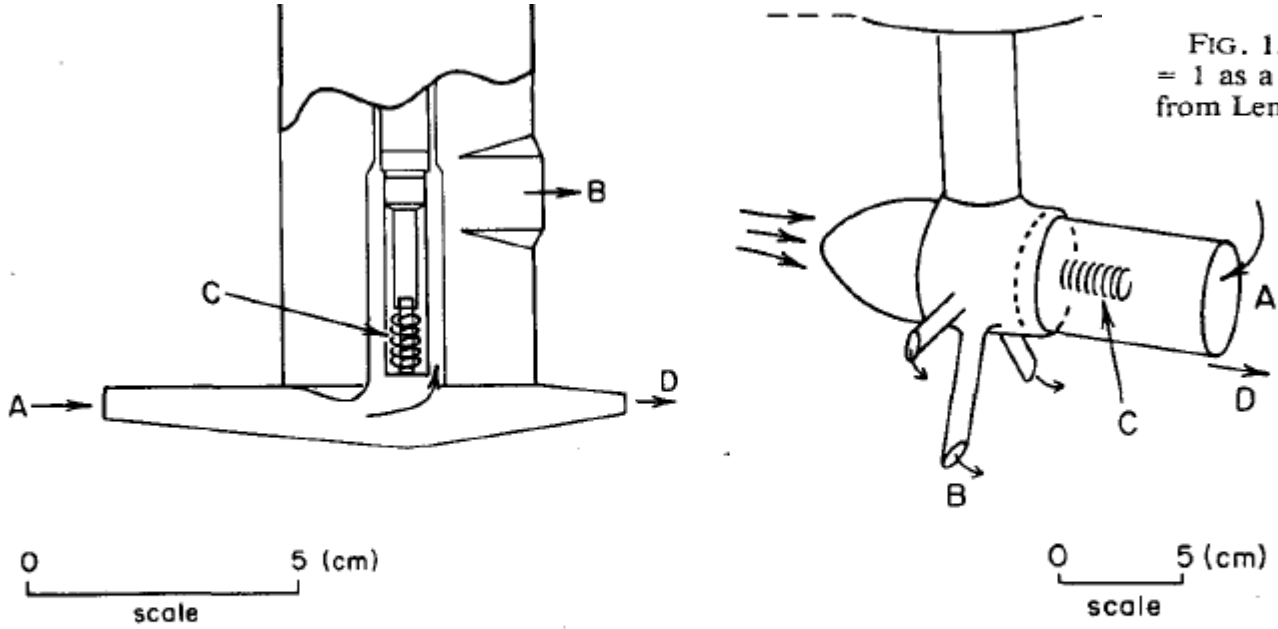


FIG. 3. Principal components of two immersion thermometers used in this study, the Rosemount total temperature probe (left) and the NCAR reverse-flow probe (right). Air enters through port (A) and is exhausted through ports (B) after coming in thermal contact with platinum wire sensor (C). The probes are designed to separate cloud hydrometeors (D) from the airstream reaching the sensing element.

Rosemount housing
vs. reverse flow housing

TABLE 1. Basic cloud properties and cloud exit EC parameters for all cumuli used in this study, in three campaigns. Cumulus depths were estimated from the zenith antenna of the WCR and the lifting condensation level. The quality of fit is discussed in the text.

| | HiCu-03 | RICO-04 | CuPIDO-06 |
|---|---|---|---|
| Environment | Continental | Maritime | Continental |
| Number of clean cloud exit samples ($T > -12.3$°C) | 77 | 153 | 76 |
| Number of clean cloud entrance samples ($T > -12.3$°C) | 291 | 188 | 162 |
| Mean in-cloud temperature before EC correction (°C) | −9.0 | +15.5 | +0.6 |
| Approx range of cumulus depths (km) | 1.0–3.8 | 0.8–2.7 | 0.7–10 |
| Mean cloud droplet number concentration ($cm^{-3}$) | 446 | 56 | 216 |
| Mean droplet diameter ($\mu$m) | 8.6 | 19.2 | 16.3 |
| Mean cloud liquid water content ($g\ m^{-3}$) | 0.35 | 0.43 | 0.83 |
| Quality of cloud exit EC bias fit (K) | 0.088 | 0.094 | 0.101 |
| Mean cloud exit EC amplitude $\Delta T_o$ (K) | −0.77 | −1.07 | −1.75 |
| Mean cloud exit EC time constant $\tau_d$ (s) | 2.20 | 2.33 | 1.88 |
| Standard error of the regression estimate of $\Delta T_o$ (K) | 0.70 | 0.76 | 0.80 |

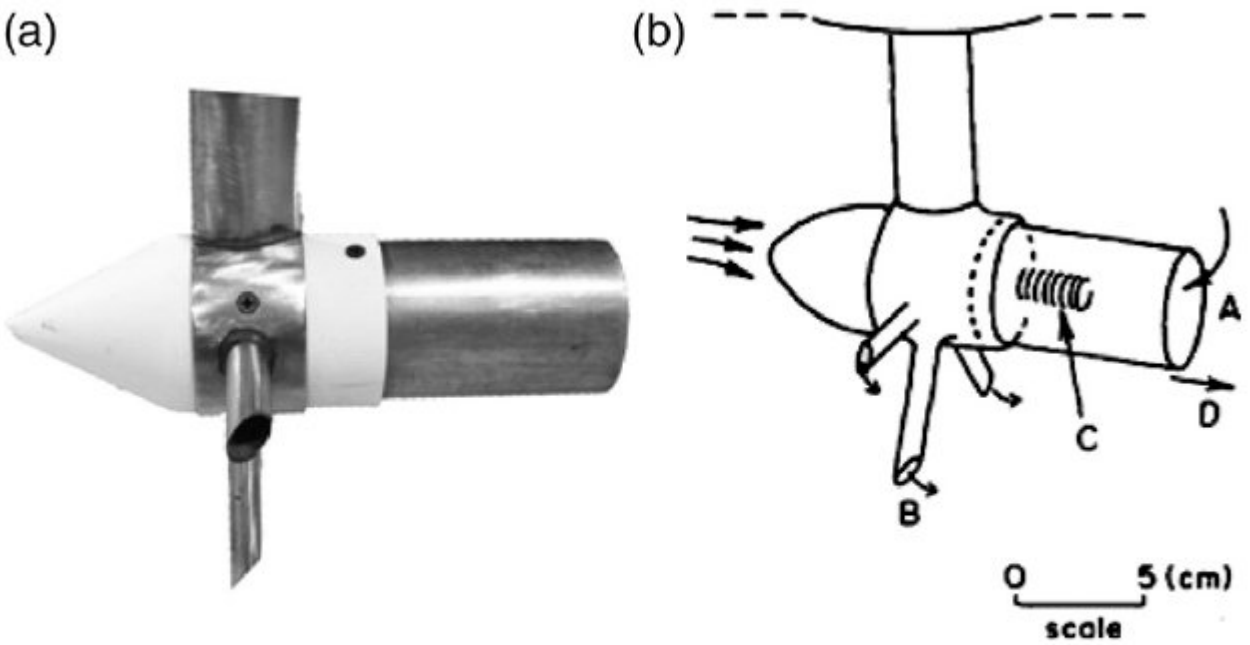


FIG. 2. Photo and schematic of the reverse-flow thermometer. Air enters through port (A) and exits through any of several ports (B). Inside the housing, the air flows past a platinum wire sensor (C) wound in a spiral, 25 $\mu$m in diameter. The reverse-flow design is intended to separate hydrometeors (D) from the airstream that enters the probe. The schematic on the right is from LC90.

Wang and Gerets, 2009

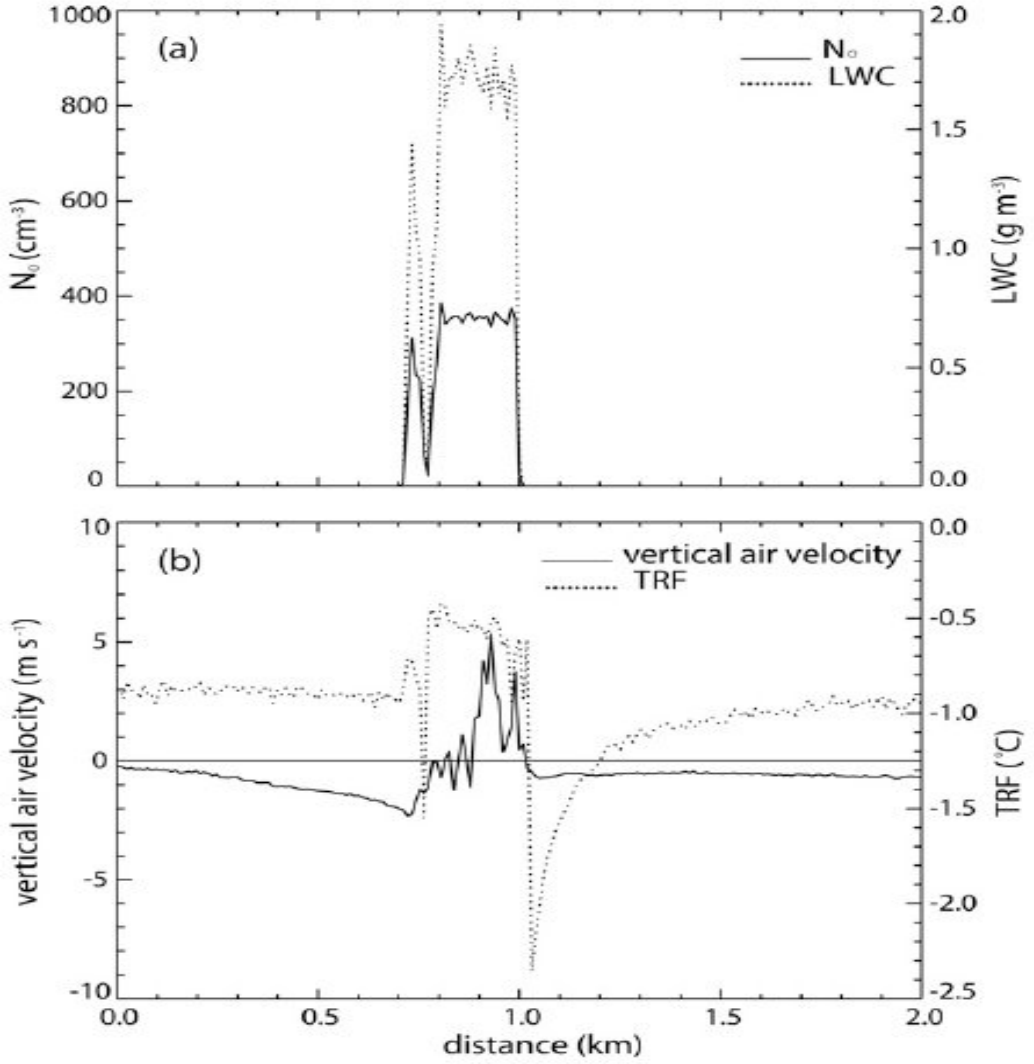


FIG. 1. WKA measurements of a cumulus penetrated during CuPIDO-06 at 1707 UTC 24 Jul 2006. (a) FSSP cloud droplet number concentration ($N_o$) and LWC; (b) vertical air velocity and TRF. The flight direction in this figure and all other transects shown in this paper is from left to right.

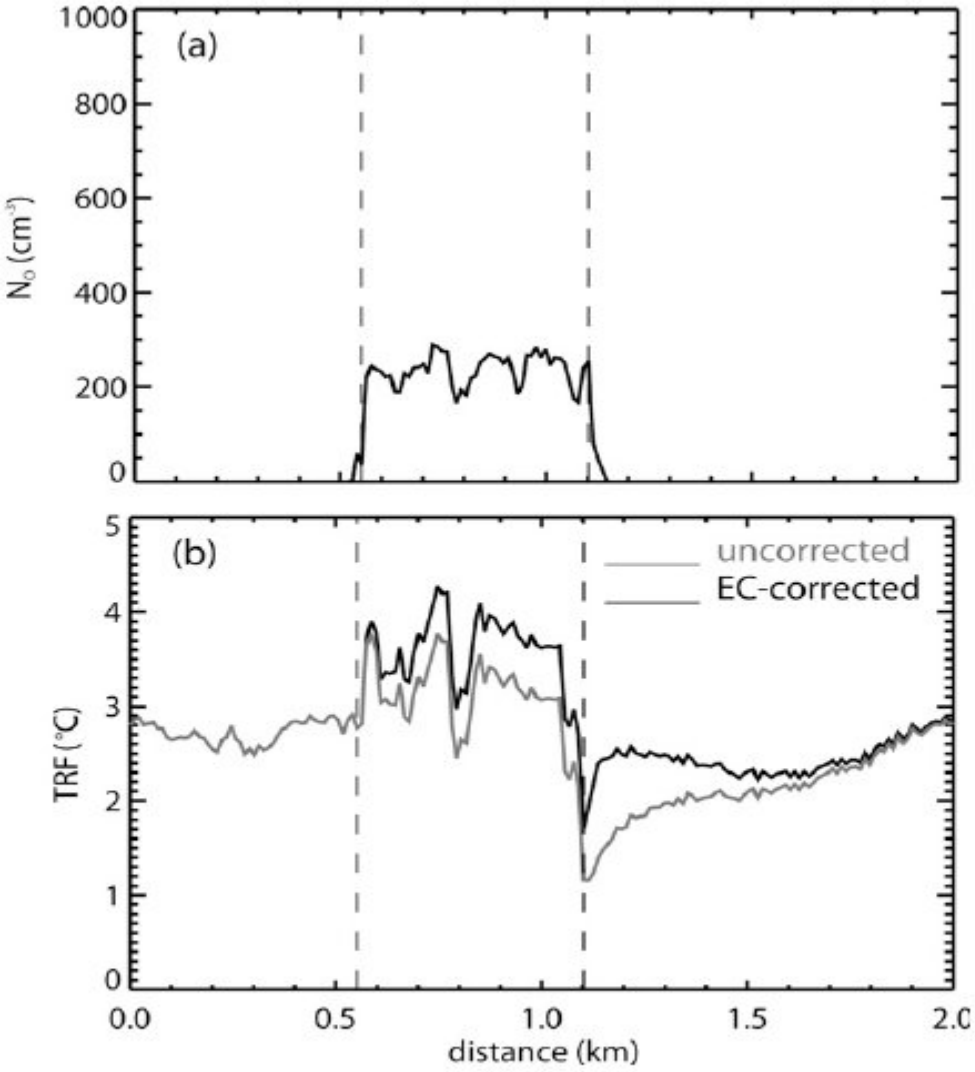


FIG. 13. Illustration of the in-cloud and cloud exit EC bias corrections for an isolated cumulus in CuPIDO-06 at 1637:02 UTC 17 Aug 2006: (top) $N_o$ and (bottom) TRF.

Wang and Gerets, 2009 >>...there is strong evidence that some wetting does occur and therefore also sensor evaporative cooling as the aircraft exits a cloud.... This cloud exit “cold spike” can be found in all cumulus clouds, even at subfreezing temperatures, both in continental and maritime cumuli.....Evaporation from the wetted sensor in cloud is surmised because air decelerates into the thermometer housing, and thus is heated and becomes subsaturated. <<

# Fast Temperature and True Airspeed Measurements with the Airborne Ultrasonic Anemometer–Thermometer (AUSAT)

D. CRUETTE, A. MARILLIER, J. L. DUFRESNE, AND J. Y. GRANDPEIX
*Laboratoire de Météorologie Dynamique, CNRS, Université Pierre et Marie Curie, Paris, France*

P. NACASS AND H. BELLEC
*Météo France, CNRM, Centre d'Aviation Météorologique, Bretigny-sur-Orge, France*

(Manuscript received 8 December 1998, in final form 14 October 1999)

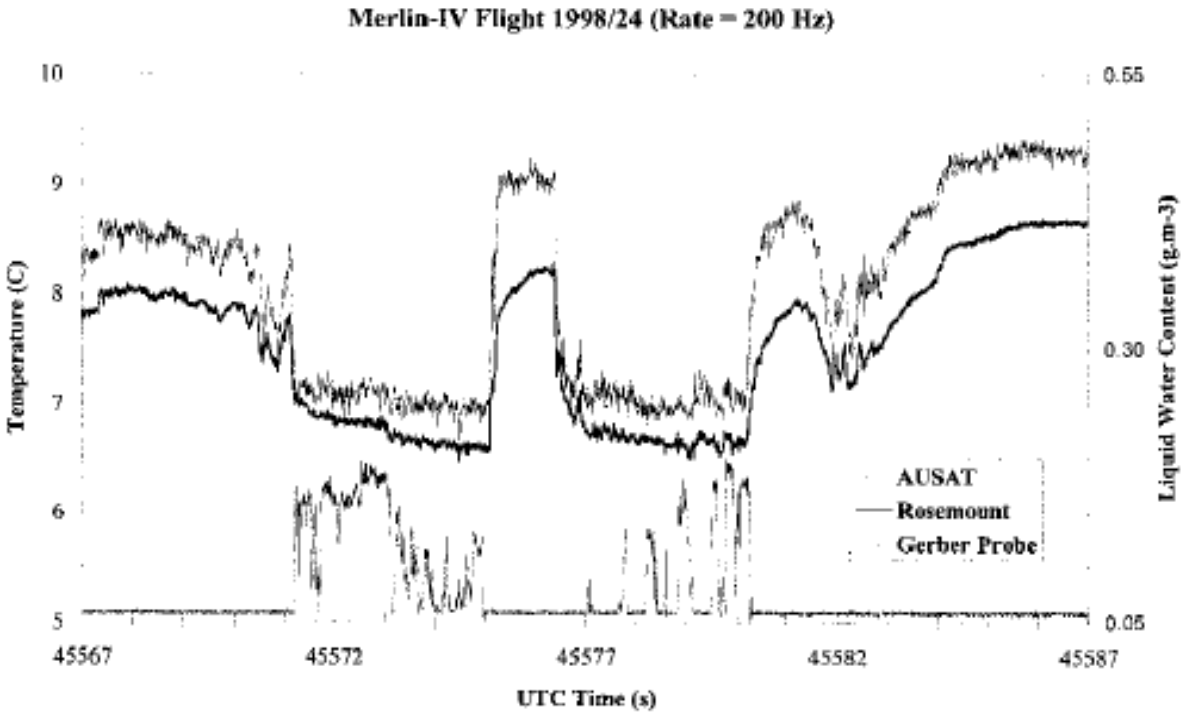


FIG. 9. High rate (200 Hz) time series (20 s) of AUSAT and Rosemount temperatures with the PMV 100 Gerber probe liquid water content.

FIG. 2. Photograph of the AUSAT mounted under the fuselage of the Merlin IV after 1997.

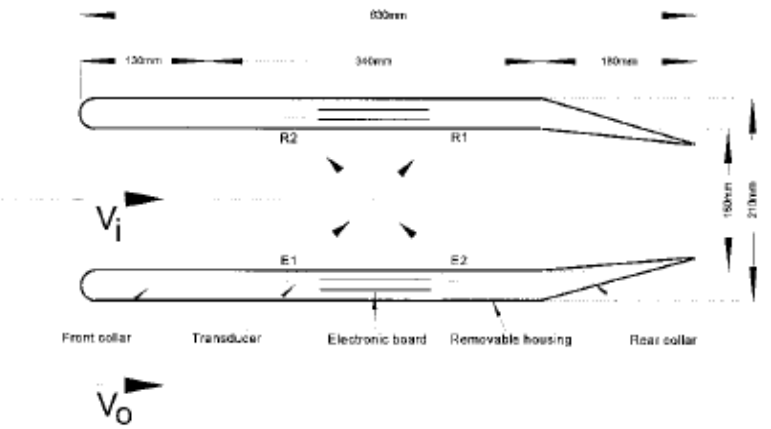


FIG. 3. Cross section of the axisymmetric body of the AUSAT with the front and rear collars, the emitters E1 and E2, the receivers R1 and R2, and the main dimensions.

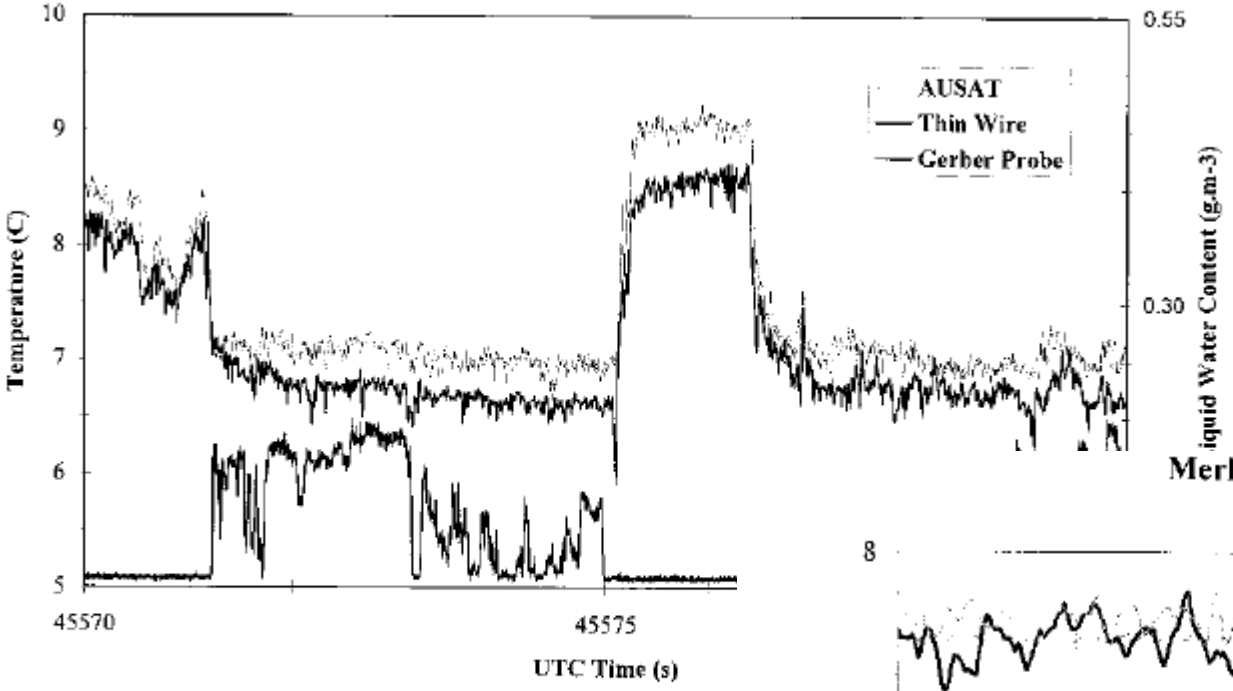


FIG. 11. Expanded portion on 10 s c
AUSAT and Rosemount temperatures v
probe liquid water content. (Same flight a

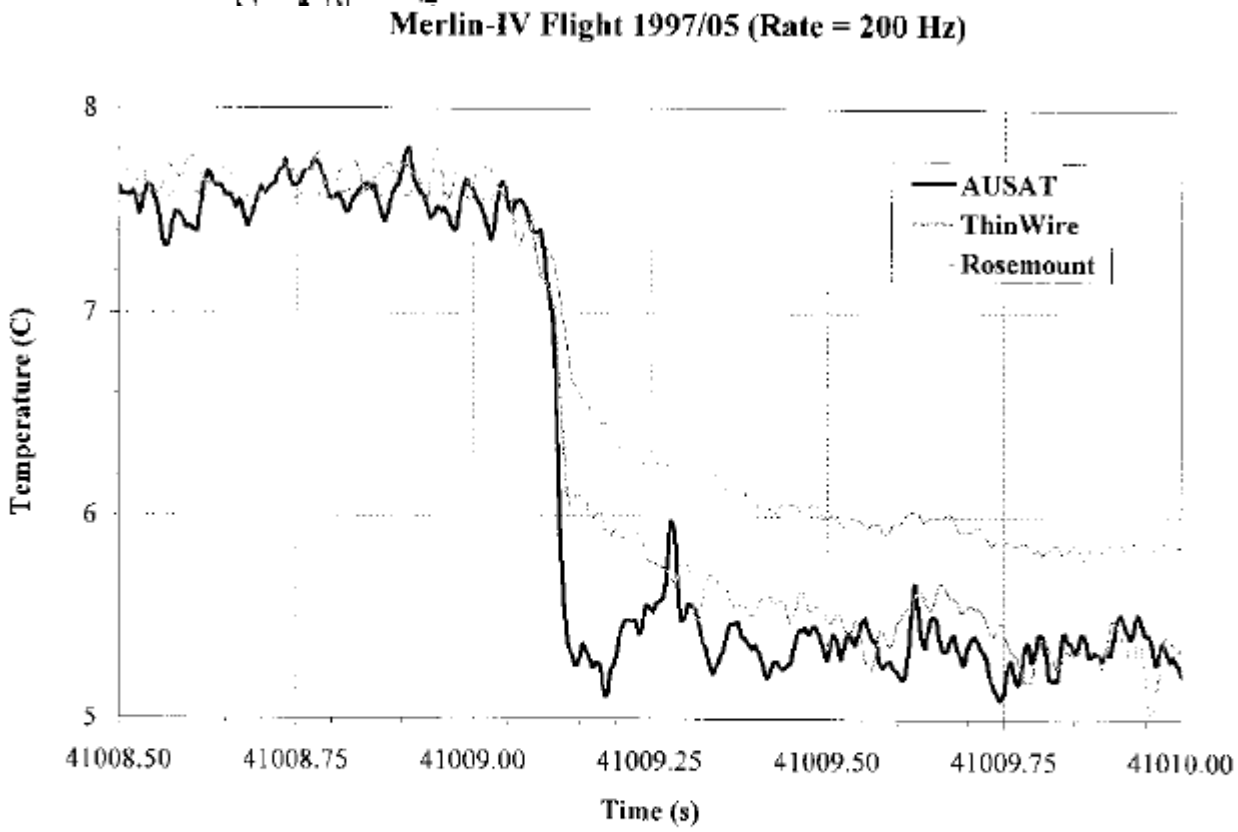


FIG. 12. Expansion, after adjustment, of 1.5 s of high rate time series of AUSAT, thin wire, and Rosemount temperatures through a sharp cloud exit. (Same flight and same rate as in Fig. 9.)

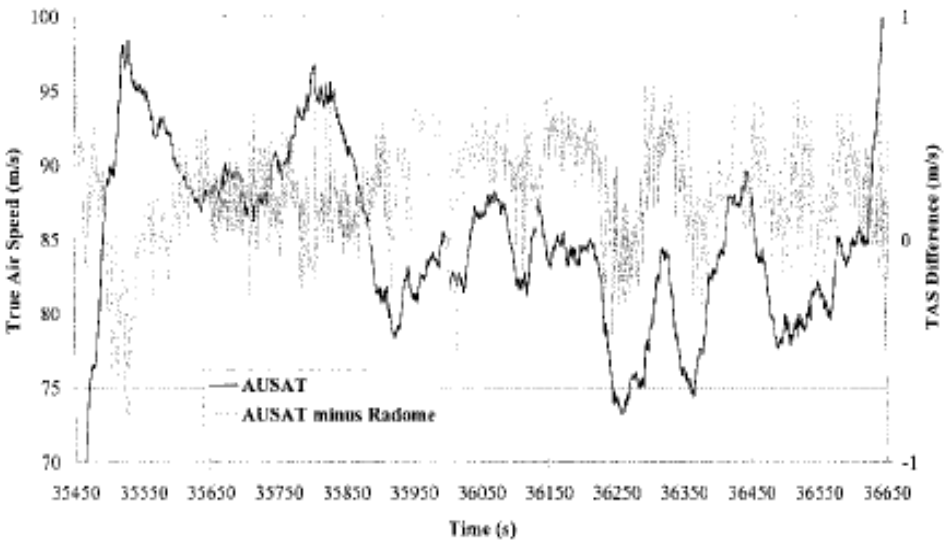


FIG. 18. Time series of the true airspeed of the aircraft measured by the AUSAT and of the difference between the true airspeed of AUSAT minus that of radome. (Same flight and same rate as in Fig. 17.)

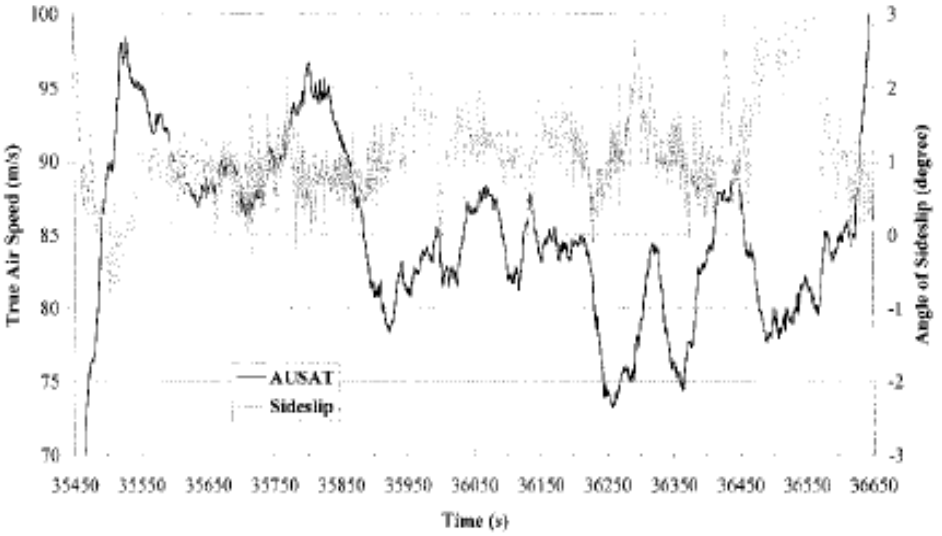


FIG. 20. Time series of the true airspeed of the aircraft measured by the AUSAT and of the angle of sideslip measured by the radome differential pressure probe. (Same flight and same rate as in Fig. 17.)

IGH UF SZD-45 „Ogar”, 1986

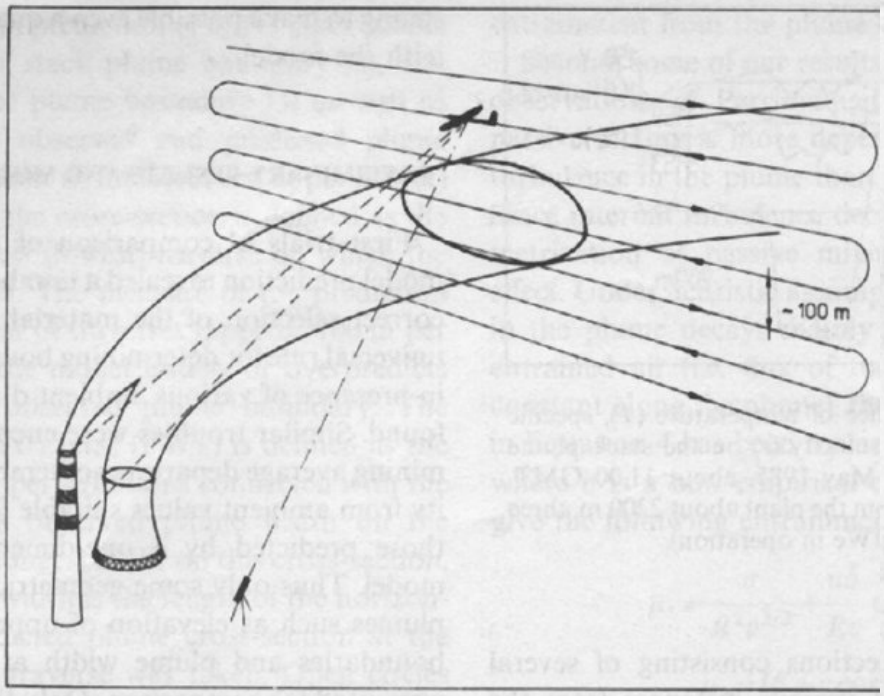


Fig. 1. Typical flight pattern in Bełchatów experiment.

Measurements in cooling tower plumes

Haman and Malinowski 1989

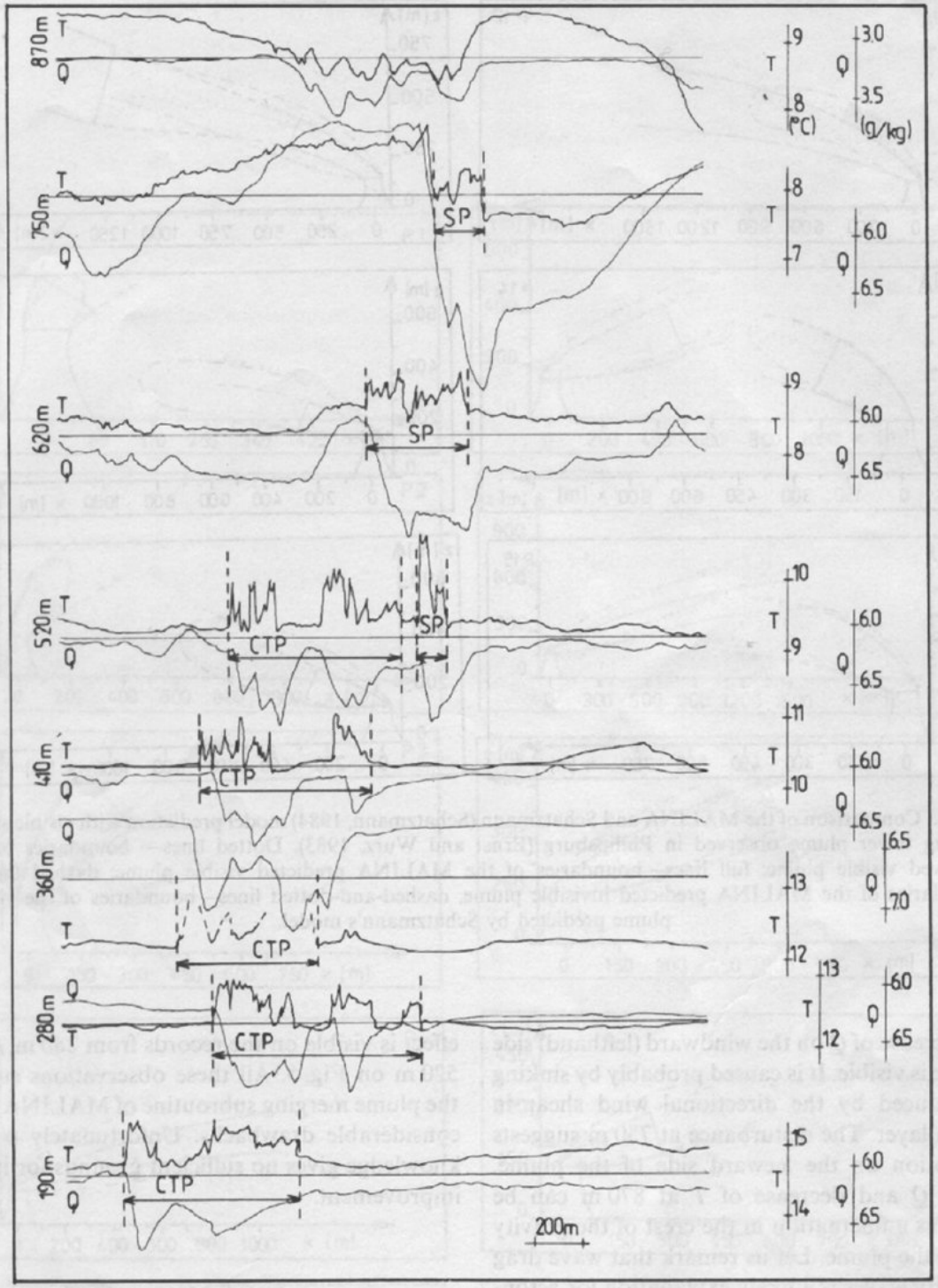


Fig. 5. Cross-section of the cooling towers and stack plumes (one stack, three cooling towers, six units in operation), taken on 27 September 1985, 13.45–14.30 GMT about 1100 m from the plant (flight 28/85). The horizontal position of the plume on this figure is arbitrary.

# A New Ultrafast Thermometer for Airborne Measurements in Clouds

KRZYSZTOF E. HAMAN, ANDRZEJ MAKULSKI, AND SZYMON P. MALINOWSKI

*Warsaw University, Warsaw, Poland*

REINHOLD BUSEN

*DLR Oberpfaffenhofen, Wessling, Germany*

(Manuscript received 21 August 1995, in final form 10 July 1996)

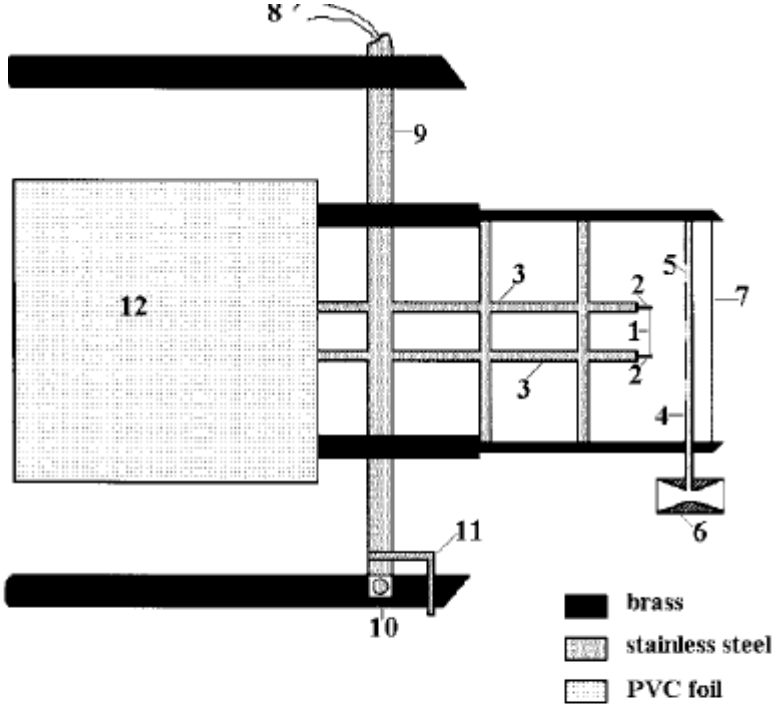


FIG. 1. Schematic view of the UFT sensor: (1) sensing element (tungsten wire, diameter 2.5 $\mu$m, length 5 mm); (2) Teflon-insulated copper supports; (3) stainless-steel tubes; (4) protecting rod made of stainless steel; (5) holes for water removal from the rod; (6) Venturi nozzle for water removal; (7) protective nylon thread; (8) copper connectors; (9) shaft; (10) ball-point bearing; (11) shaft stops; (12) vane.

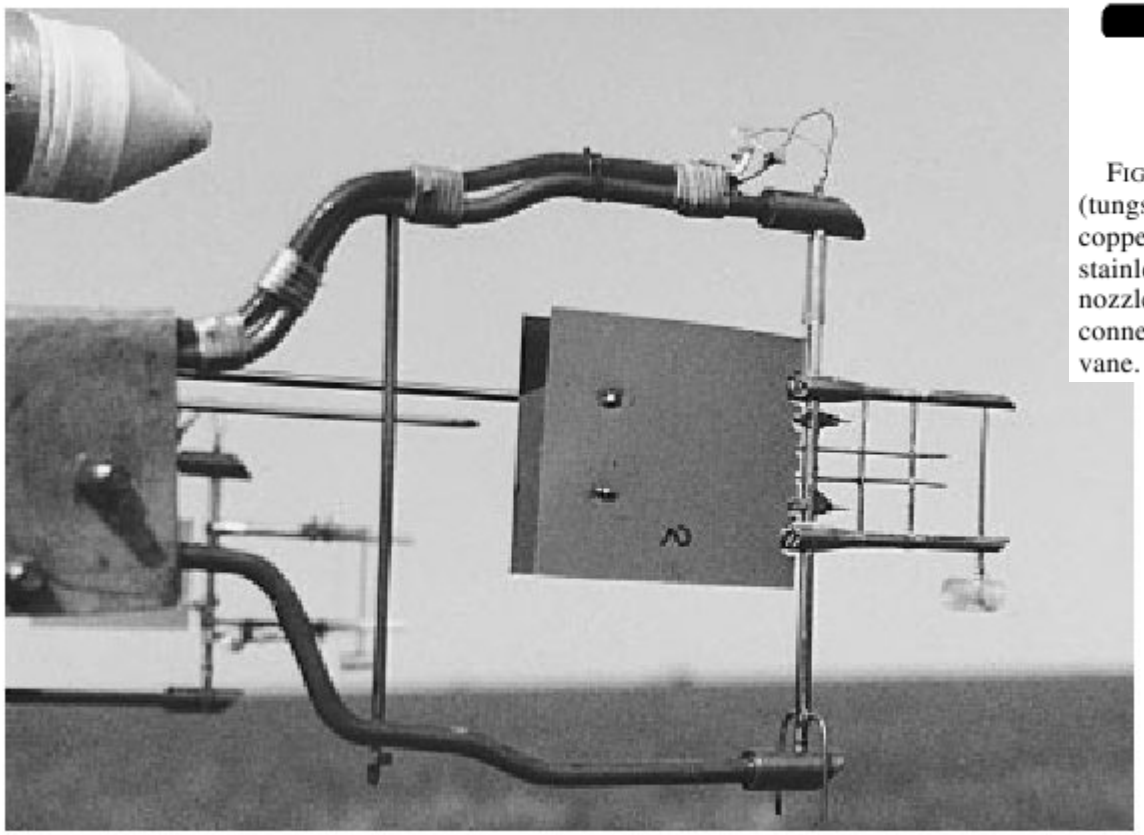

FIG. 7. UFT sensor mounted on the nose boom of the SZD-45 OGAR motorglider. The 5-mm length of the sensing wire may serve as a scale.

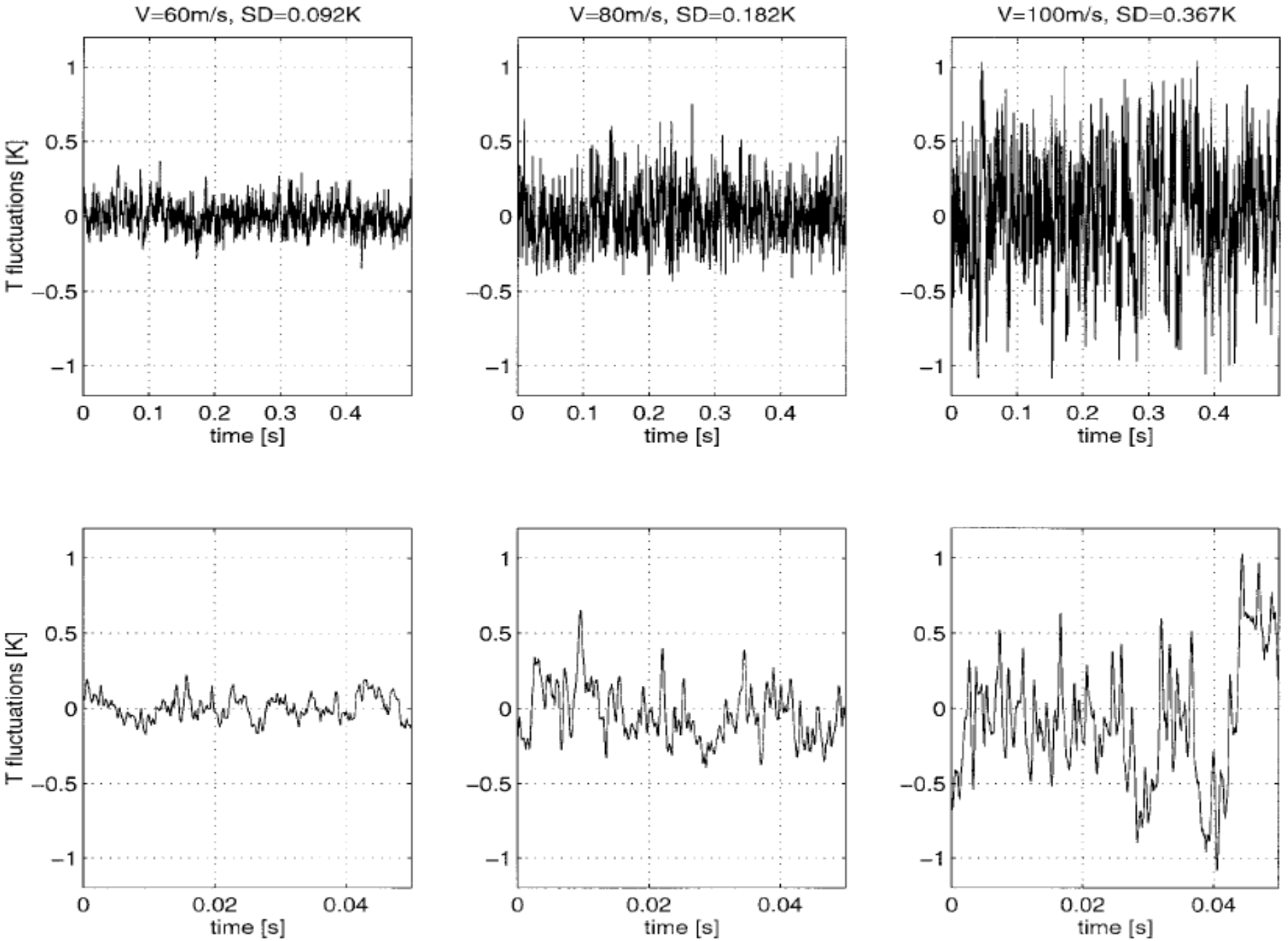


FIG. 3. The examples of temperature fluctuations at various airspeeds in horizontal flight in clear air recorded on the Do-228 aircraft. Records are made with 10-kHz sampling frequency, after conditioning with a 5-kHz low-pass filter and presented in two time resolutions (upper and lower plots). Speed and standard deviation of temperature fluctuations are given in plot titles.

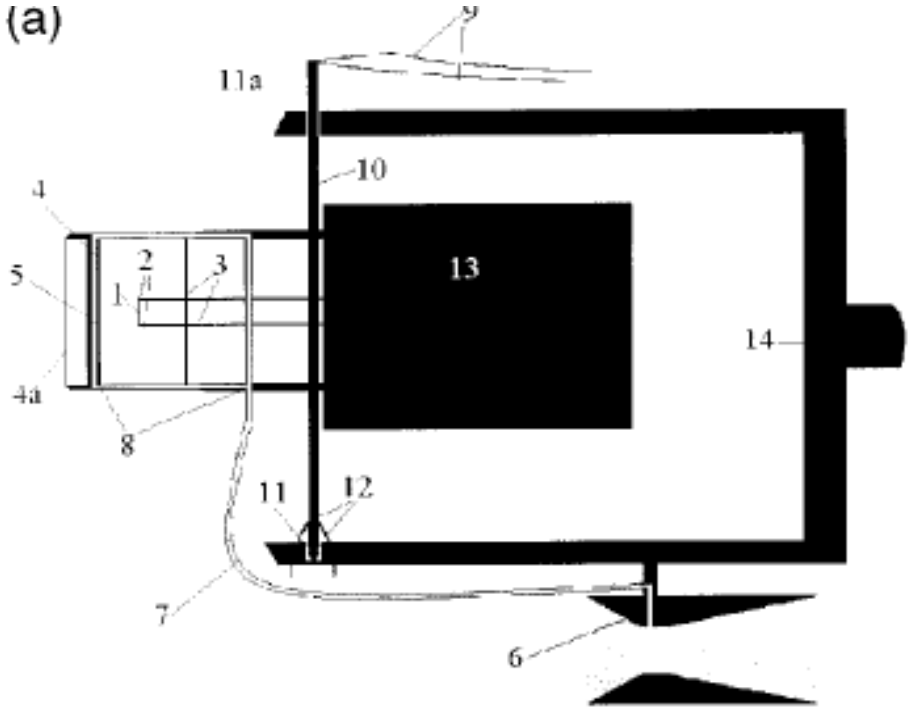


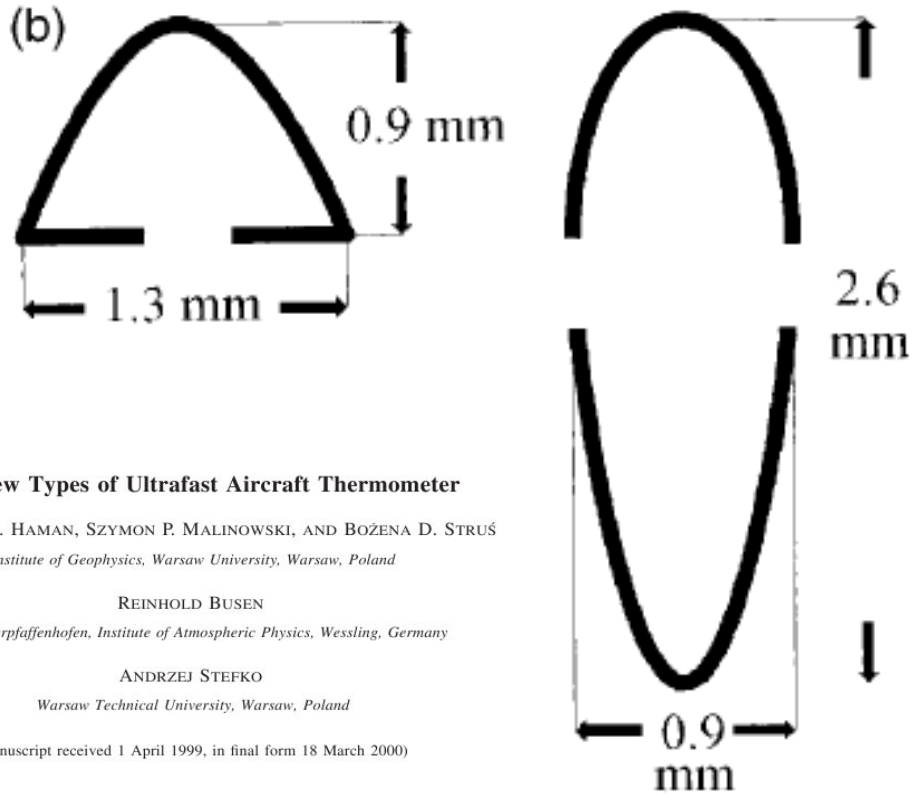


**Two New Types of Ultrafast Aircraft Thermometer**

KRZYSZTOF E. HAMAN, SZYMON P. MALINOWSKI, AND BOŻENA D. STRUŚ
*Institute of Geophysics, Warsaw University, Warsaw, Poland*

REINHOLD BUSEN
*DLR Oberpfaffenhofen, Institute of Atmospheric Physics, Wessling, Germany*

ANDRZEJ STEFKO
*Warsaw Technical University, Warsaw, Poland*

(Manuscript received 1 April 1999, in final form 18 March 2000)

FIG. 1. (a) Schematic view of the UFT-F sensor:
(1) sensing element (platinum-coated tungsten wire, ø 2.5 , length 5 mm);
(2) Teflon-insulated copper supports;
(3) stainless-steel tubes;
(4) airfoil-shaped protecting anti-droplet rod made of stainless steel;
(4a) additional protection in form of 0.25-mm nylon string (in newer versions of the instrument);
(5) slots for suppressing wake eddies and water removal from the rod;
(6) Venturi nozzle for creating suction;
(7) elastic tube connecting the sensor frame with the Venturi nozzle pneumatic ducts in gray;
(8) sensor frame;
(9) insulated copper connectors;
(10) shaft;
(11) ball-point bearing;
(11a) sleeve bearing;
(12) shaft bumpers;
(13) vane,
(14) supporting fork.

(b) ( Cross section of an antidroplet protective rod of UFT-F [part (4) in (a)] compared with (left) that of UFT-S.

**Theoretical and Experimental Characterization of the Ultrafast Aircraft Thermometer: Reduction of Aerodynamic Disturbances and Signal Processing**

BOGDAN ROSA, KONRAD BAJER, KRZYSZTOF E. HAMAN, AND TOMASZ SZOPLIK

*Institute of Geophysics, Warsaw University, Warsaw, Poland*

(Manuscript received 22 June 2004, in final form 1 December 2004)

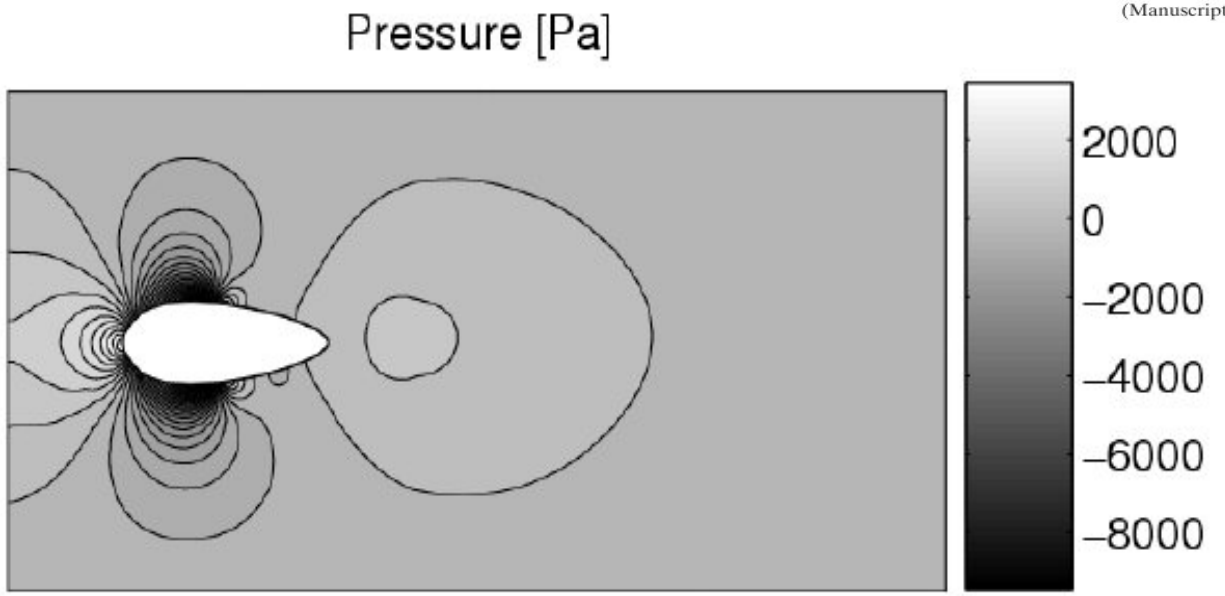


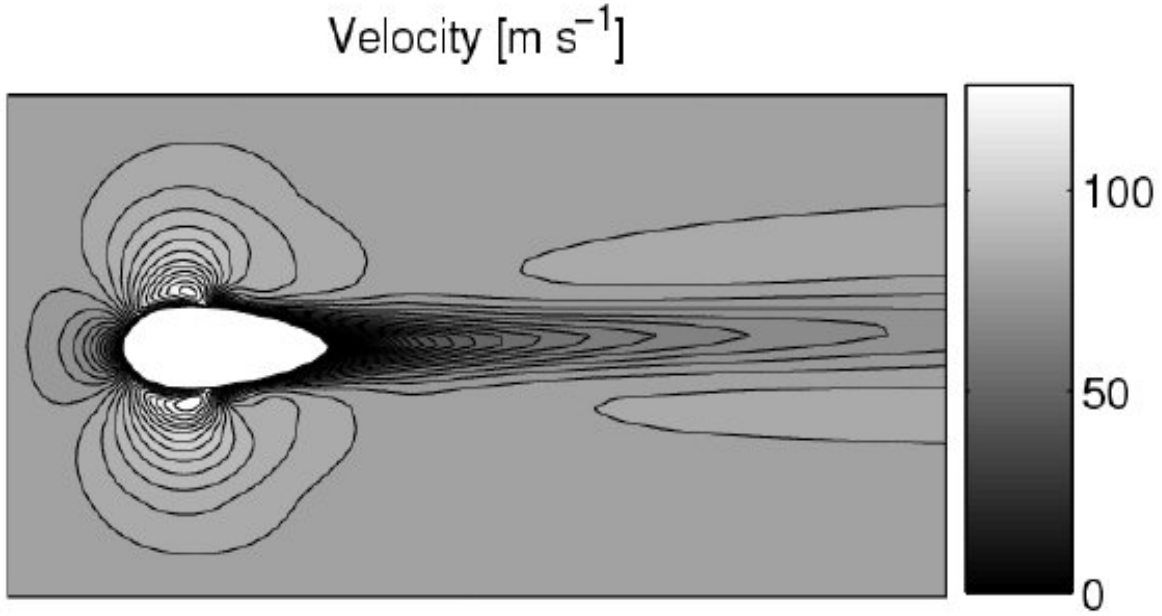


The pressure distribution and the velocity field at t = 0.34 [ms] with suction turned on.

Such a steady states is established after about 0.34 [ms] and then does not change.

Zero value on the pressure scale corresponds to the atmospheric pressure.

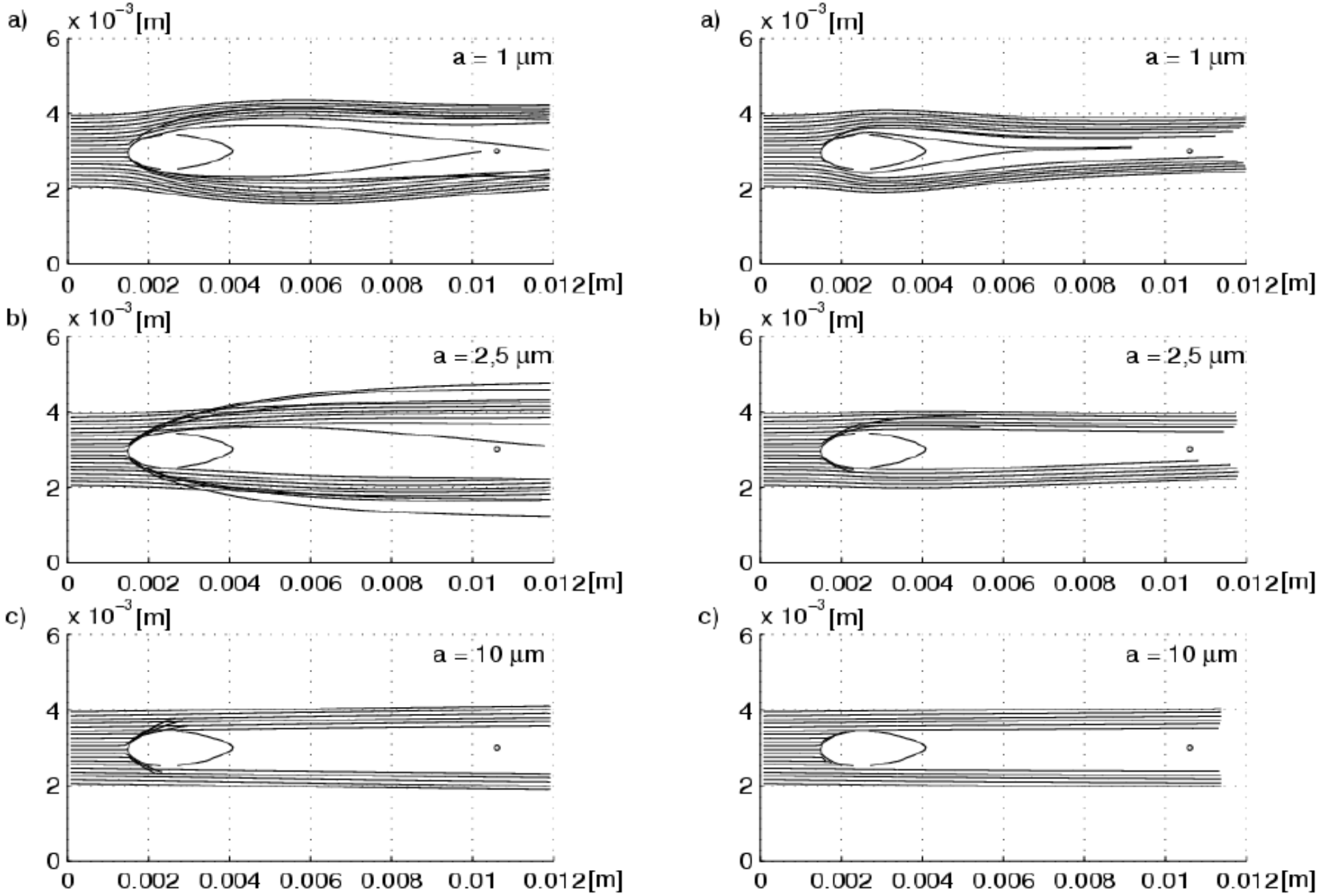


Droplet paths, computed in the Stokes approximation, in the flow with suction off (left column) and with suction on (right column). The droplets start at the inlet with zero relative velocity. The radii of the droplets are: (a) 1 μm, (b) 2,5 μm and (c) 10 μm and diameter of the wire sensor is 2.5 μm. The dot on the right represents position of the tungsten wire sensor.

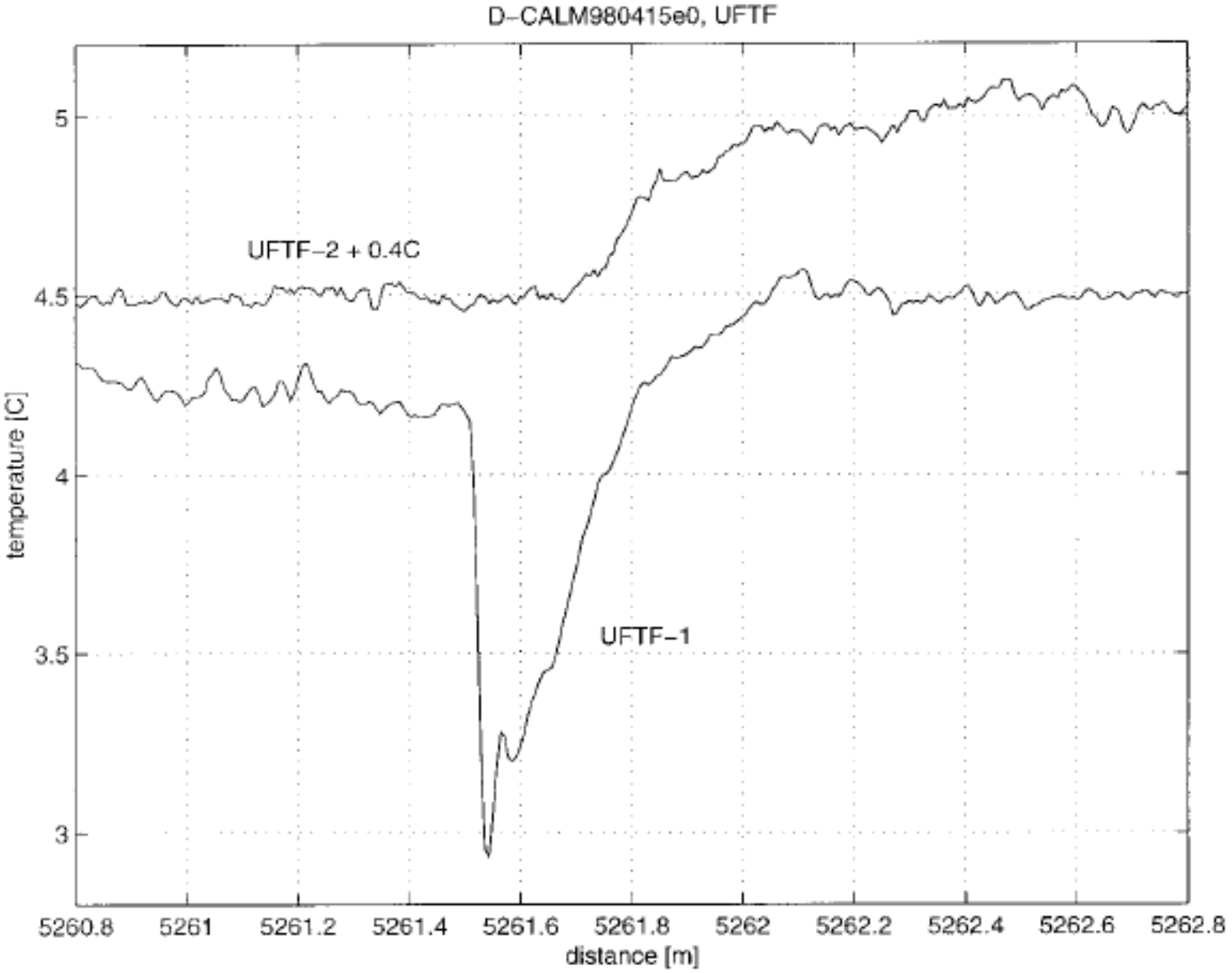


FIG. 4. Fragment of a temperature record taken with two UFT-F sensors in flight through Cu med cloud at an airspeed of 70 m $s^{-1}$. A drop of temperature lasting about 5 ms recorded with UFT-F1 might result from a wet-bulb effect on the sensing wire wetted while passing the cloud. Distance on the horizontal scale is measured from the beginning of recording.

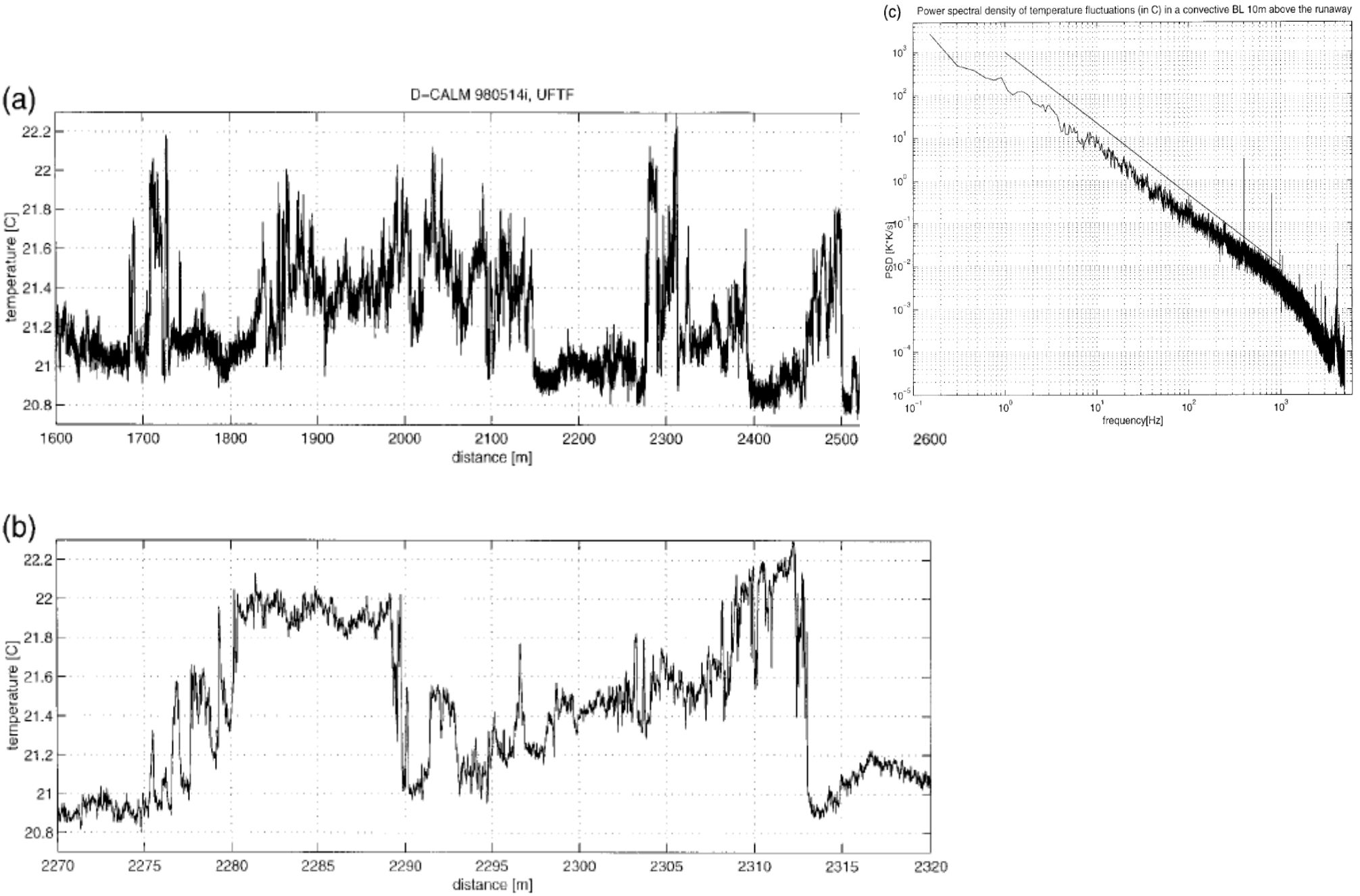


FIG. 10. Temperature fluctuations recorded with the UFT-F sensor on a 2-km pass 10 m above the airfield runway in convective weather. (a) 1-km fragment of the record. (b) Expanded segment of (a). (c) Power spectrum of the record; −5/3 slope plotted as a reference. Note the spikes at 400 Hz (frequencies of the aircraft AC network). For frequencies above 1500 Hz, influence of the signal low-pass filter is visible. The cleaner appearance than in Fig. 8 results from averaging over a longer time interval and from the fact that the record was taken shortly before landing, when some electrically noisy equipment had already been switched off.

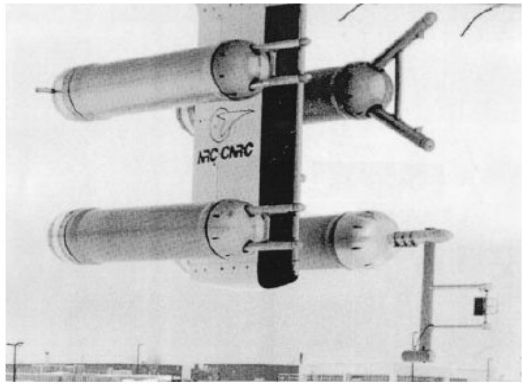

FIG. 12. UFT-D mounted in the lower-left-hand PMS container on the Convair 580 of the Canadian AES.

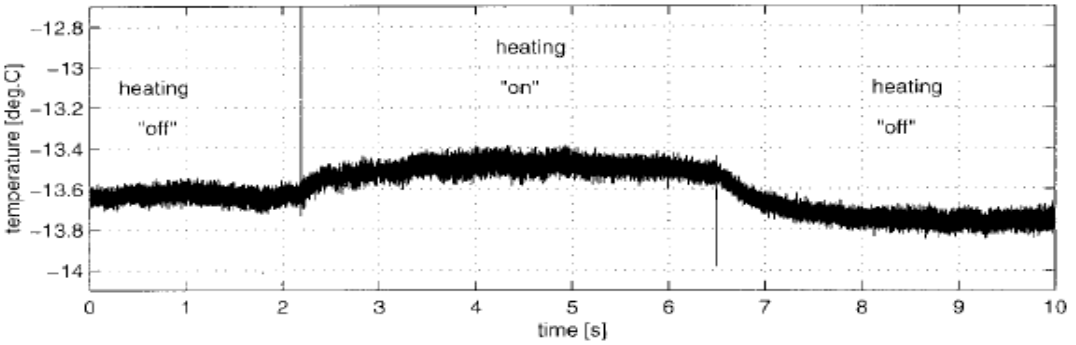


FIG. 14. Fragment of temperature record made with UFT-D outside the cloud, with heating switched off, on, and off. Pressure is 576 hPa, and airspeed is 110 m $s^{-1}$. Slight asymmetry of the record follows from variation of temperature along the flight path.

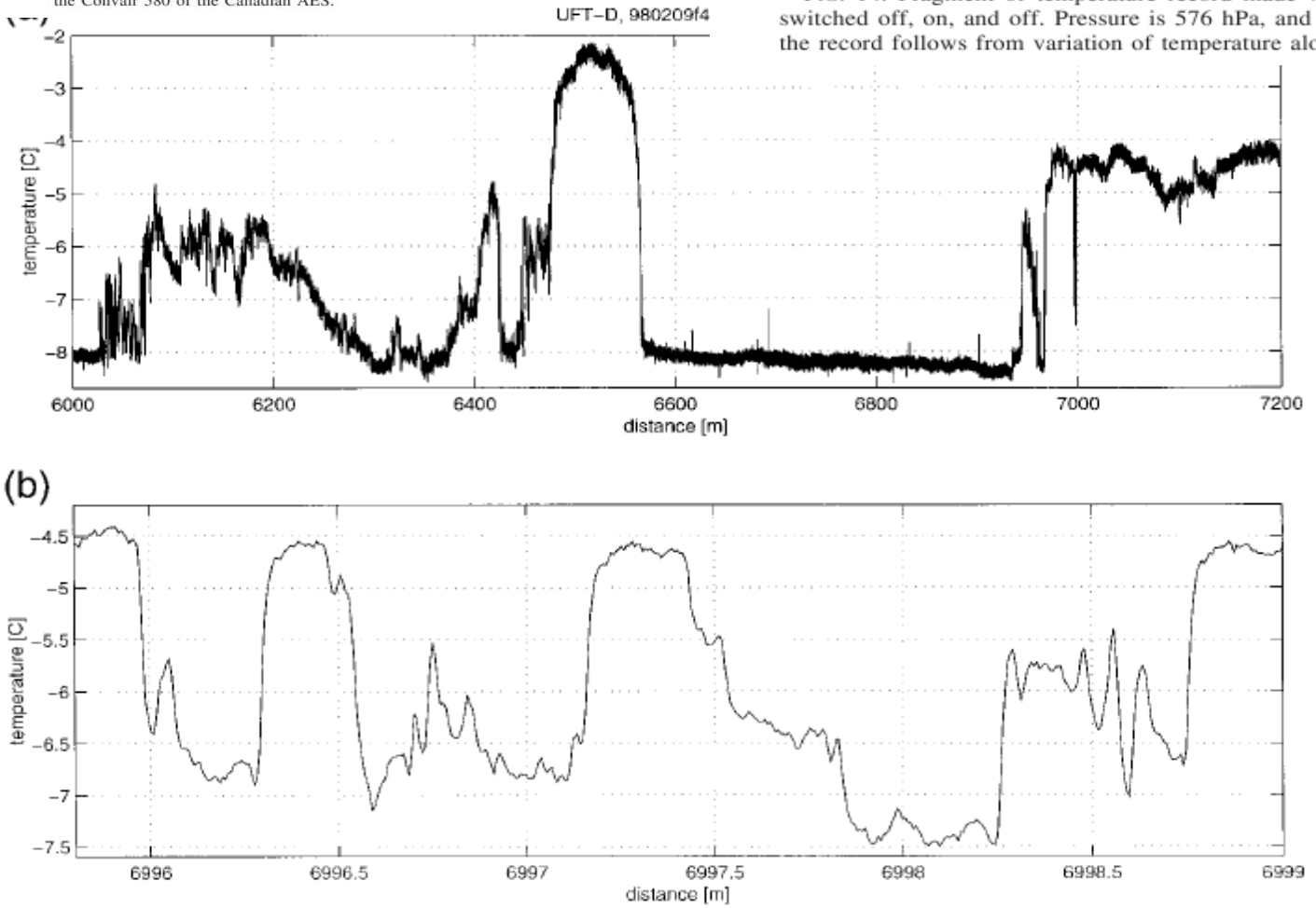


FIG. 13. Fragment of a UFT-D record taken during the CFDE3, with 10-kHz sampling rate, showing rapid variations of temperature over a few centimeters in distance. Airspeed is 70 m $s^{-1}$, and distance is measured from the beginning of the record. The temperature scale is according to the reference Rosemount thermometer. (a) General view. (b) Selected fragment of (a), with expanded distance scale.


UFT-F
PVM
FFSSP

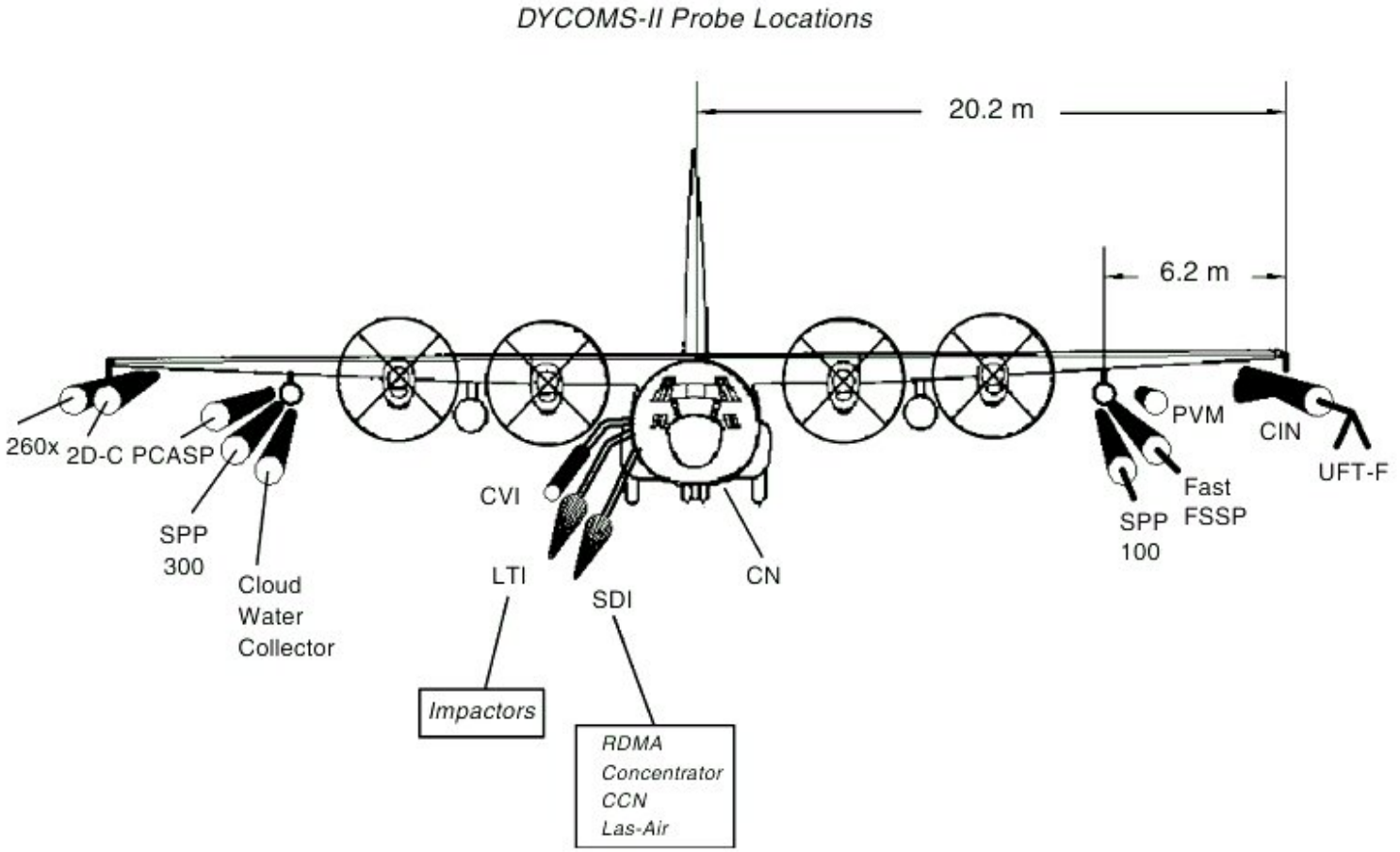


Figure 1. Location of the UFT-F, PVM-100A, and FFSSP sensors on the NCAR C-130 Hercules aircraft during the DYCOMS-II campaign. (Courtesy David C. Rogers).

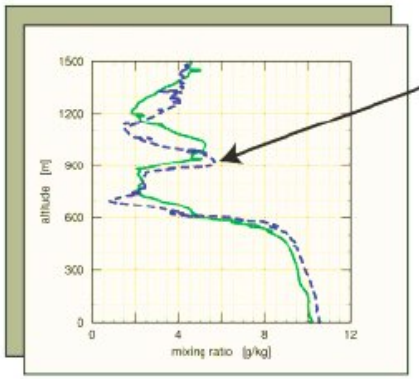


RF08 Composite dropsonde humidity soundings illustrating approximately 120 m descent of an elevated moist layer during the 6.5 hours spent on target.

*Nocturnal Flights greatly simplified dynamics and forcing of the layer.*

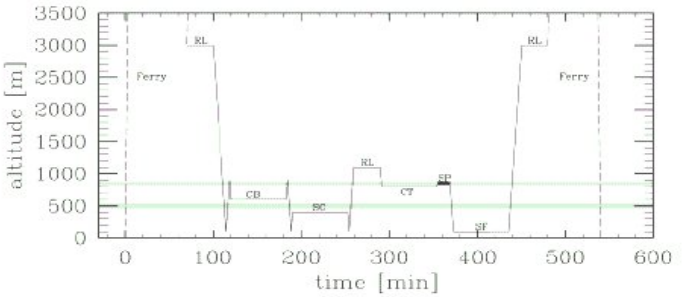


**FIG. S2. Time–height cross section for basic entrainment flight plan. Approximately 410 min are spent in the target area. Shaded bars denote cloud top and base.**

*Remote sensing legs: Three 30 min circles at the beginning, middle and end of time on target. These provided a basis for surveying cloud structure using lidar and cloud radar; 3-5 GPS dropsondes were launched on first and third circles.*

*30 minute cloud top profiling circle to estimate cloud top jumps.*

*4-6 PBL soundings interspersed during time on target, profile data indicated by lines on figure below.*

*30 minute circles flown in alternating directions are used to estimate divergence and vorticity. Flights timed so surface leg is last flux leg, just around sunrise, so as to allow operation of aircraft nearer surface. Data from these legs indicated by red dots on figure below.*

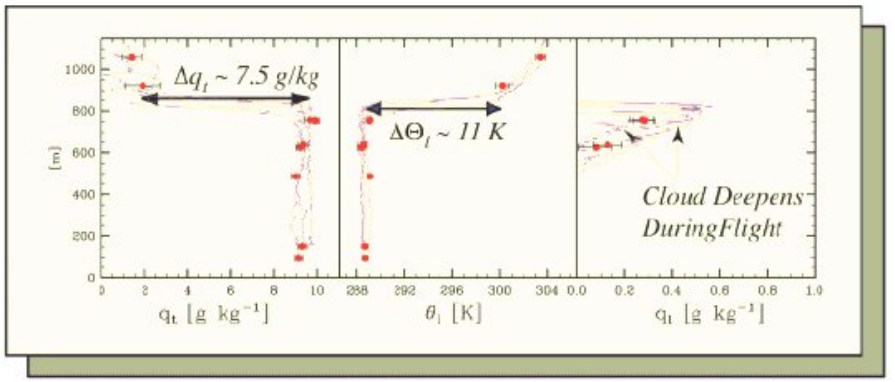


Eight 30 minute circles at four different levels in PBL and profiling allows one to reconstruct profiles and map evolution of the mean state. Shown here are the profiles and leg means from RF01. The level legs will be most useful for estimating flux profiles (and flux divergence) through the depth of the PBL.

Stevens et al., 2003

## DYNAMICS AND CHEMISTRY OF MARINE STRATOCUMULUS—DYCOMS-II

BY BJORN STEVENS, DONALD H. LENSCHOW, GABOR VALI, HERMANN GERBER, A. BANDY, B. BLOMQUIST, J.-L. BRENGUIER, C. S. BRETHERTON, F. BURNET, T. CAMPOS, S. CHAI, I. FALOONA, D. FRIESEN, S. HAIMOV, K. LAURSEN, D. K. LILLY, S. M. LOEHRER, SZYMON P. MALINOWSKI, B. MORLEY, M. D. PETTERS, D. C. ROGERS, L. RUSSELL, V. SAVIC-JOVCIC, J. R. SNIDER, D. STRAUB, MARCIN J. SZUMOWSKI, H. TAKAGI, D. C. THORNTON, M. TSCHUDI, C. TWOHY, M. WETZEL, AND M. C. VAN ZANTEN

**FIG. 2. DYCOMS-II flight strategy. Symbols in bottom panel refer to total water mixing ratio $q_t$; its change across cloud top, $\Delta q_t$; liquid water potential temperature, $\theta_l$; its change across cloud top, $\Delta\theta_l$; and liquid water mixing ratio $q_l$.**

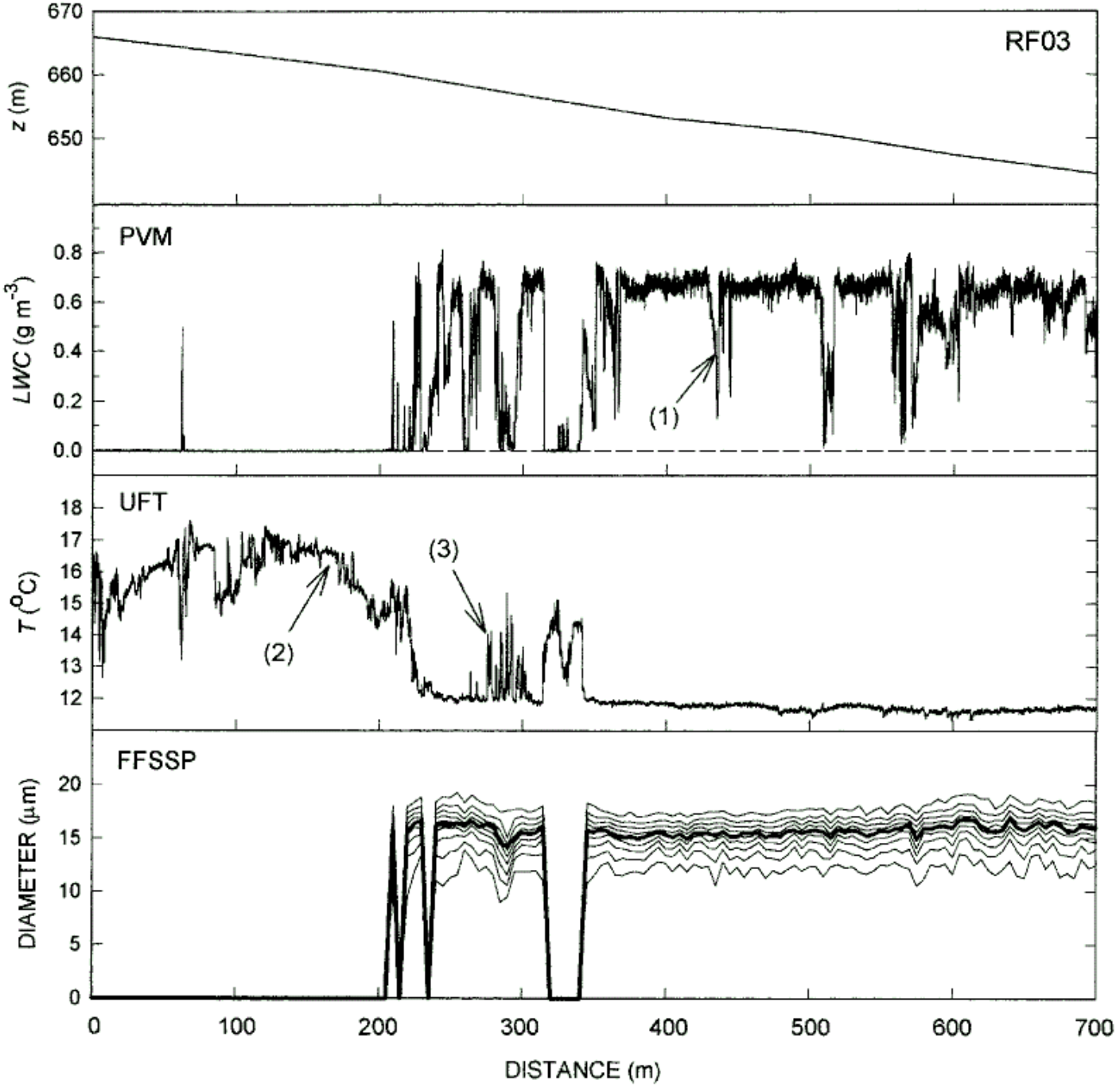


FIG. 16. (top) Gradual descent of the aircraft into cloud top during RF03 showing 1000 Hz (~10 cm spatial resolution) PVM and UFT and 50-Hz FFSSP (~2 m resolution) measurements. The thin lines in the FFSSP data are 10% percentiles of the droplet concentration, and the thick line gives the mass median diameter. One of the holes with depleted LWC′ is indicated by "(1)"; temperatures in the entrainment interface layer by "(2)"; and a region with finescale mixing by "(3)" [from Gerber et al. (2002) with changes].

Gerber et al., 2005

**Holes and Entrainment in Stratocumulus**

H. GERBER AND G. FRICK
*Gerber Scientific Inc., Reston, Virginia*

S. P. MALINOWSKI
*Warsaw University, Warsaw, Poland*

J.-L. BRENGUIER AND F. BURNET
*Météo-France, Toulouse, France*

(Manuscript received 26 November 2003, in final form 31 July 2004)

# Small scale mixing processes at the top of a marine stratocumulus – a case study

Krzysztof E. Haman,[a] Szymon P. Malinowski,[a]* Marcin J. Kurowski,[a] Hermann Gerber[b] and Jean-Louis Brenguier[c]

[a] *Warsaw University, Institute of Geophysics, Poland*
[b] *Gerber Scientific Inc. Reston, VA, USA*
[c] *CNRM, Météo-France, Toulouse, France*

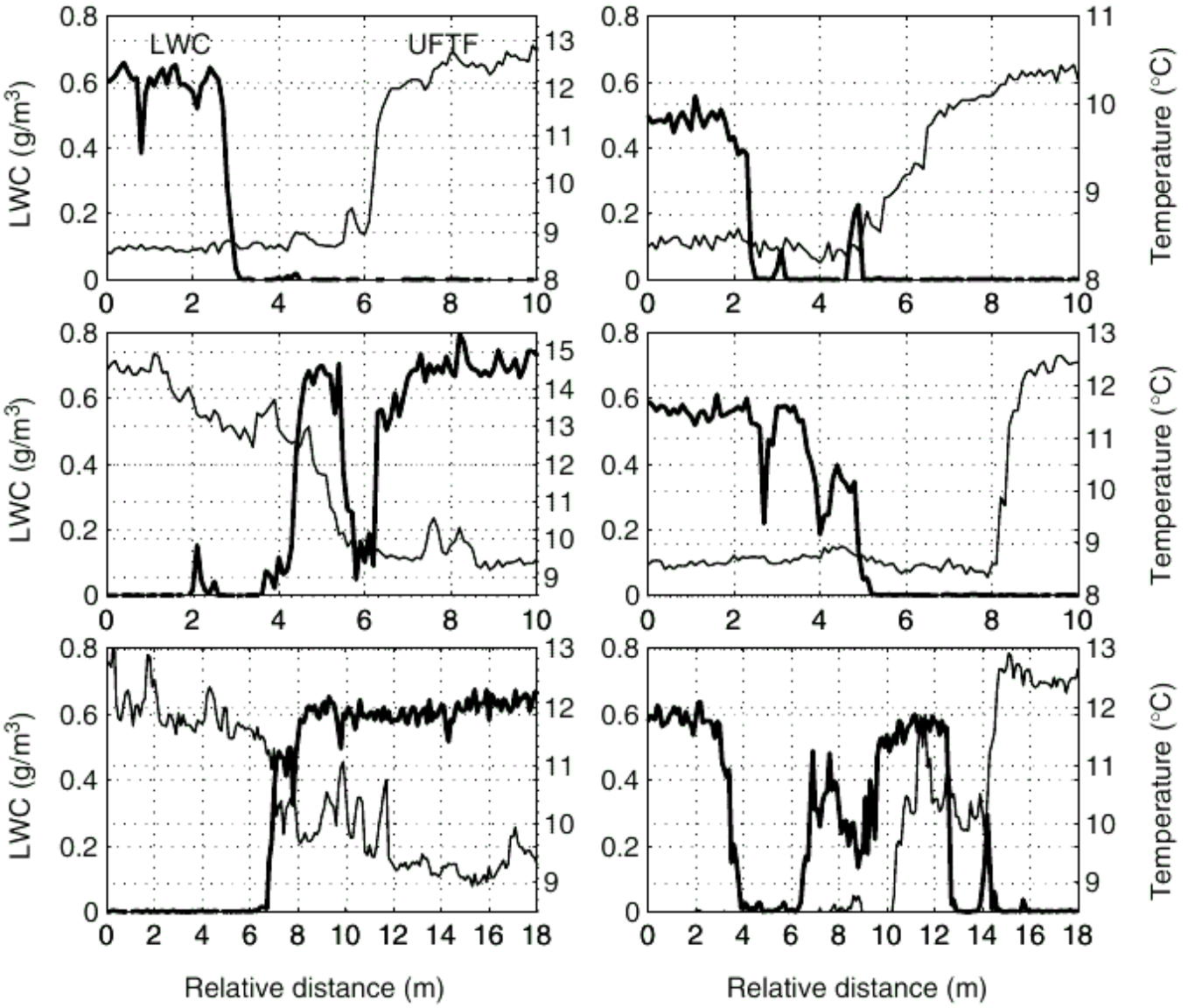


Figure 4. Examples of the cloud edge in 1000 Hz temperature (thin line) and LWC (thick line) records. Sharp jumps in LWC and temperature at distances of the order of 10 cm (data resolution) are currently observed. Notice a shift between the temperature and LWC records resulting from the 6 m separation between the instruments and the low pitch angle of the aircraft with respect to the cloud clear air interface.

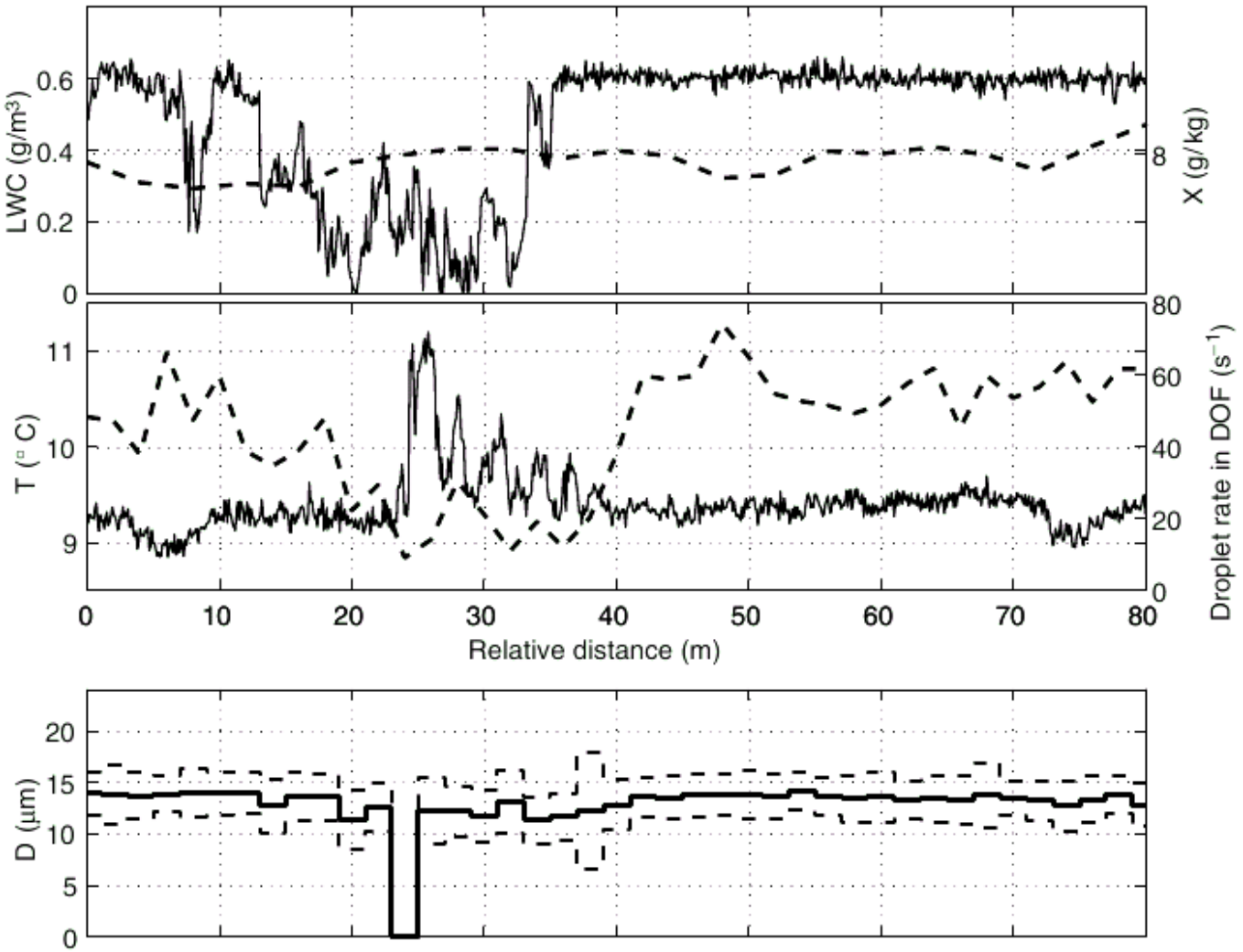


Figure 9. An example of the pattern CII – an intrusion of the cloudy air with reduced LWC into the unmixed cloudy environment (∼12–35 m); the temperature is intermediate between that of unmixed cloudy and dry air. For the description see Figure 6. Notice that disturbances in the temperature and LWC are shifted with respect to each other, which may follow from the 6 m separation between the UFT and PVM.

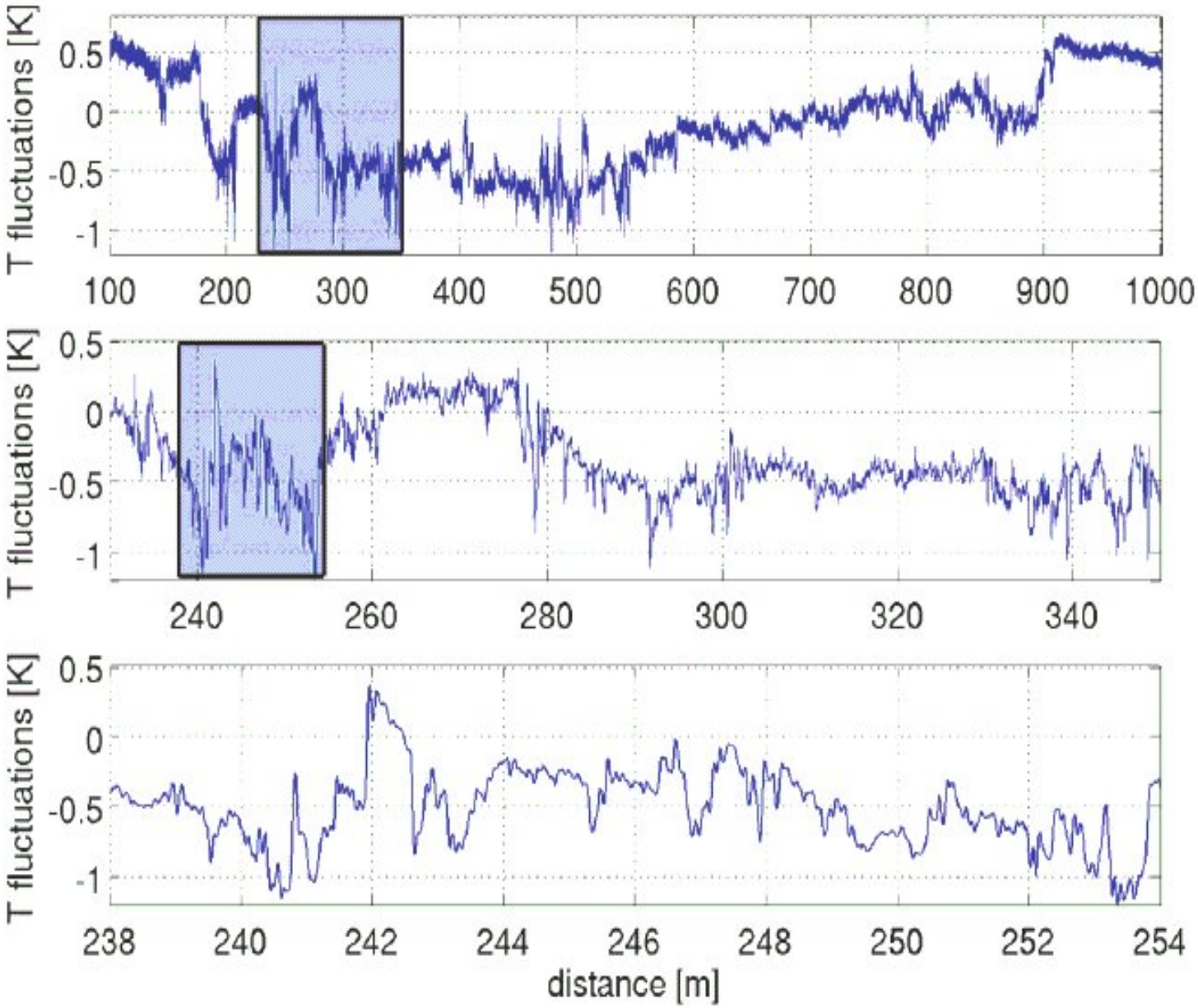


**Figure 1.** An example of the temperature time series recorded during aircraft penetration of a convective cloud. The rectangular areas marked in the upper and central plates are magnified, respectively, in the central and lower plates.

http://www.eol.ucar.edu/projects/post/

## POST – Physics of Stratocumulus Top, California, summer 2008


microphysics


temperature,
humidity,
liquid water,
turbulence,

droplet counting

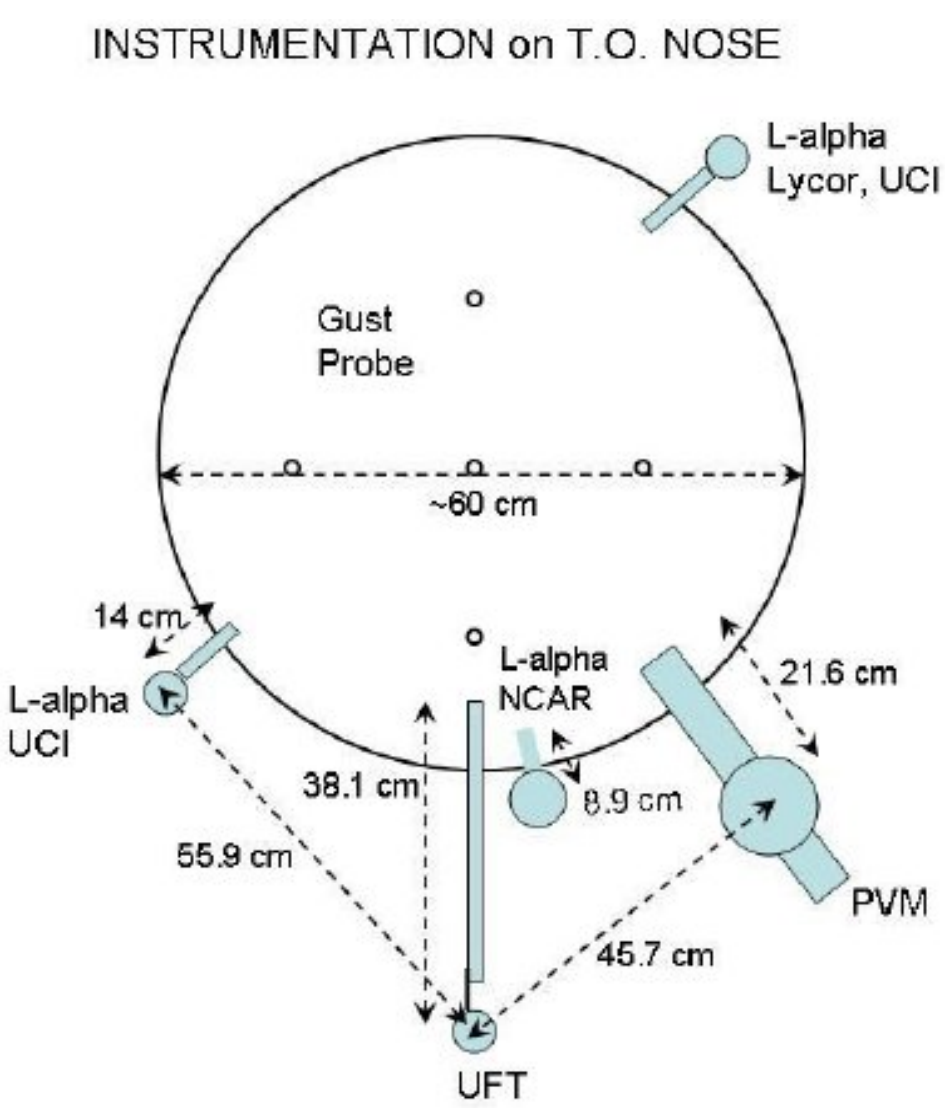


***Figure 1*** - Head-on view of the CIRPAS Twin Otter research aircraft showing the location of the UFT and PVM probes, and the Lyman-alpha probes which surround the 5-hole gust probe on the aircraft nose.

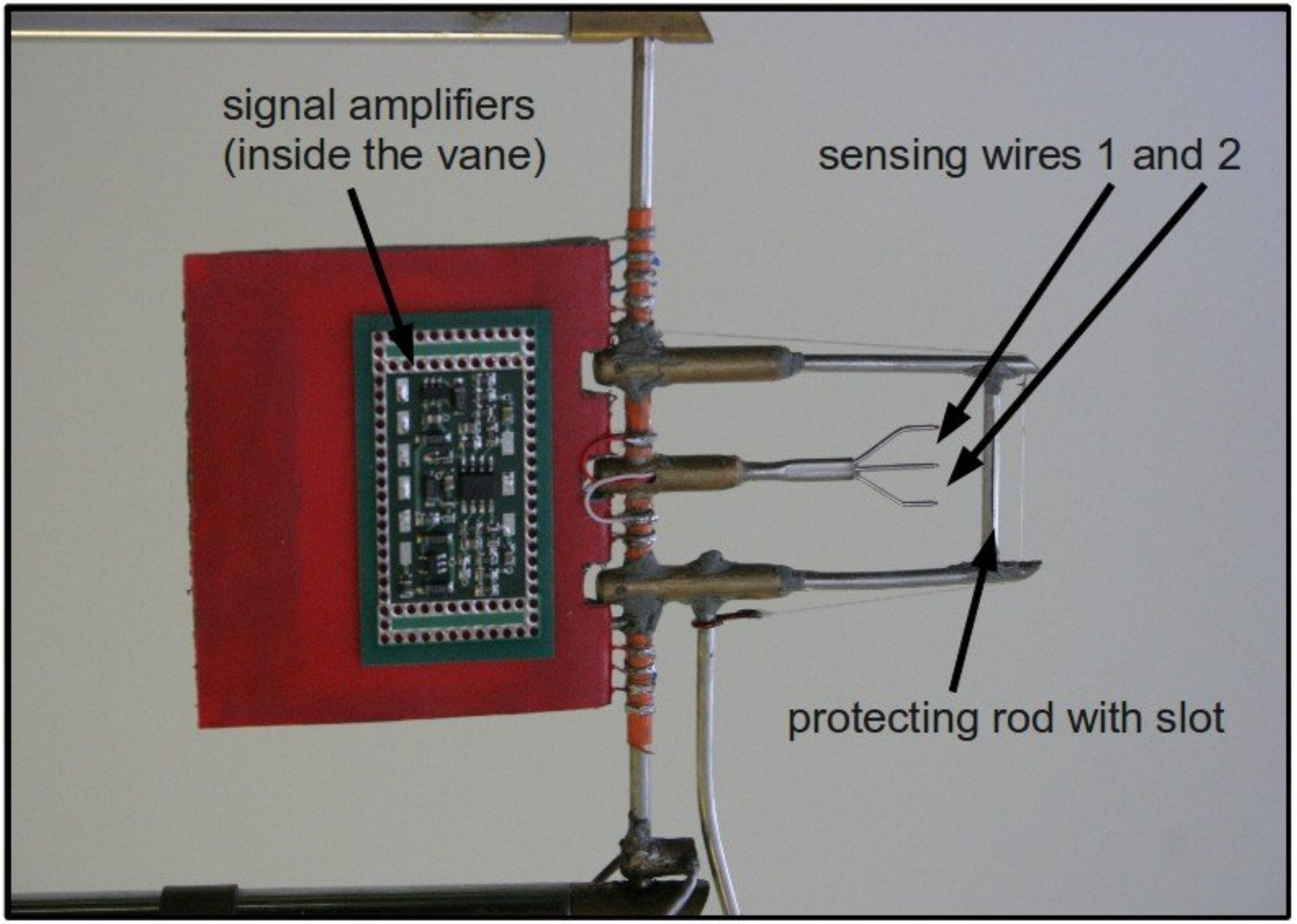
signal amplifiers
(inside the vane)
sensing wires 1 and 2
protecting rod with slot


256
NAVY


256

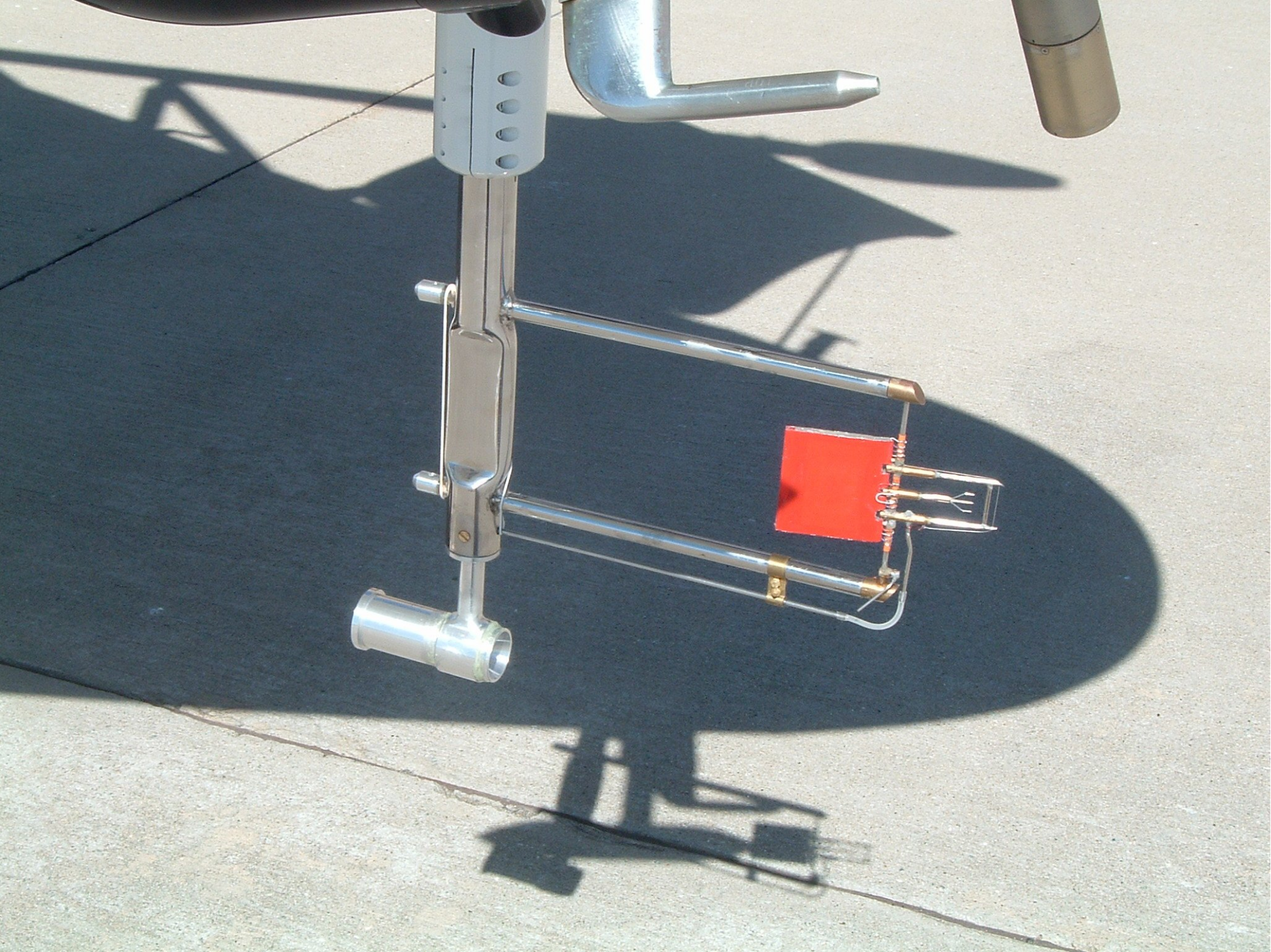


WARNING

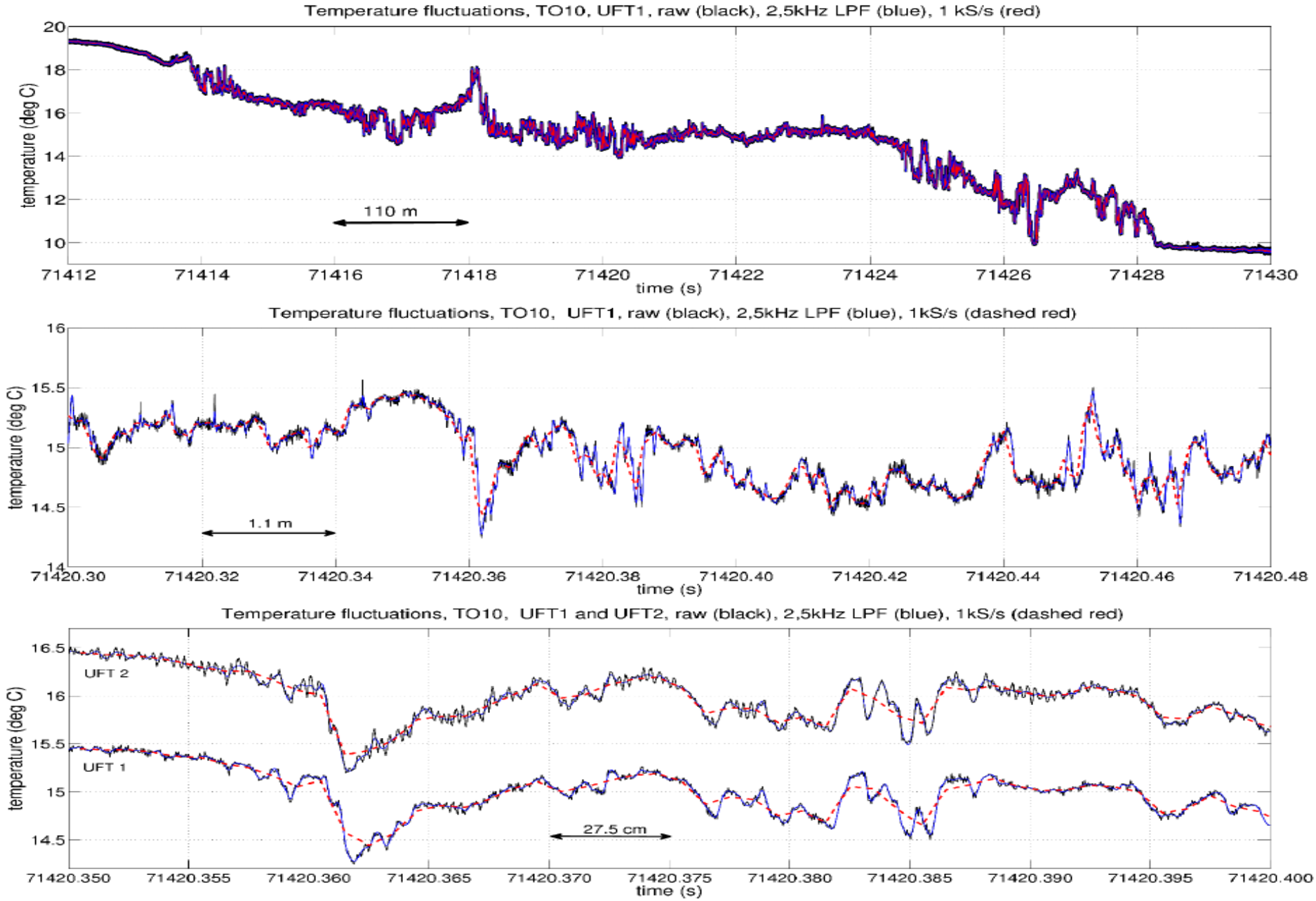


***Fig.5.*** *Examples of recorded temperature fluctuations in the cloud-top region. Upper panel shows full range of temperature fluctuations recorded during descent of Twin-Otter from capping inversion into Sc cloud. Middle panel presents temperature fluctuations as recorded by despiked, low-pass filtered and averaged signals. Lowest panel compares records from two sensing wires of the UFTM (shift between the records is artificial). Colour code as in Fig.4.*

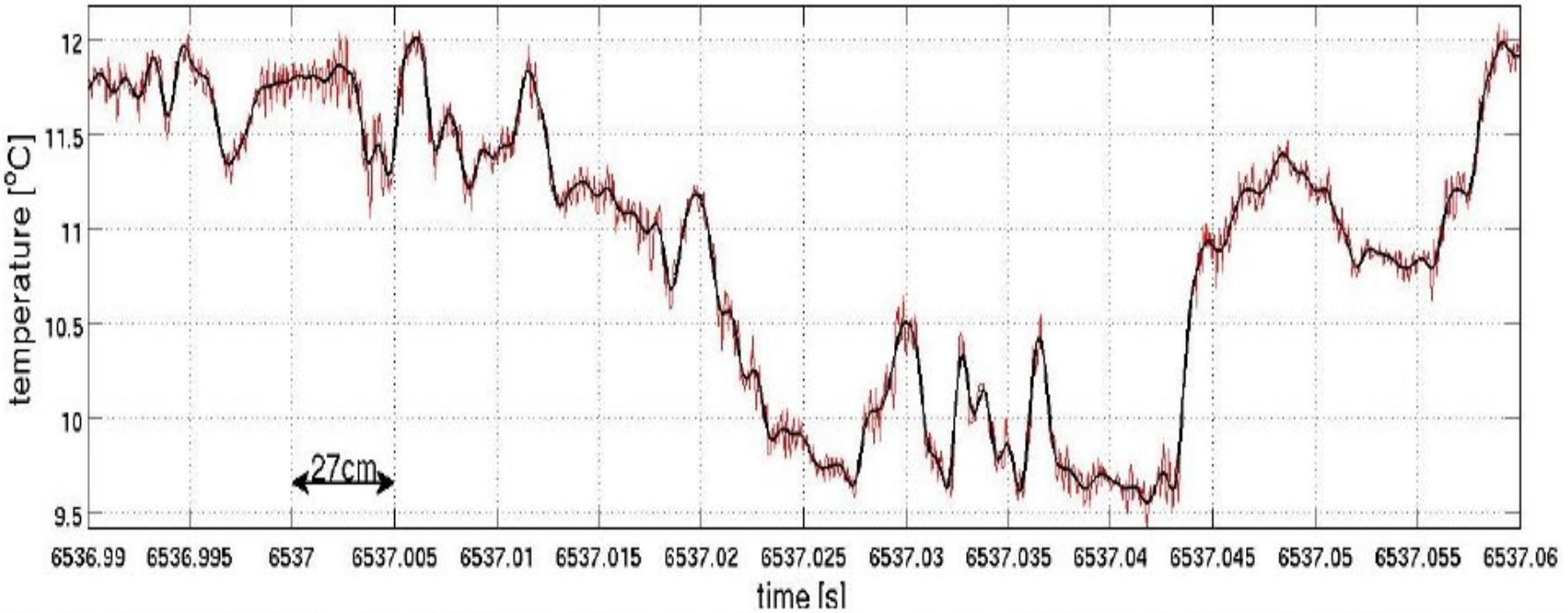


***Fig.3*** *Example temperature record from UFT-M. Red line – raw, unfiltered signal. Visible temperature fluctuations in vortices shedding from the anti-droplet protecting rod. These fluctuations of order of 0.1 K are effectively filtered with 20$^{th}$ order low-pass Butterworth filter of 2.5 kHz cut-off frequency without phase shift (black line).*

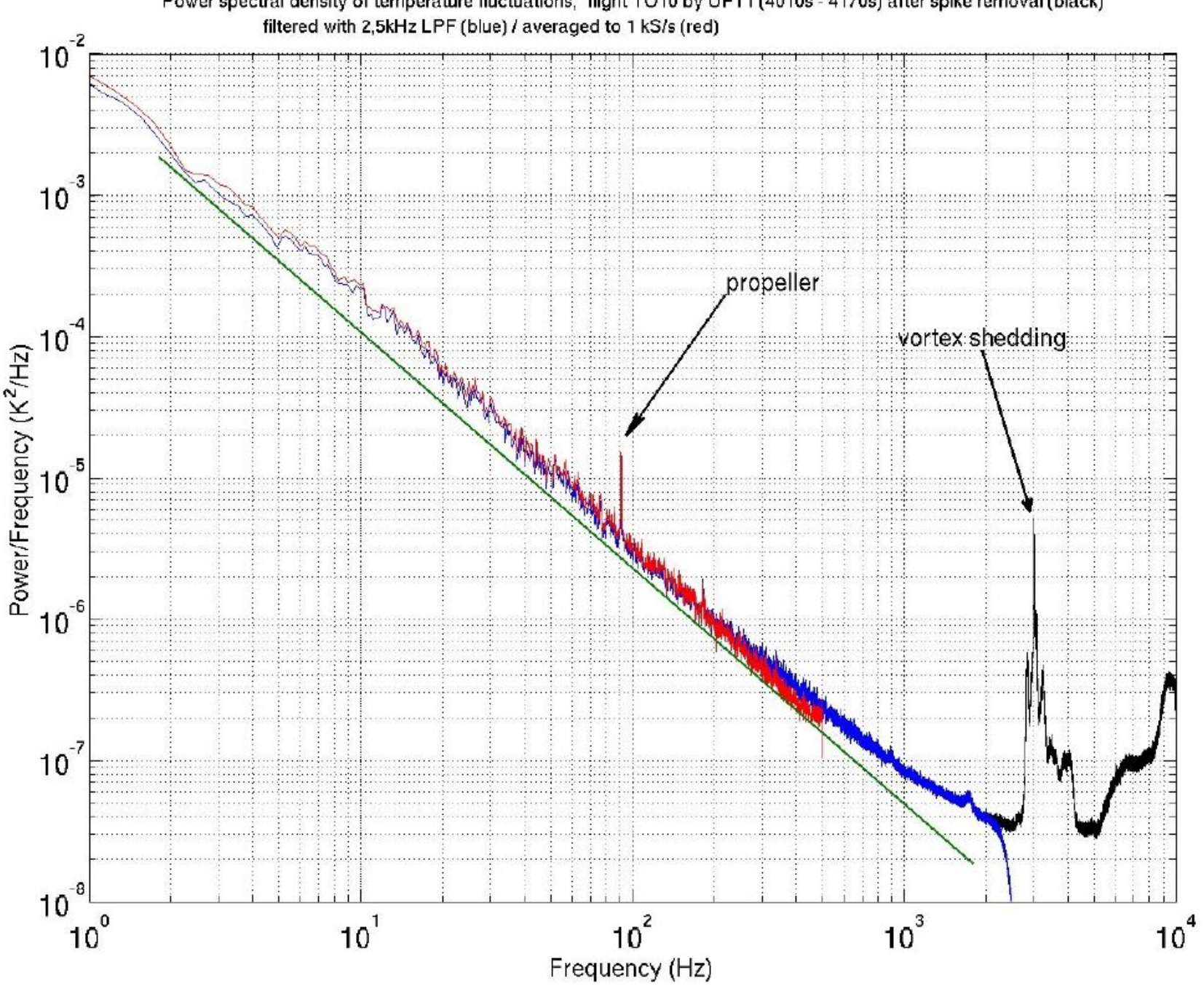


***Fig. 4*** *Power spectral density of temperature fluctuations in clod-top region. -5/3 slope plotted for reference. Black: 20kS/s data after spike removal, blue: 20kS/s data low-pass filtered with 2.5 kHz cut-off frequency, red: 1KS/s data stored in the database http://www.eol.ucar.edu/projects/post/.*

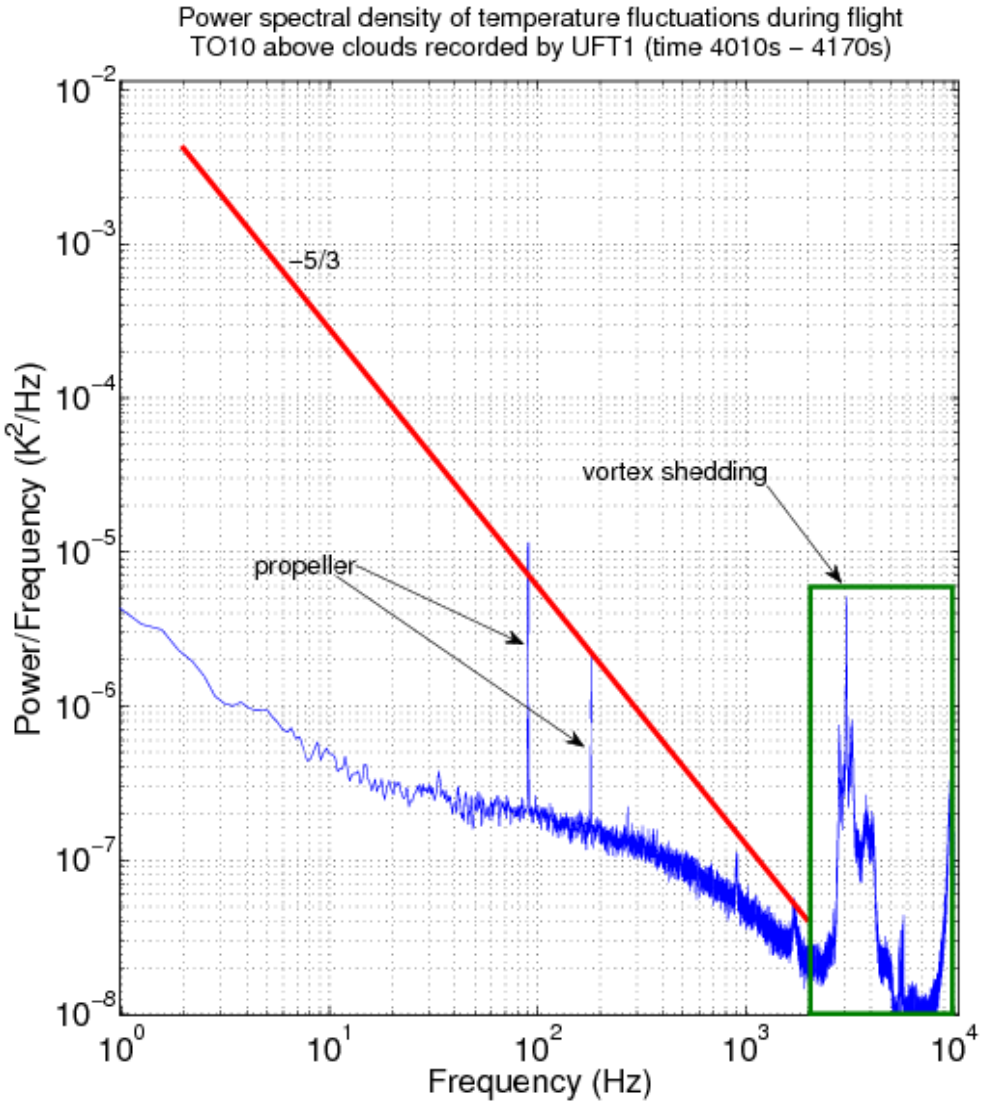
Power spectral density of temperature fluctuations during flight
TO10 above clouds recorded by UFT1 (time 4010s – 4170s)
Power/Frequency (K²/Hz)
Frequency (Hz)
−5/3
propeller
vortex shedding

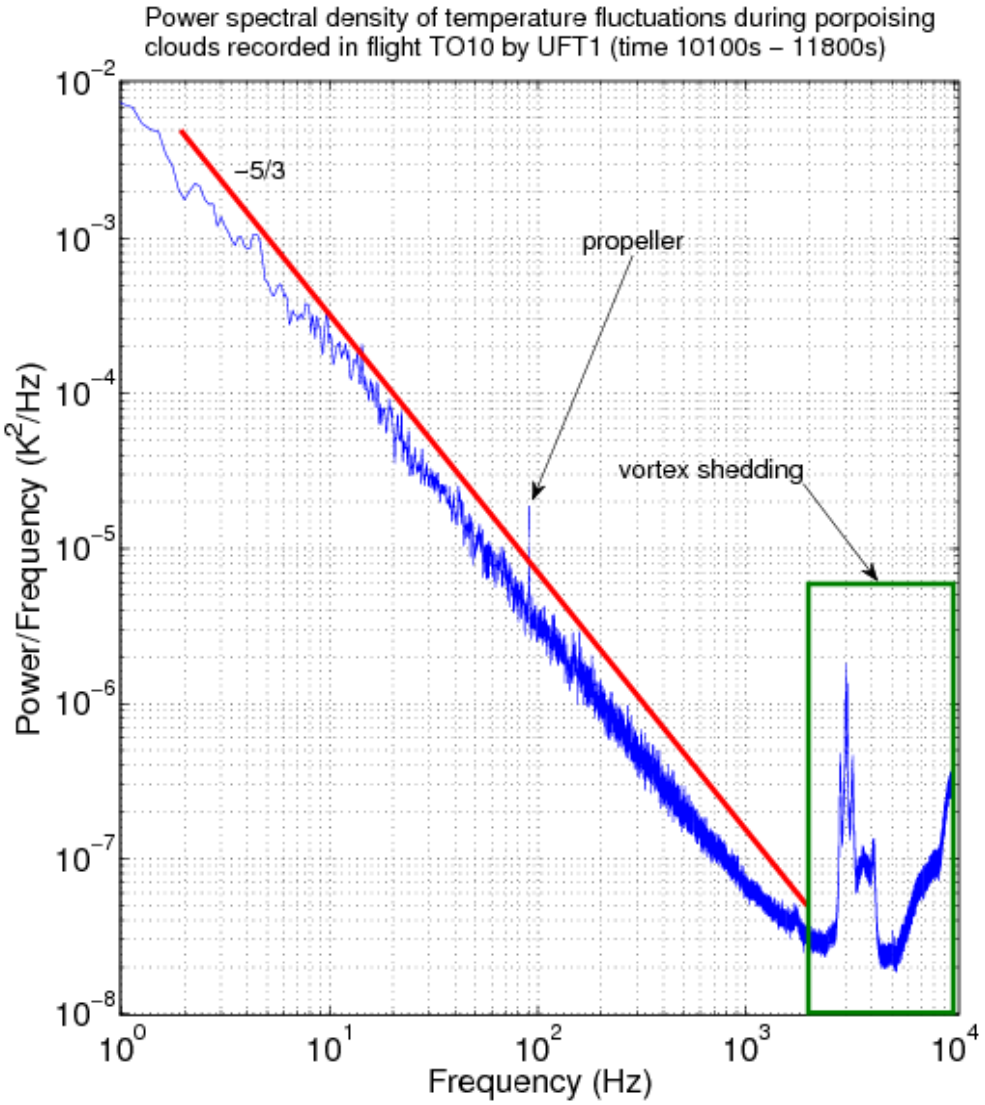
Power spectral density of temperature fluctuations during porpoising
clouds recorded in flight TO10 by UFT1 (time 10100s – 11800s)
Power/Frequency (K²/Hz)
Frequency (Hz)
−5/3
propeller
vortex shedding

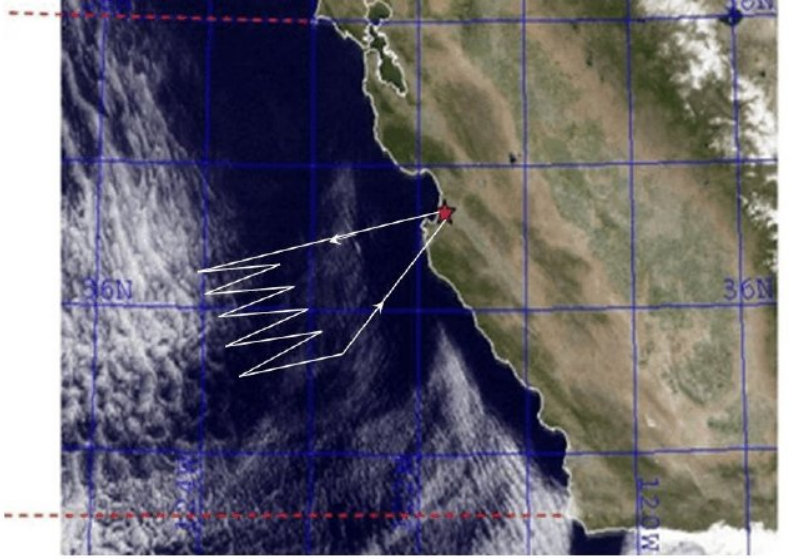


***Figure 2*** - NexSat image (courtesy Naval Research Laboratory, Monterey) of CA and the Pacific Ocean showing the typical horizontal flight track used for each quasi Lagrangian Twin Otter flight. The red star indicates the Marina airport near Monterey Bay.

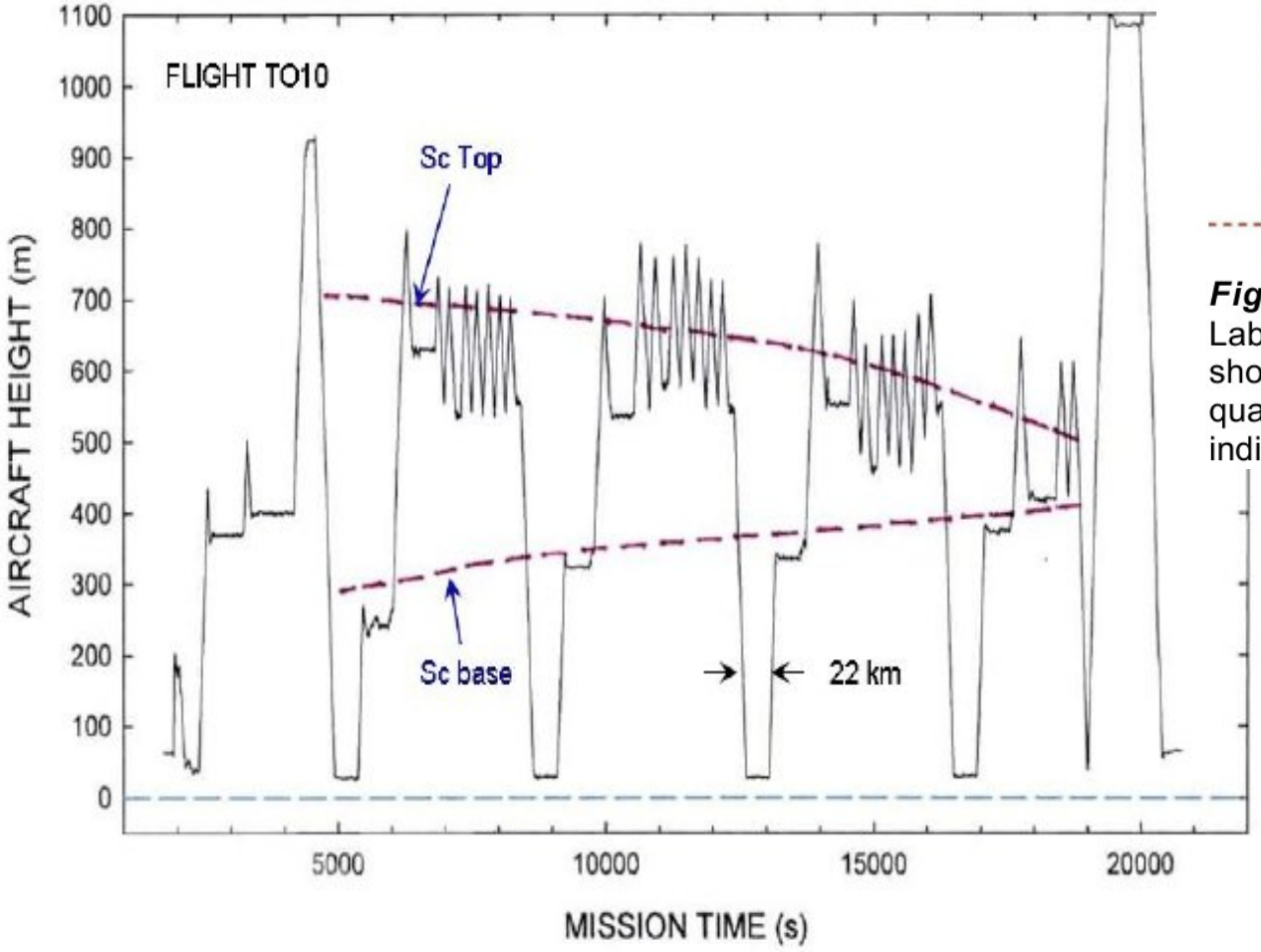


***Figure 3*** - Typical vertical flight pattern of the Twin Otter during POST flights. Porpoising through cloud top is the dominant feature.

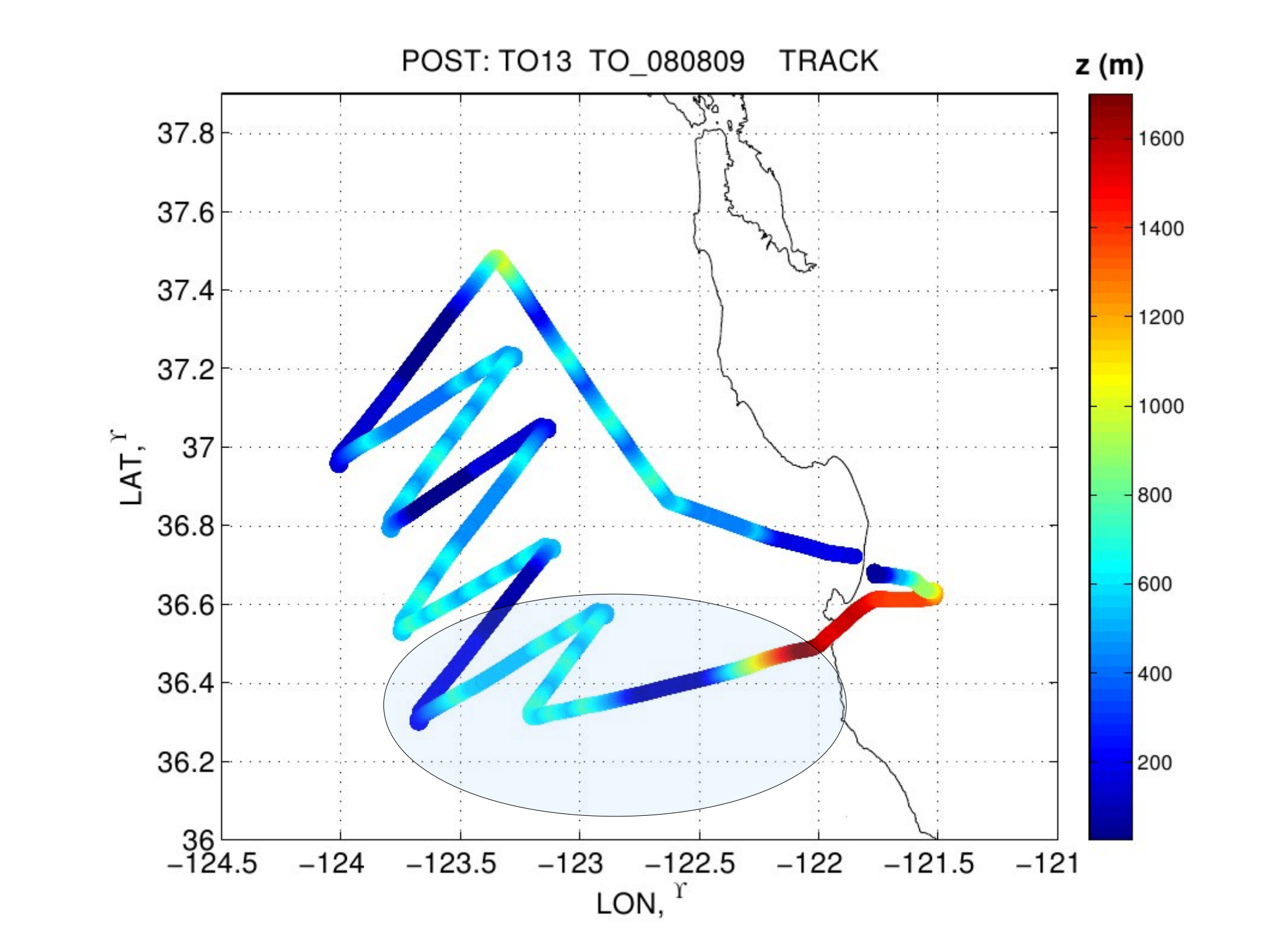
POST: TO13 TO_080809 TRACK
z (m)
1600
1400
1200
1000
800
600
400
200
37.8
37.6
37.4
37.2
37
36.8
36.6
36.4
36.2
36
LAT, ϒ
−124.5
−124
−123.5
−123
−122.5
−122
−121.5
−121
LON, ϒ

TO13, segment

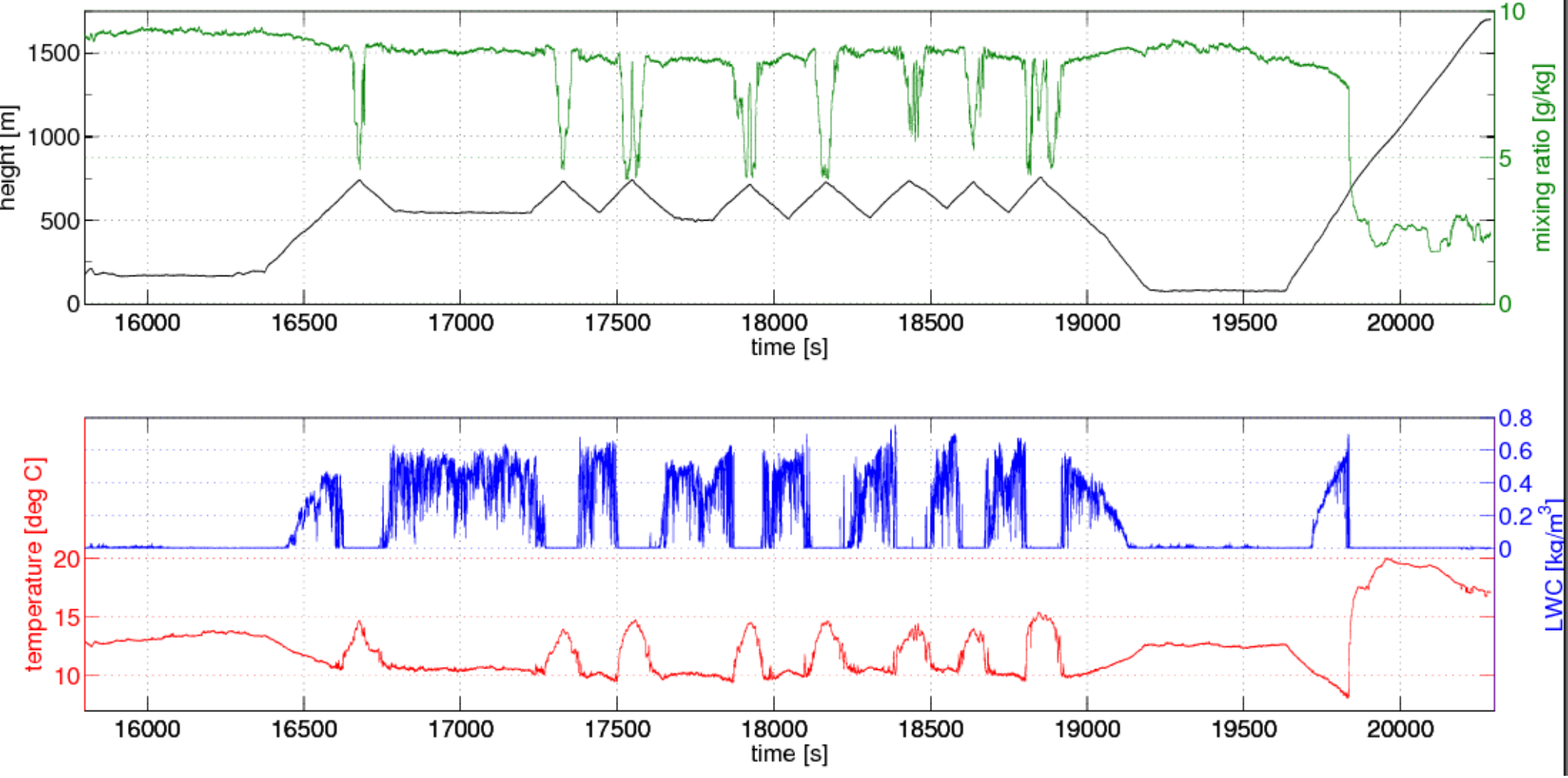


10Hz data

100Hz data

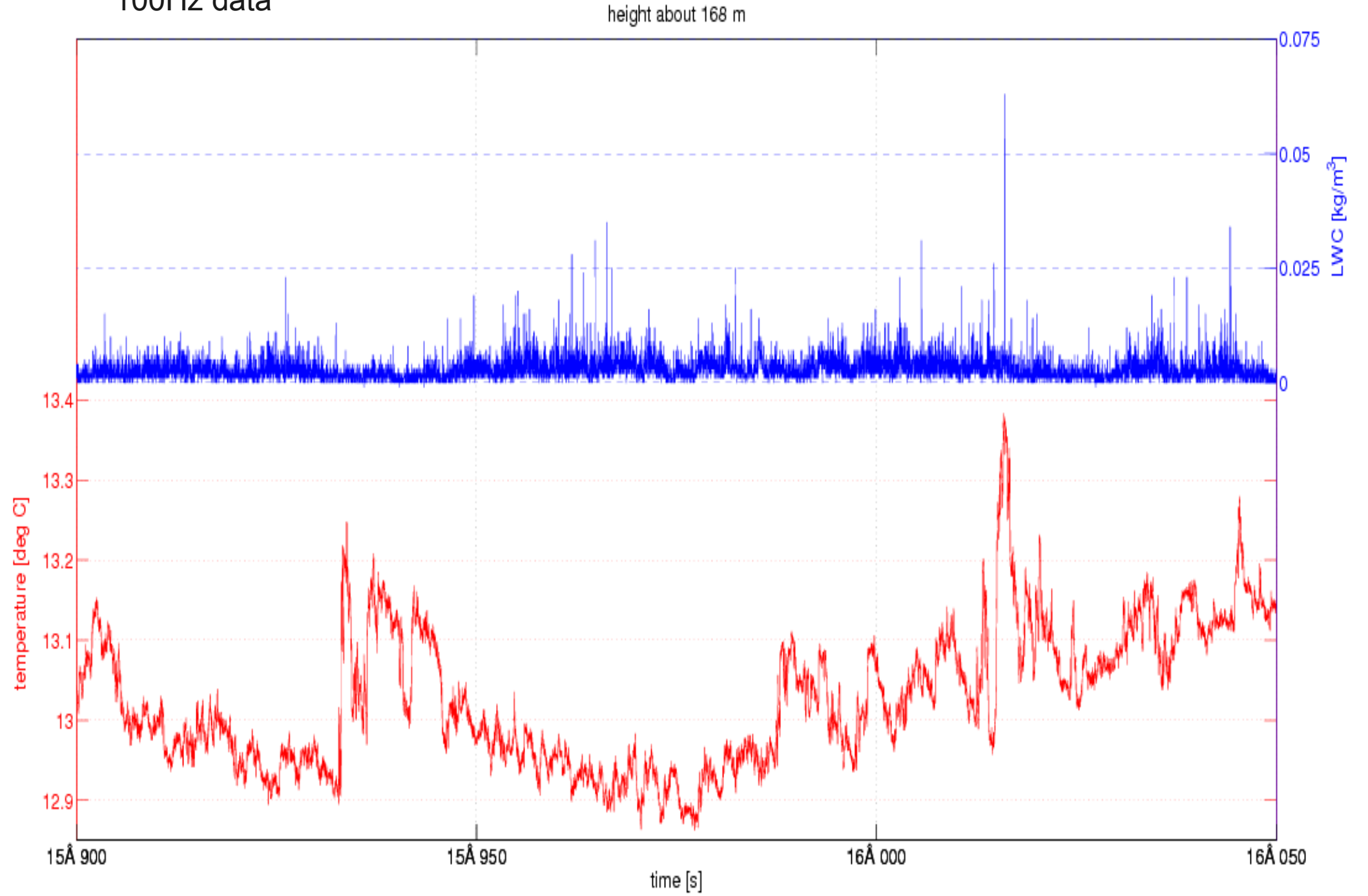
height about 168 m
0.075
0.05
0.025
0
LWC [kg/m3]
13.4
13.3
13.2
13.1
13
12.9
temperature [deg C]
15Å 900
15Å 950
16Å 000
16Å 050
time [s]

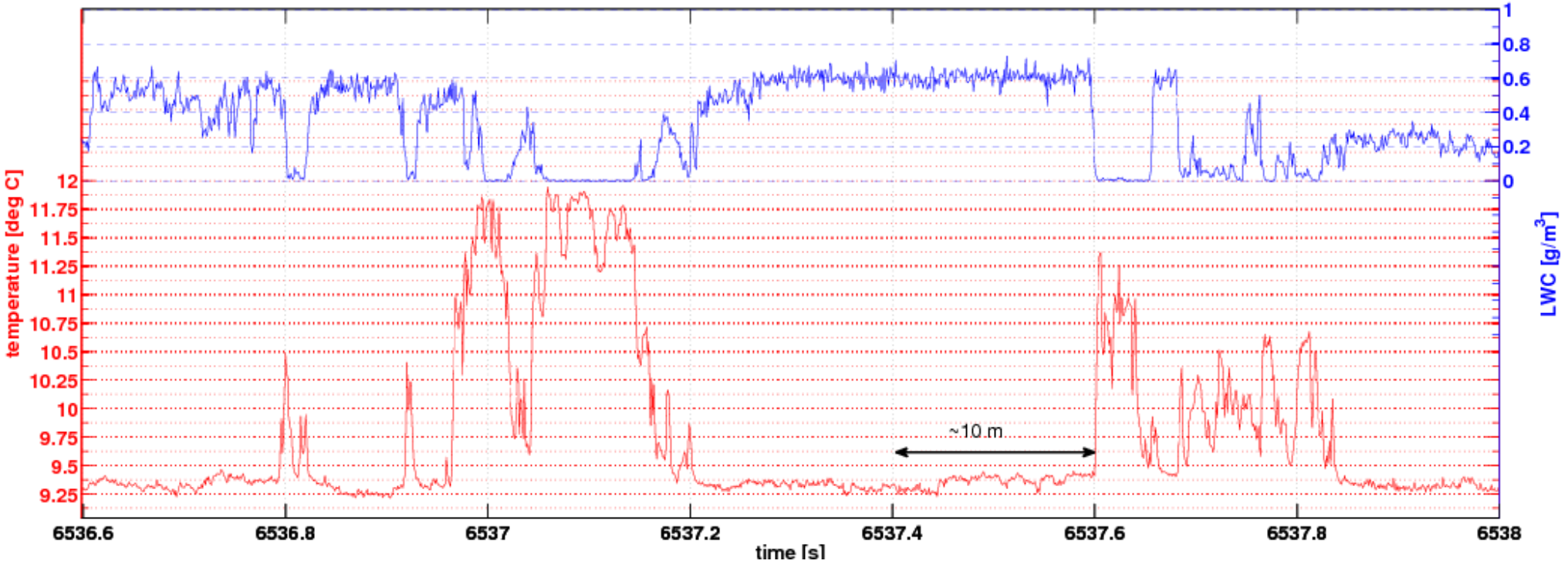
temperature [deg C]
12
11.75
11.5
11.25
11
10.75
10.5
10.25
10
9.75
9.5
9.25
LWC [g/m3]
1
0.8
0.6
0.4
0.2
0
~10 m
6536.6
6536.8
6537
6537.2
6537.4
6537.6
6537.8
6538
time [s]

# 100Hz data

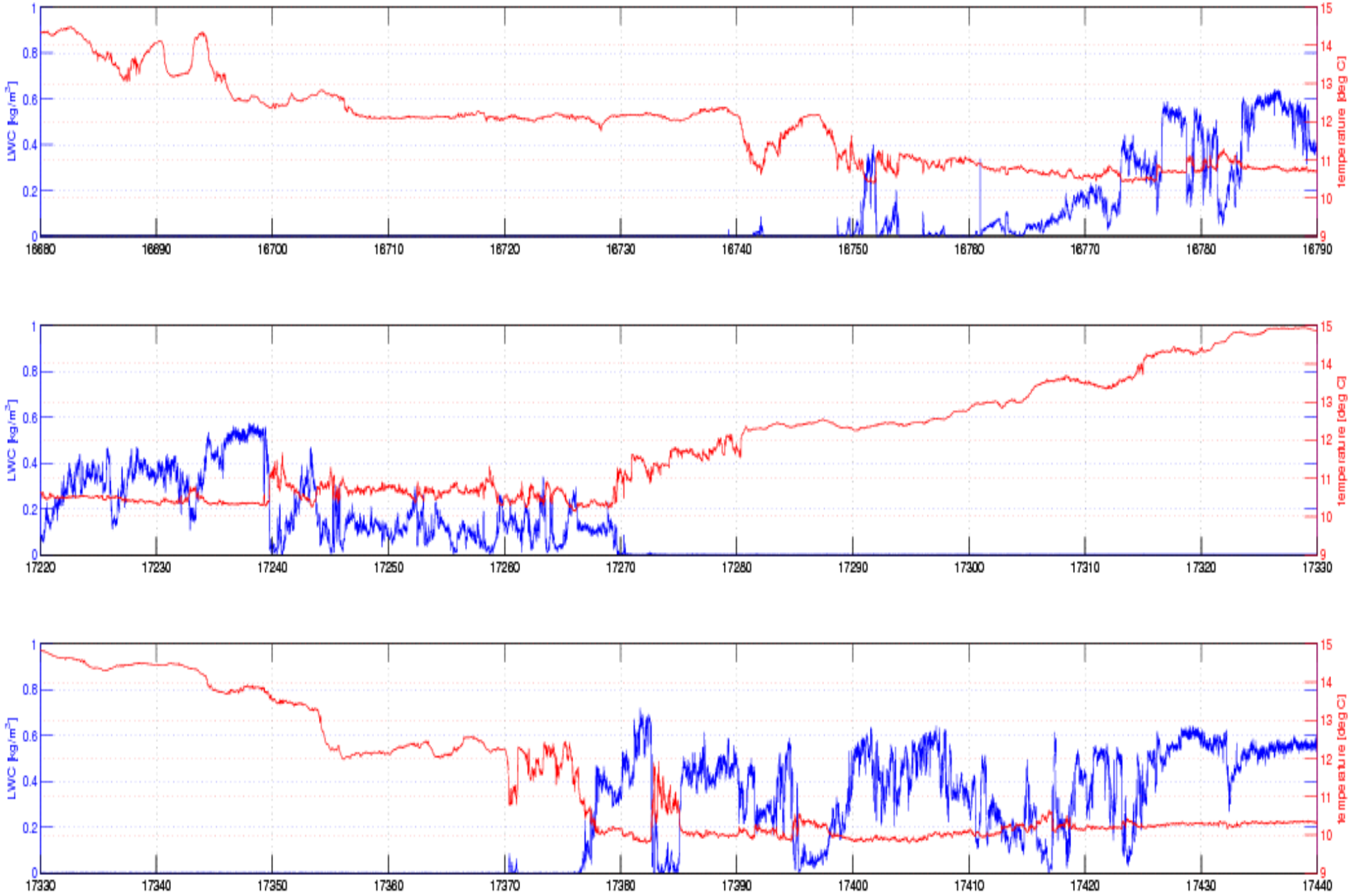
LWC [kg/m³]
temperature [deg C]
16680
16690
16700
16710
16720
16730
16740
16750
16760
16770
16780
16790
17220
17230
17240
17250
17260
17270
17280
17290
17300
17310
17320
17330
17330
17340
17350
17360
17370
17380
17390
17400
17410
17420
17430
17440

100Hz data

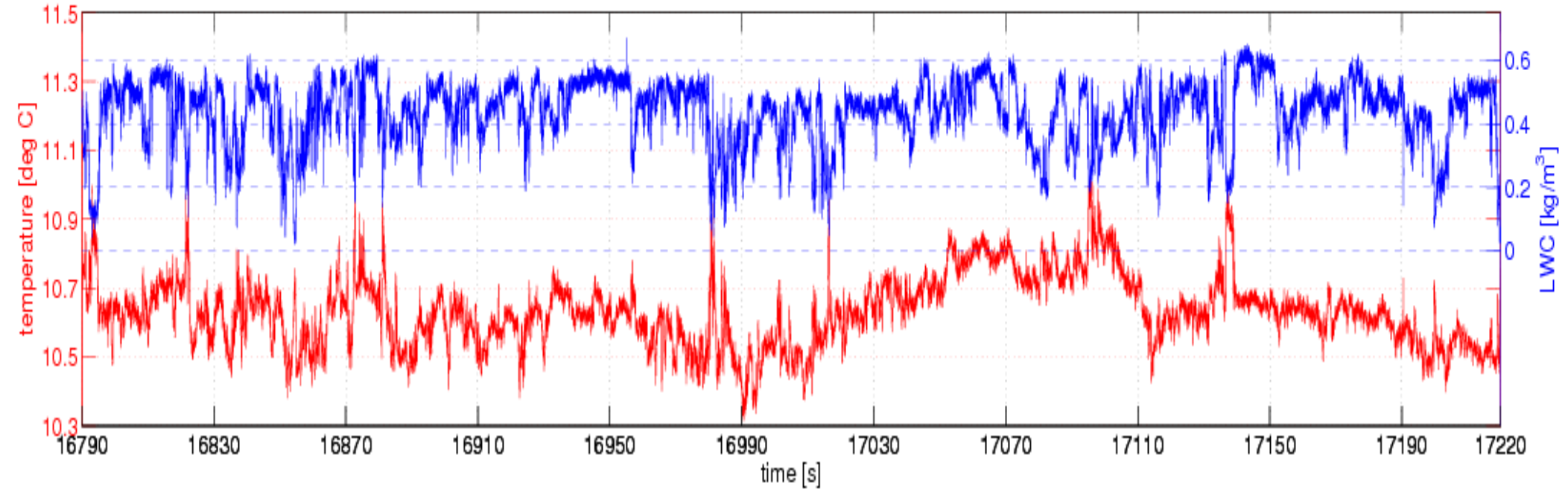
temperature [deg C]
LWC [kg/m$^3$]
time [s]
11.5
11.3
11.1
10.9
10.7
10.5
10.3
0.6
0.4
0.2
0
16790
16830
16870
16910
16950
16990
17030
17070
17110
17150
17190
17220

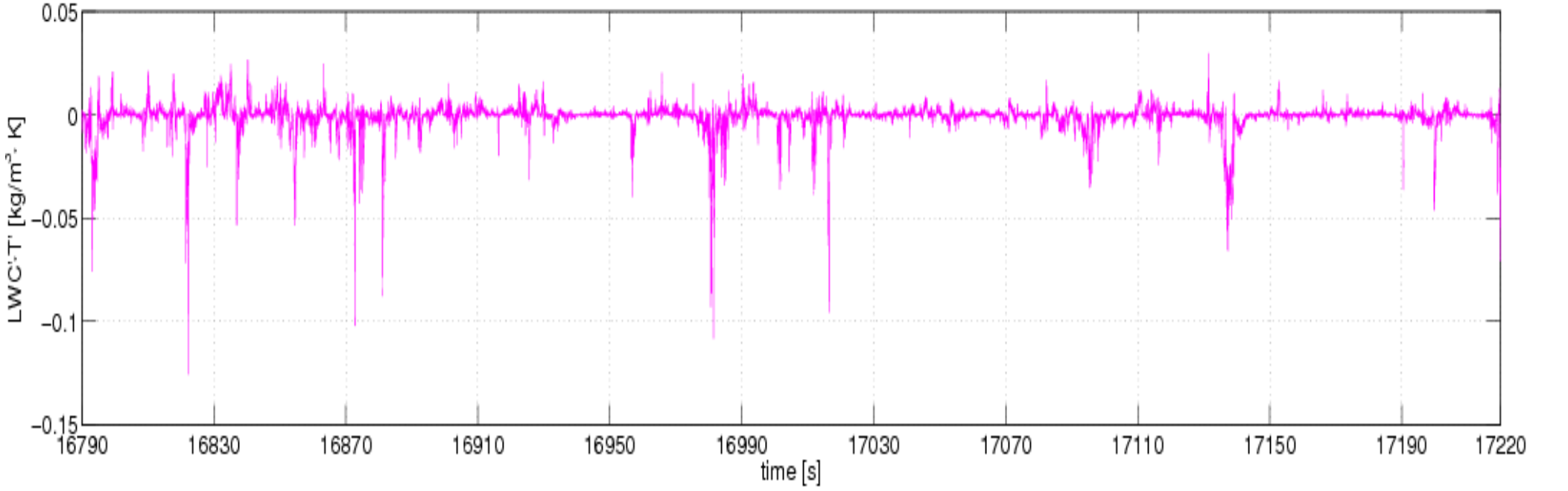
LWC'·T' [kg/m$^3$· K]
time [s]
0.05
0
−0.05
−0.1
−0.15
16790
16830
16870
16910
16950
16990
17030
17070
17110
17150
17190
17220

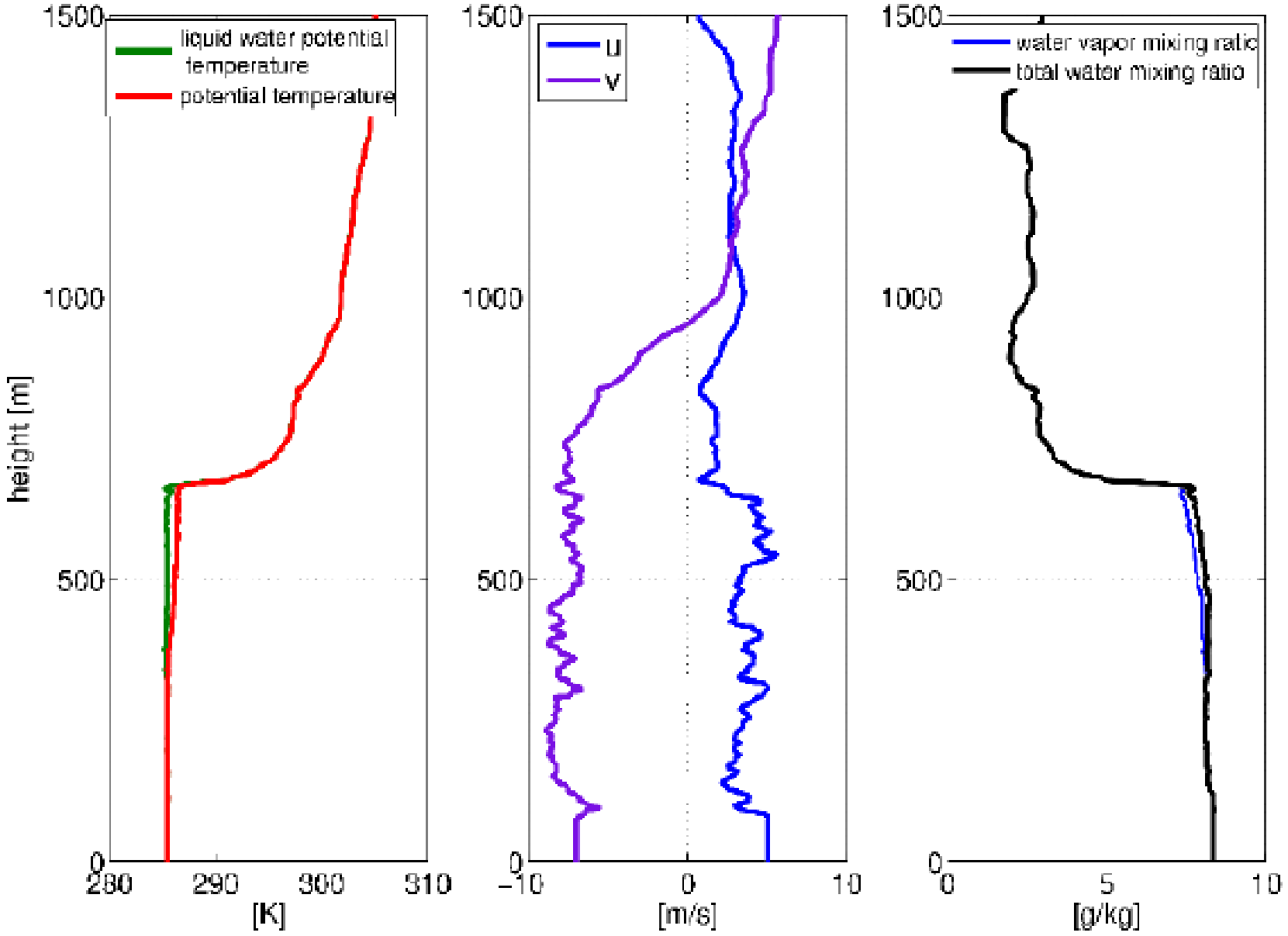


***Fig.3*** *Vertical profiles of temperature, water mixing ratio and wind taken at the end of TO13 research flight.*

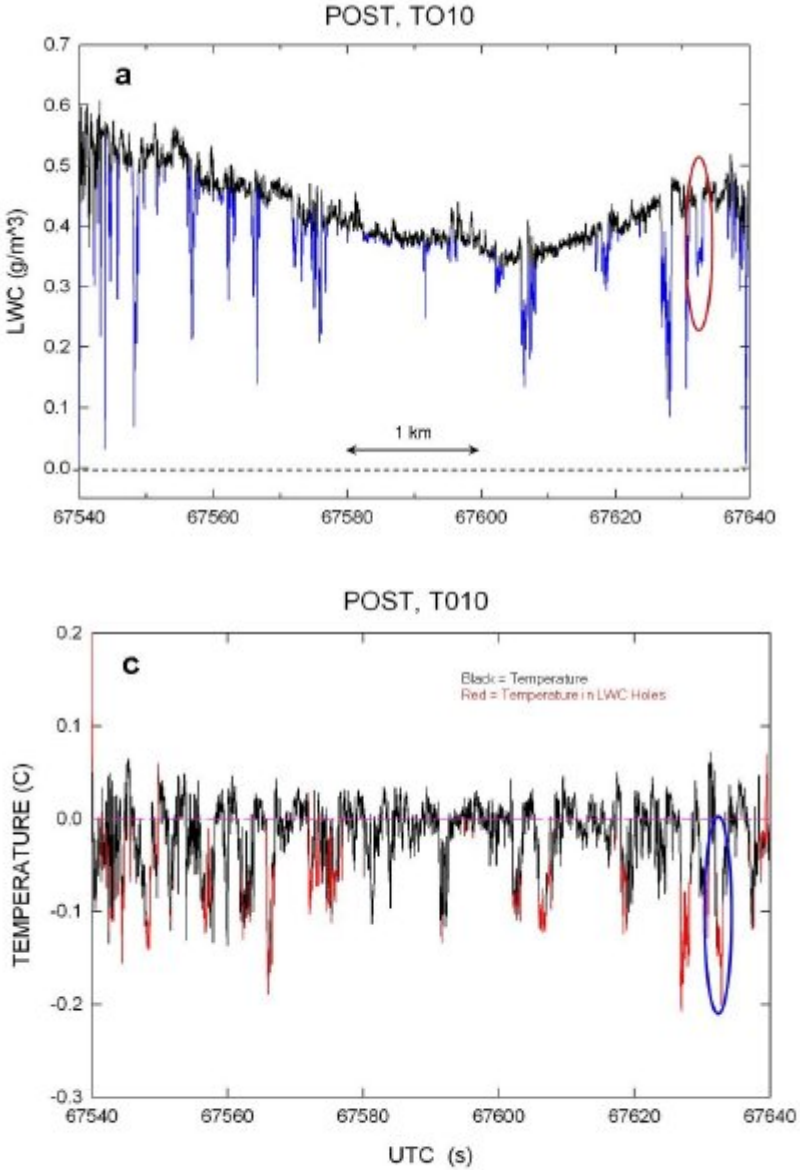


***Fig. 4*** - A 5-km segment of flight TO10 showing conditionally sampled "cloud holes in (a, blue lines), the flux of depleted LWC in (b), and the correlation between UFT temperature and cloud holes in (c).

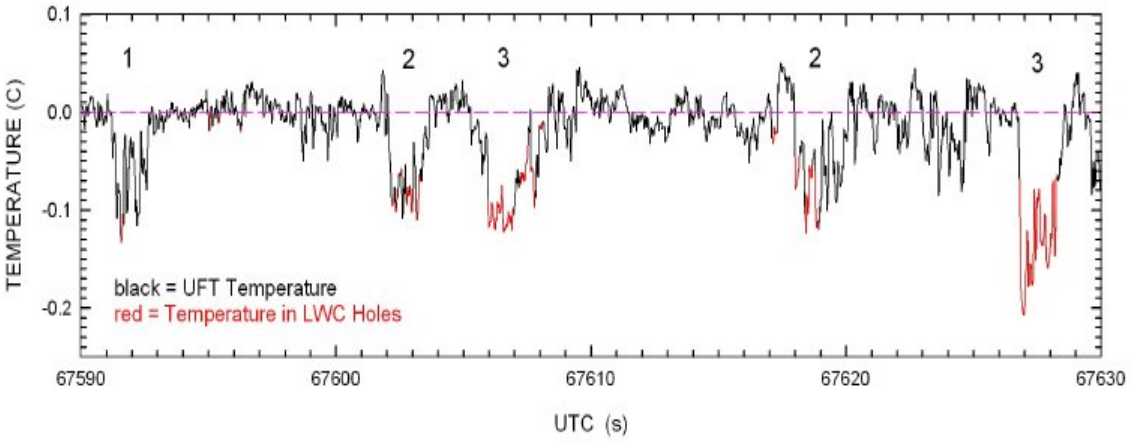


***Figure 5*** - A 40-s segment of Fig. 4 showing locations in the UFT temperature record that coincide with the depleted LWC in the cloud holes.

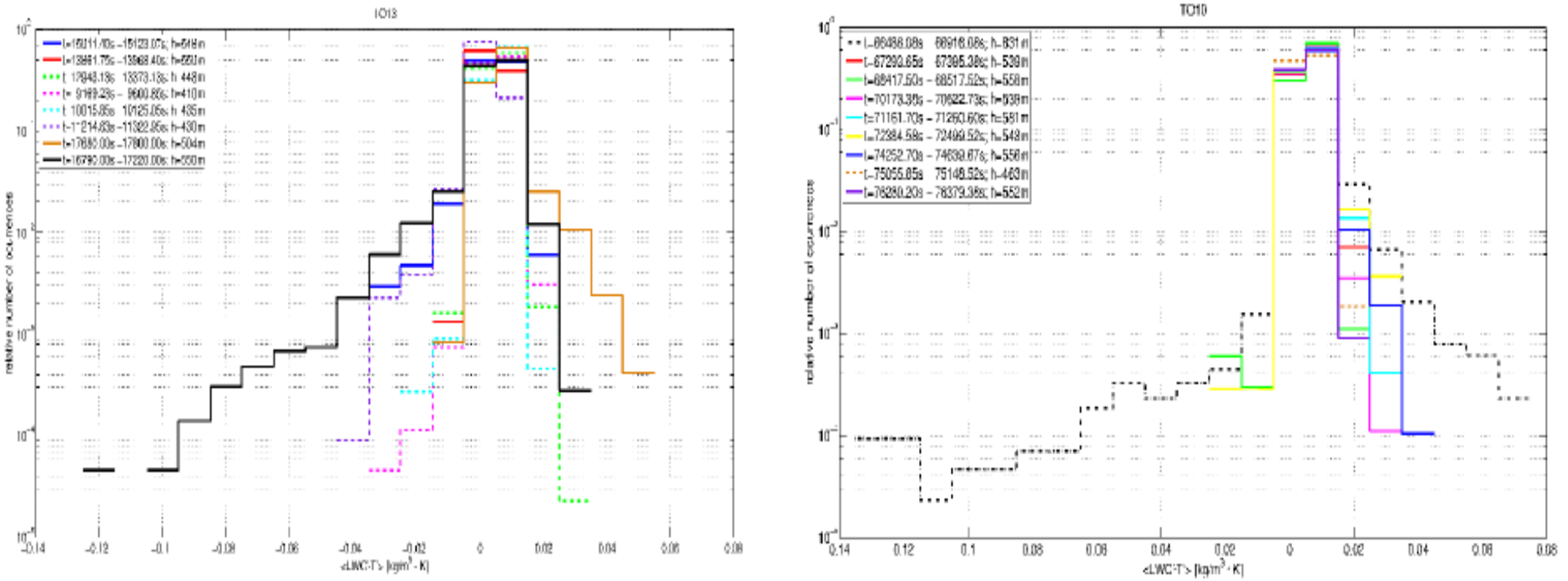


***Fig.7*** *Histograms of correlations <LWC' T'> on horizontal legs inside cloud deck in flights TO13 (left panel) and TO10 (right panel). It can be seen that weak positive correlations prevail. Strong negative correlations occur frequently in some legs of TO13 only.*

# References and suggested reading:


Beswick, K. M., Gallagher, M. W., Webb, A. R., Norton, E. G., and Perry, F.: Application of the Aventech AIMMS20AQ airborne probe for turbulence measurements during the Convective Storm Initiation Project, Atmos. Chem. Phys., 8, 5449-5463

Crawford, T. L. and R. J. Dobosy, 1992: A sensitive fast-response probe to measure turbulence and heat flux from any airplane. Bound.-Layer Meteor., 59, 257-278.

Cruette, D., A. Marillier, J. L. Dufresne, J. Y. Grandpeix, P. Nacass, H. Bellec, 2000: Fast Temperature and True Airspeed Measurements with the Airborne Ultrasonic Anemometer–Thermometer (AUSAT). J. Atmos. Oceanic Technol., 17, 1020–1039.

Friehe, C. A. and D. Khelif, 1993: Fast response aircraft temperature sensors. J. Atmos.Oceanic Technol., 9, 784–795.

Gerber, H, G. Frick, S. P. Malinowski, W. Kumula, and S. Krueger, 2010: POST—A New Look at Stratocumulus, http://ams.confex.com/ams/13CldPhy13AtRad/techprogram/paper_170431.htm

Gerber, H., G. Frick, S. P. Malinowski, J-L. Brenguier, F. Burnet, 2005: Holes and Entrainment in Stratocumulus. J. Atmos. Sci., 62, 443–459.

Haman KE, SP Malinowski, 1989: Observations of cooling tower and stack plumes and their comparison with plume model 'ALINA', Atmospheric Environment 23, 1223-1234

Haman, KE., A Makulski, SP. Malinowski, R Busen, 1997: A New Ultrafast Thermometer for Airborne Measurements in Clouds. J. Atmos. Oceanic Technol., 14, 217–227.

Haman, KE., SP. Malinowski, BD. Struś, R Busen, A Stefko, 2001: Two New Types of Ultrafast Aircraft Thermometer. J. Atmos. Oceanic Technol., 18, 117–134

Haman, KE., SP. Malinowski, MJ. Kurowski, H Gerber, and J.-L. Brenguier, 2007: Small-acale mixing processes at the top of a marine strotocumulus - a case study. Quart. J. Roy. Meteor. Soc., 133, 213–226.

Lawson, RP, WA. Cooper, 1990: Performance of Some Airborne Thermometers in Clouds. J. Atmos. Oceanic Technol., 7, 480–494.

Mayer, J.-C., K. Hens, U. Rummel, F. X. Meixner, and T. Foken, 2009: Moving measurements platforms - specific and corrections. Meteorologishe Zeitschrift, 18, 477–488.

MacPherson, J. I., G. A. Isaac, 1977: Turbulent Characteristics of Some Canadian Cumulus Clouds. J. Appl. Meteor., 16, 81–90

Rosa, B, K Bajer, KE. Haman, T Szoplik, 2005: Theoretical and Experimental Characterization of the Ultrafast Aircraft Thermometer: Reduction of Aerodynamic Disturbances and Signal Processing. J. Atmos. Oceanic Technol., 22, 988–1003.

Sinkevich, A. A. and R. P. Lawson, 2005: A survey of temperature measurements in convective clouds. J. Appl. Meteor., 44, 1133–1145.

Stevens, B, and Coauthors, 2003: Dynamics and Chemistry of Marine Stratocumulus—DYCOMS-II. Bull. Amer. Meteor. Soc., 84, 579–593.

Wang, Y, B Geerts, 2009: Estimating the Evaporative Cooling Bias of an Airborne Reverse Flow Thermometer. J. Atmos. Oceanic Technol., 26, 3–21.